THEORY & FUNDAMENTALS
How to Ensure Accuracy and Repeatability in Absorbance Measurements

ICP
Tutorials on Configuring Sample Introduction Systems and Controlling Contamination

TECHNIQUE FOCUS
Dispelling Confusion about Self-Absorption in LIBS—and Learning How to Harness It

AUGUST 2022
VOLUME 37 | NO. 8

Spectroscopy®

SOLUTIONS FOR MATERIALS ANALYSIS

The Resource Issue 2022–2023

IR
Quantitative Analysis of Co-crystallized Diastereomers with THz–TDS

Our Annual Directory of Products and Services

Scan the QR code to visit our new online directory

SPECTROSCOPYONLINE.com

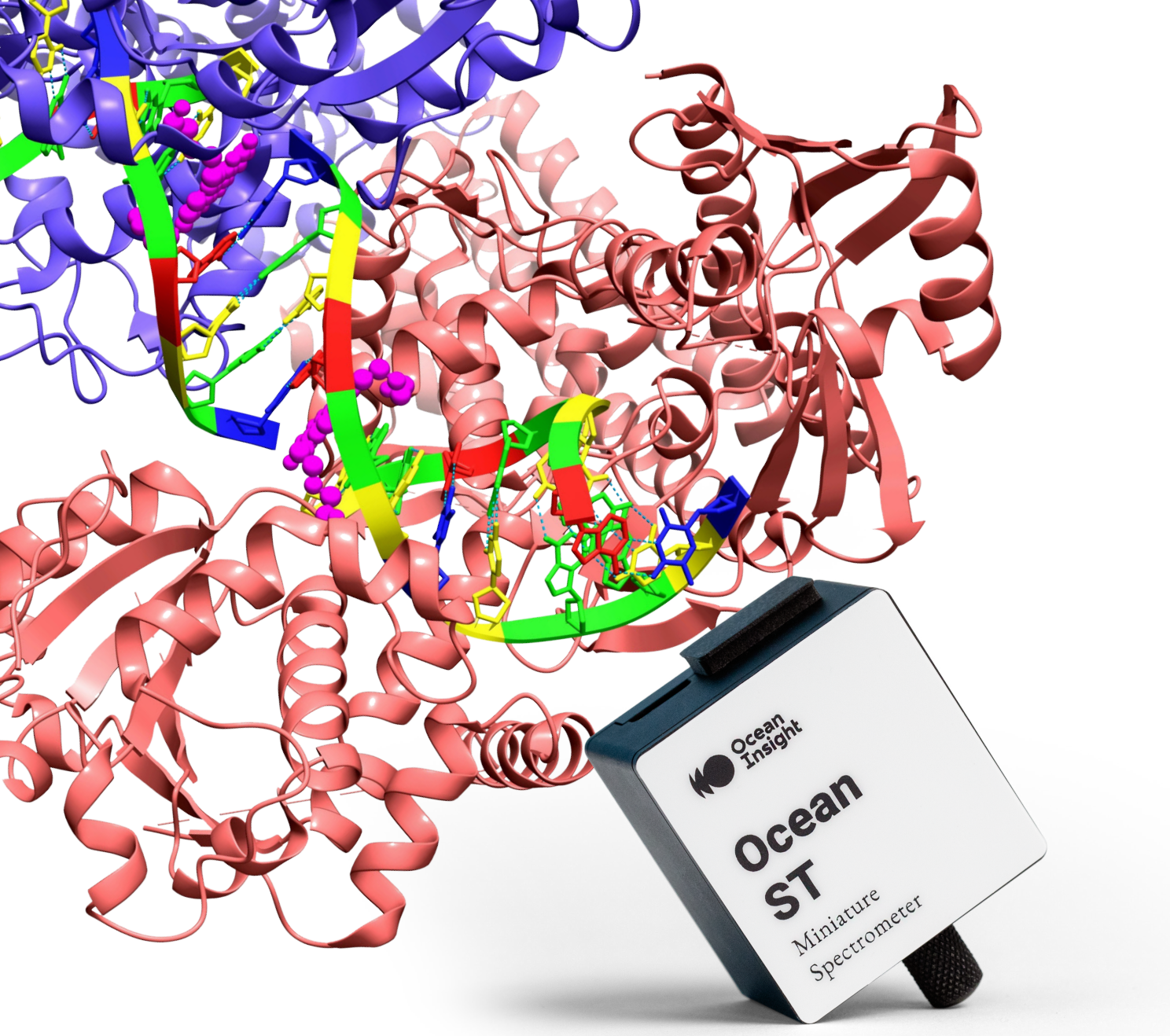

Remarkable Spectral Performance in a Compact Footprint

The ultra-compact new Ocean ST microspectrometer combines advances in detector technology with smart optoelectrical design to provide spectral performance comparable to a large-bench spectrometer. Use Ocean ST for everyday lab applications, integration into other devices, and setups where space is limited.

Ocean Insight

oceaninsight.com

multi EA 5100

Micro-elemental Analyzer

Versatile, Fast, and Sensitive Micro-Elemental Analysis

multi EA 5100 | Your entire C/N/S/X lab in one device

In addition to the testing of carbon, nitrogen, sulfur, and chlorine; the multi EA 5100 analyzes for important environmental parameters such as TOC, AOX/TOX, and EOX. C/N/S/X testing is carried out in one analysis cycle, the change between C/N/S and X determination is fully automatic, with no conversion of the instrument required. Preset standard methods simplify your work further and reduce measuring time.

- Optimal for oil and gas, petrochemical and chemical, and polymer industries
- Compliant with a large number of common international and national regulations (ASTM, EPA, DIN, ISO, EN, etc.)
- The modular principle allows for the system to be designed individually – additional detection modules may be added at at any time should your requirements change
- **HiPerSens** detection provides a broad linear measuring range at the highest levels of detection

For more information, contact us:

info@us.analytik-jena.com
www.analytik-jena.us

analytikjena
An Endress+Hauser Company

Spectroscopy

MANUSCRIPTS: To discuss possible article topics or obtain manuscript preparation guidelines, contact the editorial director at: (732) 346-3020, e-mail: LBush@mjhlifesciences.com. Publishers assume no responsibility for safety of artwork, photographs, or manuscripts. Every caution is taken to ensure accuracy, but publishers cannot accept responsibility for the information supplied herein or for any opinion expressed.

SUBSCRIPTIONS: For subscription information: *Spectroscopy*, P.O. Box 457, Cranbury, NJ 08512-0457; email mmhinfo@mmhgroup.com. Delivery of *Spectroscopy* outside the U.S. is 3–14 days after printing.

CHANGE OF ADDRESS: Send change of address to *Spectroscopy*, P.O. Box 457, Cranbury, NJ 08512-0457; provide old mailing label as well as new address; include ZIP or postal code. Allow 4–6 weeks for change. Alternately, send change via e-mail to mmhinfo@mmhgroup.com for address changes or subscription renewal.

C.A.S.T. DATA AND LIST INFORMATION: Contact Stephanie Shaffer, (774) 249-1890; e-mail: SShaffer@mjhlifesciences.com

Reprints: Contact Stephanie Shaffer, e-mail: SShaffer@mjhlifesciences.com

INTERNATIONAL LICENSING: Contact Kim Scaffidi, e-mail: KScaffidi@mjhlifesciences.com

CUSTOMER INQUIRIES: Customer inquiries can be forwarded directly to MJH Life Sciences, Attn: Subscriptions, 2 Clarke Drive, Suite 100, Cranbury, NJ 08512; e-mail: mmhinfo@mmhgroup.com

Alliance for Audited Media

50% Recycled Paper, 10-20% Post Consumer Waste

AN MJH life sciences® BRAND

485F US Highway One South,
Suite 210
Iselin, NJ 08830
(609) 716-7777

Founder
Mike Hennessy Sr
1960 - 2021

Complete FT-IR/FT-NIR analysis from laboratory to process.

ABB offers a wide portfolio of high-performance laboratory and process FT-IR/FTNIR spectrometers and packaged solutions. Its latest generation of reliable, rugged and flexible analyzers enable to address multiple applications in industry, universities and research centers. Those maintenance free instruments allow to maximize productivity and deliver unbeatable analytical performance at the industry's lowest cost of ownership. Contact us at ftir@ca.abb.com. **www.abb.com/analytical**

Spectroscopy

2022–2023

The Resource Issue

PEER-REVIEWED RESEARCH

COLUMNS & TUTORIALS

ALSO:

DIRECTORY

Visit our new online directory by **scanning the QR code** below:

Cover image courtesy of Courtney Soden

Spectroscopy (ISSN 0887-6703 [print], ISSN 1939-1900 [digital]) is published monthly by MultiMedia Healthcare, LLC., 2 Clarke Drive, Suite 100, Cranbury, NJ 08512. Spectroscopy is distributed free of charge to users and specifiers of spectroscopic equipment in the United States. Spectroscopy is available on a paid subscription basis to nonqualified readers at the rate of: U.S. and possessions: 1 year (12 issues), $83.95; 2 years (24 issues), $151.20. Canada/Mexico: 1 year, $107.10; 2 years, $168.53. International: 1 year (12 issues), $157.50; 2 years (24 issues), $281.40. Periodicals postage paid at Trenton, NJ 08650 and additional mailing offices. POSTMASTER: Send address changes to Spectroscopy, P.O. Box 457, Cranbury NJ 08512-0457. PUBLICATIONS MAIL AGREEMENT NO. 40612608, Return Undeliverable Canadian Addresses to: IMEX Global Solutions, P. O. Box 25542, London, ON N6C 6B2, CANADA. Canadian GST number: R-124213133RT001. Printed in the U.S.A.

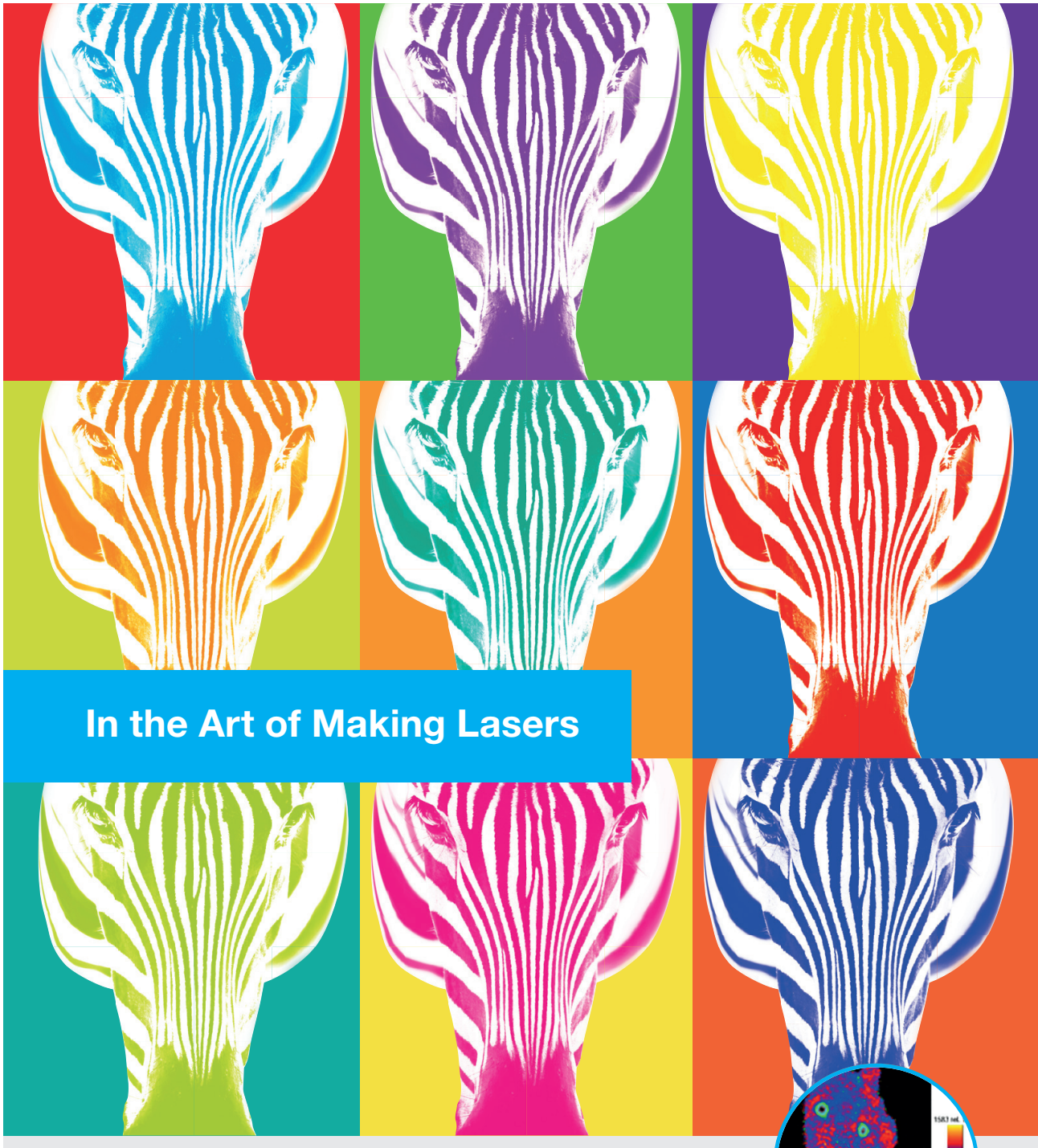

In the Art of Making Lasers

Cobolt. High performance lasers for Raman spectroscopy. All colours, same footprint – easy!

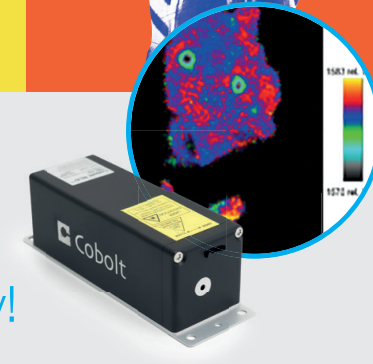

HÜBNER Photonics

hubner-photonics.com

HÜBNER

Note from the CEO

Mike Hennessy, Jr.
President & CEO, MJH Life Sciences®

Welcome to our third annual Resource Issue of *Spectroscopy*. This annual issue includes various special elements. The first is our guide to suppliers and the products and services they offer, including spectrometer systems, optics and related components, sampling and sample handling tools, services, software, and general scientific equipment, process analytical technology (PAT) instrumentation, and more. You'll want to keep this handy.

Next, we present five tutorials that will assist our readers in overcoming challenges with a range of techniques:

- Russ Algar of the University of British Columbia's examines the key steps for Förster resonance energy transfer (FRET) experiments— a versatile part of the fluorescence toolbox.
- Confused about self-absorption in laser-induced breakdown spectroscopy (LIBS)? You are not alone. Vince Palleschi of the National Research Council of Italy explains how to avoid it—or how to harness it to your advantage.
- Daniel Kutscher and Simon Nelms of Thermo Fisher Scientific offer guidance for the initial configuration and ongoing maintenance of sample introduction systems of inductively coupled plasma–optical emission spectrometry (ICP-OES) and ICP–mass spectrometry (ICP-MS) instruments.
- Key steps for controlling contamination and achieving low detection limits when using ICP-MS are provided by Ed McCurdy and Burt Woods of Agilent Technologies.
- Derek Guenther of Ocean Insight explains how to ensure repeatability in absorbance measurements.

This issue also includes three peer-reviewed articles. In the first, researchers analyze a new near-infrared (NIR) laser crystal, assessing its potential for optics and photonics devices. In the second, the authors used 3D excitation-emission matrix (EEM) fluorescence spectroscopy to track the behavior of radionuclide waste in river water, looking at how these compounds form complexes with natural organic matter. The third paper examines the use of THz–time-domain spectroscopy (THz-TDS) for quantitative analysis of co-crystallized diastereomers.

Finally, we round out the issue with our Vendor Tips and Tricks and Product Profile sections.

We hope this year's edition will be a useful source of information and inspiration to you over the next year.

Happy reading!

Editorial Advisory Board

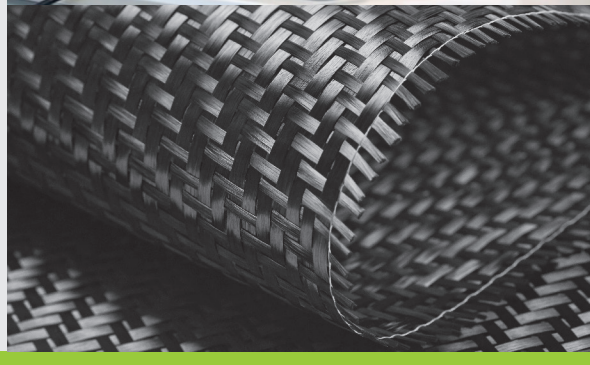

Raman Spectroscopy, Simplified

Raman spectroscopy is powerful, but doesn't have to be expensive or complex. Metrohm's Raman products cover applications from research to routine with flexible instruments, proven software, and support to deliver success.

Scan Here

Find out more
www.metrohm.com/en-us/iRaman

Metrohm

The Infrared Spectra of Polymers, VII: Polymers with Carbonyl (C=O) Bonds

Brian C. Smith

We continue our survey of the infrared (IR) spectra of polymers with a look at the spectra of polymers that contain carbonyl or C=O bonds. Our long-term goal is to examine the spectra of polymers that contain ketone, carboxylic acid, ester, and carbonate linkages. Studying these spectra is vital because these molecules are important economically and are ubiquitous in society.

We begin this installment with a discussion of the unique bonding of the carbonyl functional group and how that impacts their infrared (IR) spectra. We then review the structures and spectra of ketones and examine an example spectrum of a polymer with a ketone linkage in it.

Review of C=O Bonding and Spectroscopy

A carbon–oxygen double bond is referred to as a carbonyl bond. The structure of this bond is seen in Figure 1. As shown in Figure 1, the carbon in this bond is called the "carbonyl carbon."

Carbonyl bonds are highly polar because of the large electronegativity difference between carbon and oxygen. As a result, the carbonyl carbon has a large partial positive charge, and the oxygen has a large partial negative charge as denoted by the small Greek letter deltas in Figure 1. Recall that when in a chemical bond there are two charges separated by a distance, it forms what is called a dipole moment (1). Additionally, remember that the change in a dipole moment with respect to bond length, dμ/dx, during a molecular vibration is one of the things that determines the IR intensity (1).

Because the carbonyl group has a large dipole moment, when this group stretches and contracts, the value of dμ/dx is large, which results in an intense peak. The C=O stretching vibration is illustrated in Figure 2.

Carbonyl stretching peaks generally fall between 1900 and 1600 cm^{-1} (assume all peak positions hereafter are in wavenumber units), a relatively unique part of the IR spectrum. This area is sometimes referred to as the "carbonyl stretching region." The carbonyl stretching peak is perhaps the perfect example of a *group wavenumber*, which is a peak that shows up intensely in a unique and relatively narrow wavenumber range. This makes C=O stretches one of the easiest IR peaks to spot and assign. Therefore, an IR spectrometer is, in some respects, the perfect carbonyl detector.

Carbonyl bonds can be divided into two classes depending on what type of carbons are attached to the carbonyl carbon. A saturated carbonyl group has two saturated carbons attached to the carbonyl carbon. An aromatic carbonyl group has one or more aromatic carbons attached to the carbonyl carbon. Examples of an aromatic carbonyl group and its bonding is seen in Figure 3 (please pardon the diagram; it is hard to depict three-dimensional [3D] molecular orbitals in two dimensions).

Recall that when we introduced aromatic rings (2), we showed that some of the electrons in a benzene ring delocalize to form a cloud of electron density called

a pi cloud, and the electrons in this cloud are called pi electrons, which are illustrated in Figure 4.

Aromatic rings, such as benzene, contain p-type orbitals with electron density in them, and these orbitals stick up out of the plane of the molecule as illustrated at the top of Figure 4. The carbonyl group also contains a p-type orbital that points through space towards the orbitals on the aromatic ring, which is illustrated in Figure 3. The second carbon-oxygen bond in a carbonyl group has significant electron density perpendicular to the C=O bond axis forming what is also called a pi bond with pi electrons in it.

On the left side of Figure 3, you can see that the pi bond of the C=O group points in space towards the pi electron cloud of the benzene ring. Because of the proximity of these two pi electron clouds, there is some orbital overlap and, as a result, some of the electron density is siphoned off from the C=O bond into the benzene ring, which is illustrated by the dashed lines to the right in Figure 3. This phenomenon, whereby electrons are pulled from part of a molecule, is called *conjugation*. Conjugation weakens the C=O bond, lowers its force constant, and lowers its peak position compared to if there were only saturated carbons attached to the benzene ring.

Figure 5 shows the spectrum of acetone. Acetone has two saturated carbons bonded to the carbonyl carbon; hence, no conjugation takes place. Note that its C=O stretching peak falls at 1716 and is labeled A. It is also important to note how intense this peak is; carbonyl stretches are some of the strongest IR features you will ever see.

Figure 6 shows the spectrum of acetophenone, which has an aromatic ring bonded to the carbonyl carbon; therefore, its C=O bond is conjugated. As a result, its C=O stretch is at 1686, 30 cm^{-1} lower than in acetone.

In general, we find that conjugated C=O groups have carbonyl stretching vibrations about 20–30 cm^{-1} lower than non-conjugated carbonyl groups. That is why going forward we will be quoting two peak position ranges for each carbonyl-containing functional group we study, one for the saturated

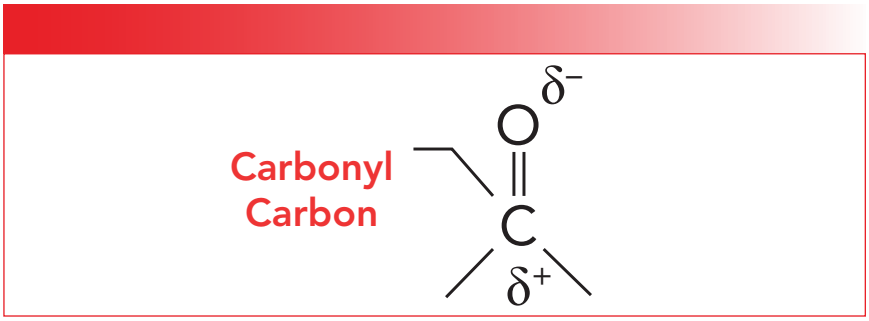

FIGURE 1: The chemical structure and charge distribution in a carbonyl bond.

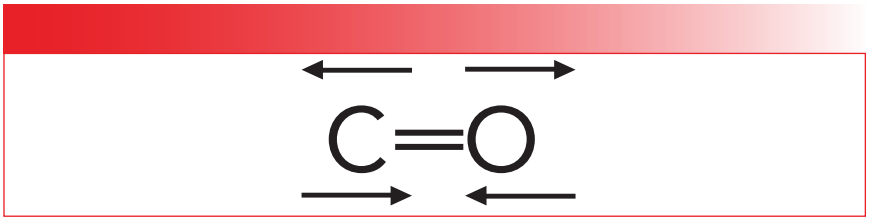

FIGURE 2: The stretching vibration of a carbonyl bond.

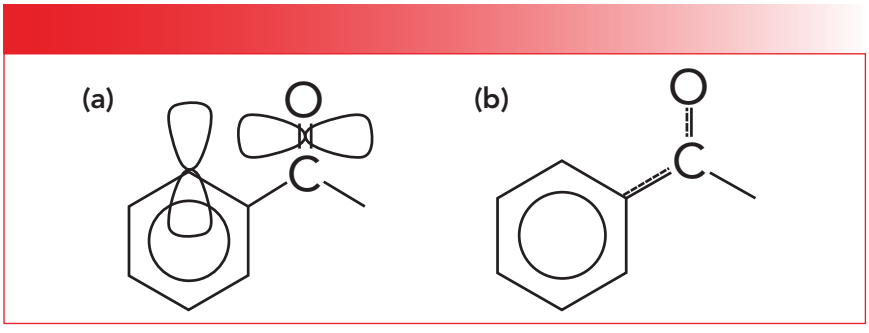

FIGURE 3: (a) The p-type orbitals and **(b)** conjugation within an aromatic carbonyl group.

TABLE I: The IR group wavenumbers for ketones

Vibration	Wavenumber Range
Saturated C=O stretch	1715±10
Aromatic C=O stretch	1700–1640
Saturated C-C-C stretch	1230–1100
Aromatic C-C-C stretch	1300–1230

version of the functional group and one for the aromatic version.

The IR Spectroscopy of Ketones

Perhaps one of the most common chemical structures to contain a carbonyl group are ketone molecules. Ketones consist of a C=O with two carbons attached, one to the left and one to the right as illustrated in Figure 7.

Note that the carbons attached to the carbonyl carbon are denoted "alpha carbons." If both alpha carbons are saturated, we speak of saturated ketones, and if one or both alpha carbons are saturated, it is called an aromatic ketone.

A common example of a ketone-containing molecule is acetone (dimethyl ketone), whose IR spectrum we have already seen in Figure 5. The carbonyl stretch of acetone falls at 1716, and it is labeled A in Figure 5. In general, for saturated ketones, this peak appears at 1715±10. Note how large this

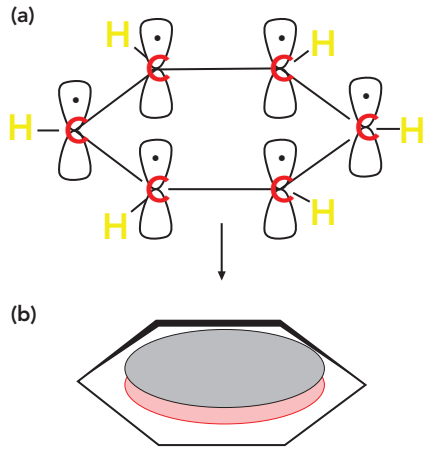

FIGURE 4: (a) The p orbitals on each of the six carbon atoms in benzene that each contribute an electron to the ring. (b) The collection of delocalized P orbital electrons that form a pi cloud of pi electron density above and below the plane of the benzene ring.

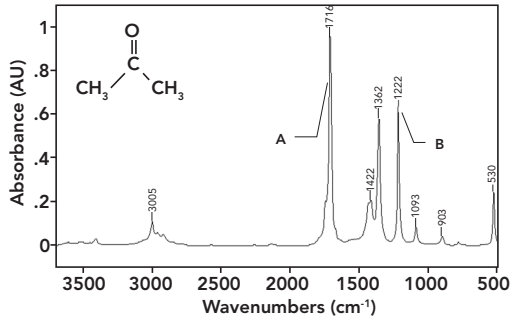

A	1716	C=O Stretch
B	1222	C-C-C Stretch

FIGURE 5: The IR spectrum of acetone, C_3H_6O.

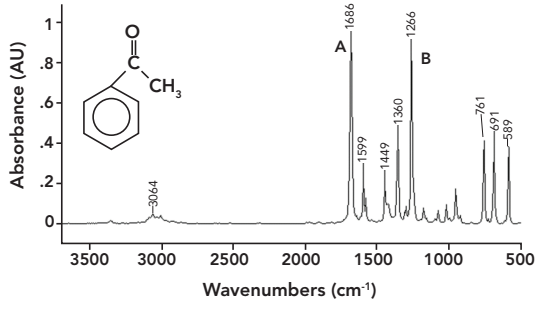

A	1686	C=O Stretch
B	1266	C-C-C Stretch

FIGURE 6: The IR spectrum of acetophenone (phenyl methyl ketone), C_6H_8O.

peak is and how it is easily the biggest in the spectrum.

It is tempting to assume that the carbonyl stretching peak for ketones uniquely identifies them, but this is not the case. Polymers containing saturated esters, aldehydes, and carboxylic acids among others have their C=O stretching peaks at approximately 1715 as we will see in future columns. Thus, the C=O stretching peak is diagnostic for carbonyl groups but not for anything else. We are dependent upon other peaks in IR spectra besides the C=O stretch to distinguish the different types of carbonyl-containing functional groups from each other.

For ketones, the peak that can help distinguish them from other functional groups is the C-C-C stretching vibration, which is illustrated in Figure 8.

Note that this vibration involves the two alpha carbons stretching asymmetrically about the carbonyl carbon. This vibration gives rise to an intense peak between 1230 and 1100 for saturated ketones. This peak appears in the spectrum of acetone in Figure 5 at 1222 and is labeled B. Note that it is the second largest peak in the spectrum.

Normally, a C-C stretching vibration peak is small because the electronegativity difference between the carbon atoms is often negligible, giving non-polar bonds and small values of dμ/dx (1). However, the carbonyl carbon in the C=O bond has a large positive partial charge on it as seen in Figure 1. This large positive partial charge polarizes the bonds to the two alpha carbons, and when these C-C bonds stretch and the dμ/dx is large, it results in a large ketone C-C-C stretching peak seen in Figure 5.

Acetophenone is an example of an aromatic ketone, and its spectrum is seen in Figure 6. Although there is an aromatic and a saturated carbon attached to the carbonyl carbon in acetophenone, it is considered an aromatic ketone, which is because it only takes the presence of a single aromatic substituent to engage in conjugation and lower the carbonyl stretching peak position. Note in Figure 6 that the C-C-C stretch is at 1266 and is labeled B. The general range for the C-C-C stretch of aromatic ketones is 1300 to 1230.

Table I summarizes the group wavenumbers for ketones.

Note in Table I that both the C=O stretch and C-C-C stretching peak positions are sensitive as to whether the ketone is saturated or aromatic. The C=O stretch of saturated ketones falls above 1705, whereas for aromatic ketones it falls below 1700. Additionally, the C-C-C stretch of saturated ketones falls below 1230, whereas for aromatic ketones it falls above 1230. Thus, either one of these peaks can be used to distinguish saturated from aromatic ketones.

Polyetheretherketone (PEEK)

The fact that the name of this polymer contains the word ether twice just might make you think that it contains ether linkages only, but it also has a ketone in it per the last part of its name.

Polyetheretherketone (PEEK) is a copolymer made from monomers that form ketone and ether linkages upon the formation of the polymer. We discussed the ether linkages of PEEK in the last column (4); here, we focus on its ketone functional group. The structure and spectrum of PEEK are shown in Figure 9.

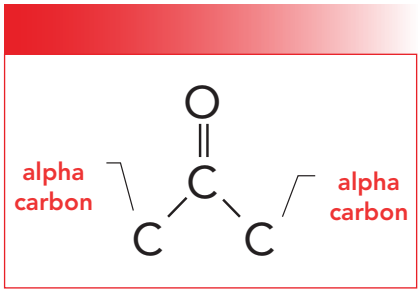

FIGURE 7: The structural framework of the ketone functional group.

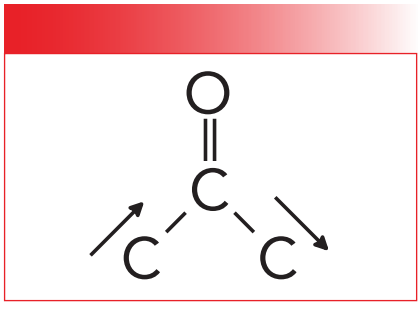

FIGURE 8: The C-C-C stretching vibration of ketones.

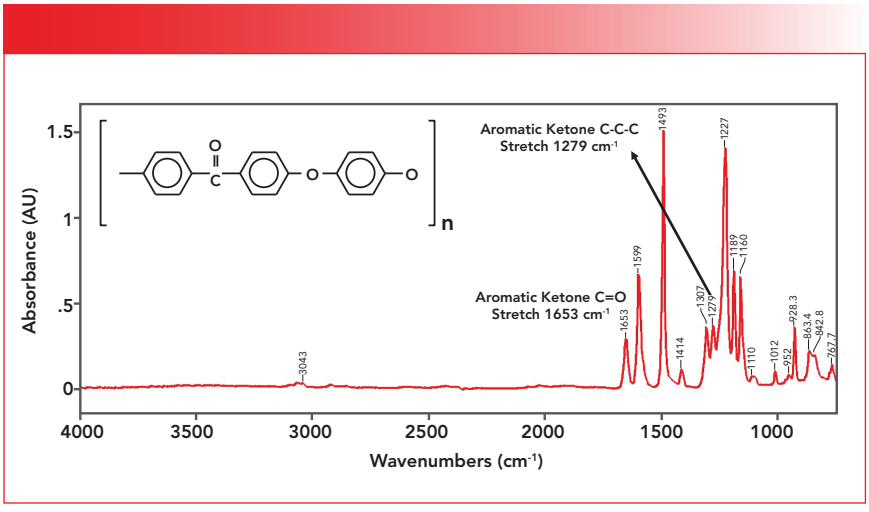

FIGURE 9: The IR spectrum of polyetheretherketone (PEEK).

The spectrum of PEEK is a little strange in that the ketone peaks are not the biggest in the spectrum. This honor goes to the C-O stretching peak of the aromatic ether linkages and ring modes from the benzene rings present. These peaks are so large because the repeat unit contains two ether linkages and three benzene rings respectively.

The C=O stretch of PEEK is at 1653, agreeing with the position of aromatic ketone C=O stretches stated in Table I. The C-C-C stretch of PEEK is seen at 1279, which also agrees with Table I. PEEK is one of the few polymers that contains a ketone linkage.

Conclusions

In this introduction to the spectra of carbonyl containing polymers, we reviewed the structure and bonding of the C=O bond. We found that the C=O bond has a large dipole moment and gives strong carbonyl stretching peaks in the 1900 to 1600 range. We also saw how conjugation can alter the force constant of the C=O bond, lowering its stretching peak position.

We then reviewed the spectra of saturated and aromatic ketones, and discussed how the diagnostic peak pattern for ketones is a C=O stretch approximately 1700 and a C-C-C stretch around 1200. Both of these peaks are sensitive as to whether the ketone is saturated or aromatic, so either can be used to determine what type of ketone is present in a sample. We then analyzed the spectrum of PEEK, a ketone-containing polymer.

References

(1) B.C. Smith, *Spectroscopy* **30**(1), 16–25 (2015).

(2) B.C. Smith, *Spectroscopy* **31**(3), 34–37 (2016).

(3) B.C. Smith, *Spectroscopy* **32**(9), 31–36 (2017).

(4) B.C. Smith, *Spectroscopy* **37**(5), 15–19,27 (2022).

Brian C. Smith, PhD, is the founder and CEO of Big Sur Scientific, a maker of portable mid-infrared cannabis analyzers. He has over 30 years experience as an industrial infrared spectroscopist, has published numerous peer-reviewed papers, and has written three books on spectroscopy. As a trainer, he has helped thousands of people around the world improve their infrared analyses. In addition to writing for *Spectroscopy,* Dr. Smith writes a regular column for its sister publication *Cannabis Science and Technology* and sits on its editorial board. He earned his PhD in physical chemistry from Dartmouth College. He can be reached at: SpectroscopyEdit@MMHGroup.com ●

FACSS PRESENTS

SCIX2022

The Great SCIentific eXchange

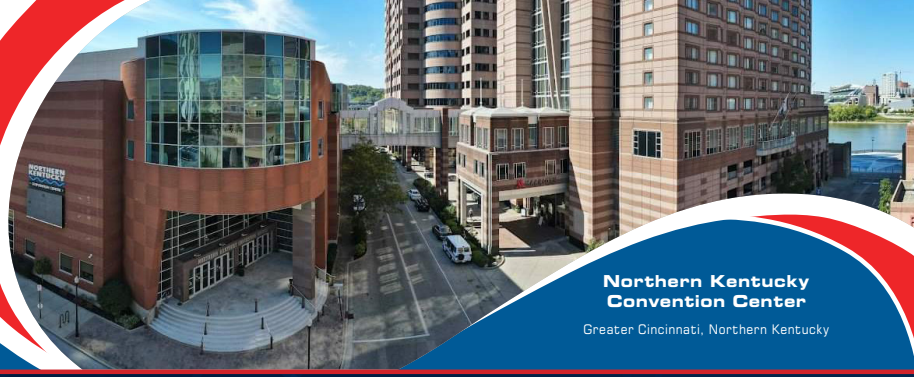

October 2–7, 2022

Northern Kentucky Convention Center

Greater Cincinnati, Northern Kentucky

SciX Sneak Preview

KEYNOTE SPEAKER

"The Future of Space Exploration: Earth-based, Deep Space-based, Robotic and Human"

Amanda Hendrix
Senior Scientist, Planetary Science Institute
Boulder, Colorado, USA

PLENARY LECTURES BY ESTEEMED SPEAKERS

View all Award Winners at **scixconference.org/awards**

- Sensitive and Selective Bioanalysis using SERS and SESORS; *Karen Faulds*
- Advances in Interfacial and Voltage-gated Two-dimensional Infrared Spectroscopy; *Martin Zanni*
- Pushing the Frontiers of Stimulated Raman Imaging for Complex Subcellular Bioanalysis; *Lu Wei*
- Raman Spectroscopy and Machine Learning for Medical Diagnostics and Forensic Purposes; *Igor Lednev*
- Stimulated Raman Scattering Imaging: From Label-free to Metabolic to Super-multiplex and to Single-molecule Imaging; *Wei Min*
- Multifaceted Laser Induced Plasma: Spectroscopy and Beyond; *Igor Gornushkin*
- Process Analytical Utility of Raman Microspectroscopy for Cell Therapy Manufacturing Validation; *James Piret*
- Mass Spectrometry Au Naturel: A Tool for Structural Biology; *Joseph Loo*
- Nonlinear Electrophoresis of Colloidal Particles; *Aditya Khair*

www.SciXconference.org

SESSIONS BY SECTION

View the complete daily scientific program at **scixconference.org/program**

AES Electrophoresis
- Extraterrestrial Electrokinetics
- Electrokinetic Fundamentals
- Microfluid Electrokinetic Devices
- Microfluidic Bioanalysis 1 & 2
- AES Lifetime Achievement Award: Adrienne Minerick
- Emerging Leaders Session

Art and Archaeology
- Student Research in Archaeological Chemistry

Atomic
- LA-ICP-MS
- Single Cell & NP ICP-MS Part I & II
- Nuclear
- Traditional and Atmospheric Glow Discharge Sources
- Food
- ICP-MS Applications

Biomedical
- New Stream of Intelligent Measurements
- Biophotonics Technologies: Fighting Infections
- Translation of Multimodal Imaging into Clinical Routine
- Machine and Deep Learning for Biomedical Diagnostics
- Nanotheranostics
- Optical Technologies for Disease Screening/Diagnostics

Chemometrics
- New Stream of Intelligent Measurements/Data Science
- Advances in Chemometrics
- Chemometrics Something Borrowed, Something New
- Chemometrics and Food Safety
- Chemometric Opportunities in the Forensic Sciences
- Pathways to Autonomous Chemometrics

Contemporary Topics/Early Career
- Entrepreneurship in the Scientific Community
- Strategies for Finding Balance
- Early Career Spectroscopists, Part 1 & 2

Forensics
- Nuclear Forensics
- Food Forensics
- Forensic Analysis in the Lab and at the Crime Scene
- Pharmaceutical Forensics

IR/Nano
- NanoIR in Material Science
- NanoIR in Life Science and Biology
- Nanoscale Spectroscopy: Advances in Instrumentation
- Mid-IR Lasers and Detectors as Enabling Technology
- Quantum Cascade Lasers for Chemical Sensing
- Photothermal Session I & II
- Advances in Vibrational Spectroscopy for PAT
- AI and Self-Optimization for Flow Chemistry
- Nurturing Talent in Vibrational Spectroscopy

LIBS
- Fundamentals
- Advanced Approaches I & II
- Molecular
- Chemometrics
- Space Applications
- Environmental and Cultural Applications
- Medical Applications
- Geological Applications
- Instrumentation

Mass Spectrometry
- Mass Spectrometry and Space
- Advances in Novel Mass-Spectral Imaging
- Elemental and Isotopic Tracers
- On-site Chemical Analysis

Process Analytical Technology
- PAT in BioPharma and Pharma
- Advances in On-Line Process Analysis
- In Situ Spectroscopy for Industrial R&D
- PAT Coblentz: Machine Learning
- Process Analytical in Petroleum and Refinery Industries

Pharmaceutical
- Characterization of Therapeutic Modalities
- Pharmaceutical Forensics
- SERS for Drug Discovery
- SERS for Diagnostics and BioPharma Manufacturing
- Industrial Applications of Vibrational Spectroscopy
- Advanced Spectroscopic Techniques in PAT
- Analysis of Nanomaterials for Health
- Bioprocess Materials and Methods
- Small Molecule Profiling

Raman
- Emerging Raman
- SERS Parts 1-3
- IRDG Raman
- Biomedical Raman (CLIRSPEC)
- Transmission and Advanced Raman Sampling Methods
- Raman Imaging and Microscopy
- Spatially Offset Raman Spectroscopy
- SAS: Spectroscopy in Space
- Raman Spectroscopy for Food Security
- Raman Spectroscopy for Security and Forensics
- Raman Spectroscopy in Regenerative Medicine and 3Rs

Special Sessions
- Coherent Multidimensional Spectroscopy Symposium
- Celebrating Peter Griffiths' 80th Birthday
- FACSS 2021 Mann Symposium Honoring Roy Goodacre
- Regional Industrial Research
- Regional Academic Research
- Molecular Microspectroscopy Laboratory (MML)
- Spectrochimica Acta B - Award Session
- Analytical Imaging - NSF Chemical Measurements
- Remembering Stanley Crouch

Spectroscopical Society of Japan
- Near-IR; Spectral Analysis, Imaging
- Near-IR; Application to Biological and Materials Sciences
- Vacuum, Far, and Deep-Ultraviolet Spectroscopy I & II

Surface Plasmon Resonance
- Emerging Plasmonic Materials and Architectures
- Optical/Chiral Properties of Plasmonic Nanoparticles
- Biosensing with Plasmonics
- Enhancing Chemical Processes with Plasmonics
- Early Career Researchers in Plasmonics

The program is subject to change. Some session titles have been abbreviated for printing purposes.

www.SciXconference.org

PEER-REVIEWED RESEARCH
Spectroscopy papers have undergone a double-blind peer review process and are available on our open-access website.

Growth and Temperature-Dependent Spectral Properties of Yb^{3+}, Tm^{3+} Co-Doped $NaY(MoO_4)_2$ Crystal

Xi Wang, Zongyue Chen, Jianyu Zhang, Shangke Pan, and Jianguo Pan

The $NaY(MoO_4)_2$:Yb^{3+}/Tm^{3+} single crystal was grown by the vertical Bridgman method using spontaneous crystallization. After annealing at 850 °C for 24 h in a muffle furnace under an air atmosphere, the obtained light black crystal became transparent and optically clear. Powder X-ray diffraction (PXRD) confirmed that the as-grown crystal had the structure of scheelite. The segregation coefficients of Tm^{3+} and Yb^{3+} were 0.589 and 0.588, respectively. Under 980 nm excitation, the temperature dependence of the emission intensity of the crystal in the temperature range of 298–473 K was measured. The results show that, because of the thermal quenching effect, the emission intensity decreases as the temperature rises. The possible energy transfer modes between Yb^{3+} and Tm^{3+} ions were analyzed. The emission cross section was calculated to be 1.97×10^{-20} cm^2 by the Füchtabauer-Ladeburg formula, and the fluorescence lifetime was fitted to be 166.67 µs.

In recent years, with the rapid development of near-infrared (NIR) optical amplifiers and mid-IR fiber lasers, new rare earth-doped solid IR luminescent materials have attracted great attention (1–5). Among rare earth ions, the energy level transitions of $^3H_4$–$^3F_4$ and $^3F_4$–$^3H_6$ of Tm^{3+} can generate fluorescence emission in the bands of 1.47–1.8 µm (6). The glass fiber with Tm^{3+} as the luminescence center is a type of material suitable for the third window fiber amplifier, which has a strong energy cross-relaxation effect between Tm^{3+} ions ($^3H_6$,$^3H_4$→$^3F_4$,$^3F_4$) (7). Tm^{3+} stimulated radiation belongs to quasi-three-level, and the emission wavelength is in the wavelength range of 1.47–1.8 µm (8–10). However, because of the concentration quenching effect, the symmetric energy level of the Tm^{3+} ion limits the effective emission of the laser (11,12). The effective way to overcome this shortcoming is to combine with the Yb^{3+} ion (13–17). Yb^{3+} is the most promising ion that can be used in all solid-state laser sources in the NIR spectrum around 1030 nm. Compared with other ions, Yb^{3+} ion is also a good sensitizer, which only has two very simple $^2F_{7/2}$ and $^2F_{5/2}$ energy levels and can absorb light near 980 nm (18,19).

In many substrates, such as glass and single crystal, the combination of the Yb^{3+} ion and the Tm^{3+} ion is considered to be an effective composition for laser crystals**.** The doped crystal needs the radius and electronegativity of the cation of the host crystal and the activated ion to be as close as possible. Moreover, a variety of solid-state lasers have been constructed for eye-safe applications using Yb^{3+} and Tm^{3+} doped YAG, $YLiF_4$ (20–22). With stable chemical properties, good luminescence properties, high thermal stability, and low phonon energy, sodium yttrium molybdate ($NaY[MoO_4]_2$) is considered to be a good luminescent matrix. Considering the above reasons, we studied the Yb^{3+} and Tm^{3+} ion co-doped with $NaY(MoO_4)_2$. The Yb^{3+} and Tm^{3+} ion can replace the Y^{3+} ion easily, so the Yb^{3+} and Tm^{3+} co-doped system could be introduced in the $NaY(MoO_4)_2$ crystal (23).

The vertical Bridgman method using spontaneous crystallization is an easily feasible way to obtain crystal samples for measurement (24–26). Here, we used the solid phase synthesis method to synthesize the precursor and the vertical Bridgman method with spontaneous crystallization to grow the $NaY(MoO_4)_2$:Re (Re=Yb/Tm) crystal.

The thermal annealing, X-ray powder diffraction analysis, absorption spectrum, and temperature dependence emission spectra of the $NaY(MoO_4)_2$:Yb^{3+}/Tm^{3+} crystal is reported in detail in this paper.

Materials and Methods

Materials

The raw materials for crystal growth of $NaY(MoO_4)_2$:Yb^{3+}/Tm^{3+} were molybdenum oxide (MoO_3, 99.99%), sodium carbonate (Na_2CO_3, 99.99%), ytterbium oxide (Yb_2O_3, 99.99%), thulium oxide (Tm_2O_3, 99.99%), and yttrium oxide (Y_2O_3, 99.99%).

Crystal Growth

The $NaY(MoO_4)_2$:Yb^{3+}/Tm^{3+} precursor for crystal growth was prepared by solid-state reaction according to the following stoichiometric relation:

$$Na_2CO_3 + 4MoO_3 + Y_2O_3 + xYb_2O_3 + yTm_2O_3 \rightarrow 2NaY_{(1-x-y)}Yb_xTm_y(MoO_4)_2 + CO_2\uparrow \quad [1]$$

where x and y are the doping concentration. To compensate for the volatilization of MoO_3 during solid phase reaction and crystal growth, an additional 0.2at% MoO_3 was added. The raw materials were mixed and grounded in a mortar for 2 h. The precursor was put into an alumina crucible and calcined in a muffle furnace at 950 °C for 24 h. The process was repeated, and the samples were held at 1000 °C for 48 h to make an adequate solid-state reaction. The synthesized $NaY(MoO_4)_2$:Yb^{3+}/Tm^{3+} polycrystalline powder was filled into a platinum crucible. The platinum crucible was then placed in a Bridgman growth furnace built in-house for crystal growth. The schematic of the Bridgman growth furnace used in this study was presented in Figure 1a. The obvious advantage of the vertical Bridgman method is that multiple crystals with a smaller size can be grown simultaneously, which helps save time, energy, and raw materials. In this experiment, the position of the four platinum crucibles in the furnace was shown in Figure 1b. The melting point of the $NaY(MoO_4)_2$ crystal was 1120 °C (27), and the controlled temperature of the furnace was 1250 °C. The lowering speed of the crucibles was fixed at 0.35 mm/h during the crystal process.

Characterization

The structure of the $NaY(MoO_4)_2$:Yb^{3+}/Tm^{3+} crystal was confirmed through powder X-ray diffraction (PXRD), using a diffractometer of Bruker D8 with Cu Kα radiation (λ=1.54056 Å) at room temperature. The measurement was carried out with the scanning step of 0.02°, the scanning scope was from 10° to 80°, the high voltage was 40 kV, and the current was 40 mA. A scanning electron microscope (SEM) with Helios G4 CX model and energy

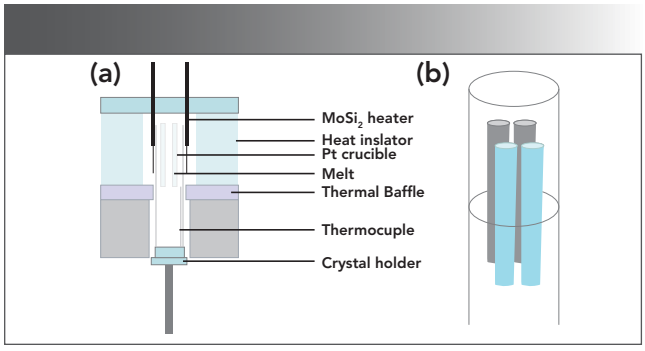

FIGURE 1: (a) Schematic of the Bridgman growth furnace, and (b) layout of platinum crucibles in the furnace.

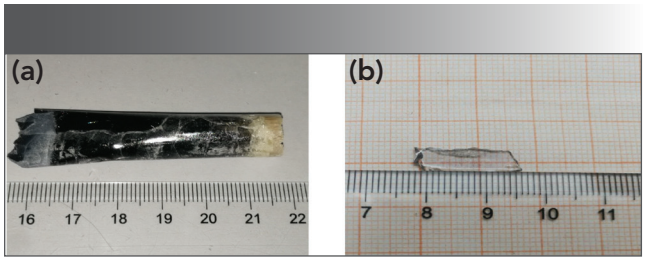

FIGURE 2: Photographs of (a) $NaY(MoO_4)_2$:Yb^{3+}/Tm^{3+} crystal, and (b) annealed $NaY(MoO_4)_2$:Yb^{3+}/Tm^{3+} crystal sample with the size of 15×5×1 mm^3.

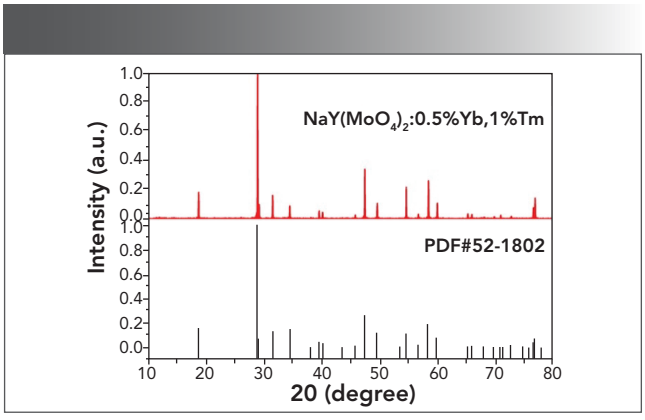

FIGURE 3: The PXRD patterns of $NaY(MoO_4)_2:Yb^{3+}/Tm^{3+}$ crystal.

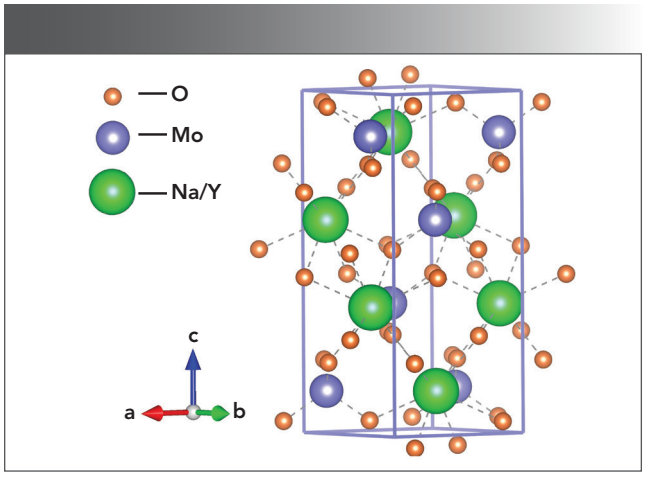

FIGURE 4: Schematic cell structure of tetragonal $NaY(MoO_4)_2:Yb^{3+}/Tm^{3+}$ single crystal.

TABLE I: EDS result of as-grown $NaY(MoO_4)_2:Yb^{3+}/Tm^{3+}$ crystal

Element	O	Mo	Y	Na	Tm	Yb
Atomic (%)	67.49	16.44	9.23	6.78	0.04	0.02

spectrum model called the Edax Apollo X was used to detect the content of the elements in the single crystal. The absorption spectrum in the range of 500–2000 nm was measured by a PerkinElmer UV-visible-NIR (UV-vis-NIR) spectrometer photometer (Lambda-950) with the resolution of 1 nm at room temperature. Under the excitation of 980 nm LD laser, the temperature-dependent emission spectra in the range of 1000–1600 nm were recorded with the Edinburgh FLS920 fluorescence spectrometer, in which the temperature of 273 to 473 K was controlled by Oxford Instruments liquid nitrogen with an isothermal titration calorimetry (ITC) temperature controller and software. The luminescence decay curve was measured by the FL 3–111 fluorescence spectrometer using a gate of 5 µs.

Results and Discussion

Crystal Growth and Powder X-ray Diffraction Analysis

The vertical Bridgman method is a very effective method to obtain the $NaY(MoO_4)_2:Yb^{3+}/Tm^{3+}$ crystal. First, the $NaY(MoO_4)_2:Yb^{3+}/Tm^{3+}$ crystal crystallized at the bottom of the crucible, so the shape of the crucible affected the spontaneous crystallization of the crystal. The crystal shape obtained by the vertical Bridgman method was similar to that of a crucible. To obtain the single crystal, the bottom of the platinum crucible was squeezed with an angle of approximately 7°, because the spontaneous crystallization could not eliminate the grain boundaries at the large shoulder angle and diameter.

The as-grown crystal showed two colors: light black from the middle to the bottom, and yellow at the top, in which the yellow at the top is polycrystalline, which is shown in Figure 2a. The reason for the yellow color at the top could be the role of transition metals in the raw materials (28). The light black color should be caused by the oxygen vacancies, which were formed by the growth of the crystal in a closed environment (5,29). This process can be explained by the following equation 2:

$$O_O^X \rightarrow V_{\ddot{O}} + \tfrac{1}{2}O_2 + 2e \qquad [2]$$

After annealing at 850 °C for 24 h in a muffle furnace under air atmosphere, the obtained light black crystal showed uniform colorlessness and transparency. The reason was that oxygen diffused into the lattice, filling and occupying the oxygen vacancies. The mechanism is shown as the following equation 3:

$$V_{\ddot{O}} + \tfrac{1}{2}O_2 \rightarrow O_O^X + 2h \qquad [3]$$

By cutting and polishing, an optical transparent sheet as shown in Figure 2b was obtained, which was used for testing and analysis.

Figure 3 shows the PXRD pattern of $NaY(MoO_4)_2:Yb^{3+}/Tm^{3+}$ powder at room temperature with the $NaY(MoO_4)_2$ standard card (PDF#82-2369) as a reference. All diffraction peaks match well with the $NaY(MoO_4)_2$ standard cards, and no additional diffraction peaks corresponding to any impurities were observed. Figure 4 shows that the crystal belonged to the tetragonal scheelite ($CaWO_4$) structure, and the phase structure of the $NaY(MoO_4)_2$ crystal had not changed by doping other rare earth ions. The $NaY(MoO_4)_2:Yb^{3+}/Tm^{3+}$ single crystal was a molybdate crystal with scheelite structure, belonging to the tetragonal system, with a $I4_{1/a}$ space group and two molecules per unit cell. In this lattice, MoO_4^{2-} tetrahedral ion groups replaced the positions of the WO_4^{2-} tetrahedral ion groups. Na^+ and Y^{3+} ions randomly occupied the crystal lattice of Ca^{2+}, and the doping of the Yb^{3+} and Tm^{3+} ions did not affect the crystal structure (30–32).

BRUKER

IR SPECTROSCOPY

We Know Spectroscopy

Providing the complete range of IR solutions

Bruker's selection of nanoscale, near, mid, far-infrared and Raman spectrometers is unrivalled in the industry. Our portfolio includes compact, portable, routine as well as powerful research spectrometers. Our solutions cover the entire spectral range from near-infrared, mid-infrared to far-infrared applications, across scales from macro to nano.
Our most innovative products include:

- FTIR: **ALPHA II** the extremely compact FT-IR spectrometer used for chemical analysis, quality control, verification of raw materials www.bruker.com/ALPHA
- NIR: **TANGO** offers efficient, cost effective analysis for material identification and quantification in a wide variety of applications www.bruker.com/TANGO
- Nanoscale IR: **IconIR** delivers the most advanced photothermal IR spectro-microscopy with nanometer resolution with Tapping AFM-IR www.bruker.com/ICONIR

For more information please visit www.bruker.com

Innovation with Integrity

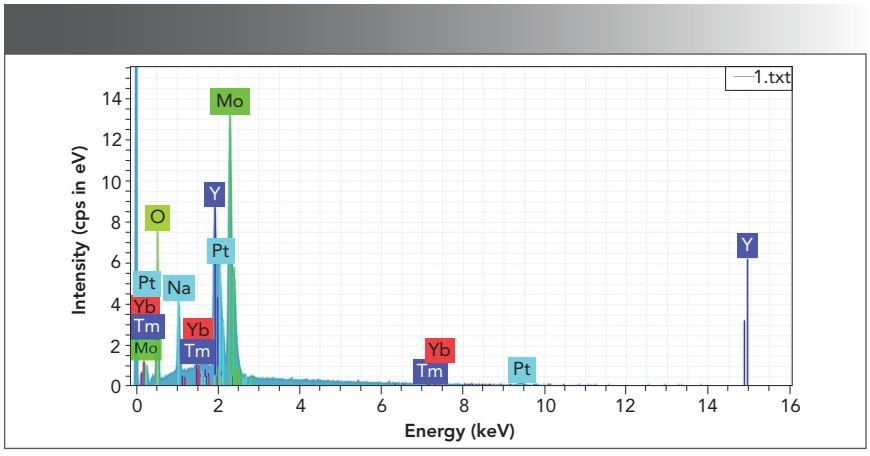

FIGURE 5: EDS analysis of as-grown $NaY(MoO_4)_2$:Yb^{3+}/Tm^{3+} crystal

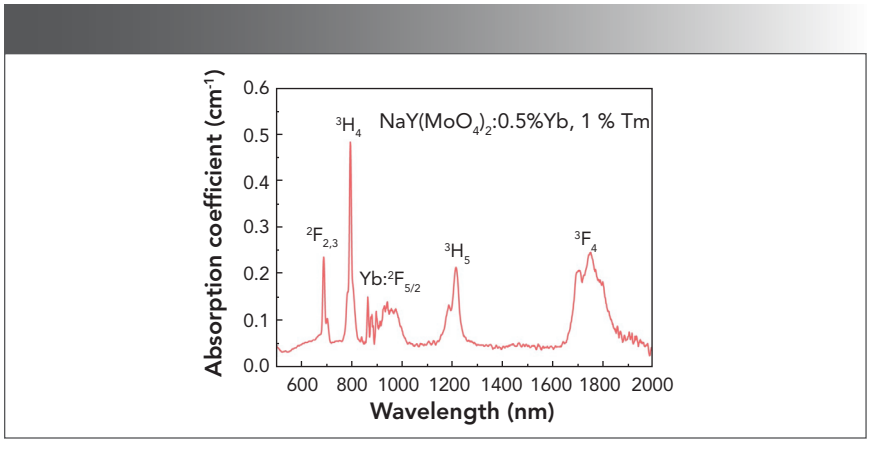

FIGURE 6: The absorption spectrum of $NaY(MoO_4)_2$ crystal co-doped by Yb^{3+} and Tm^{3+} ions.

TABLE II: Concentration and segregation coefficients of Tm^{3+} and Yb^{3+} ions in $NaY(MoO_4)_2$:Yb^{3+}/Tm^{3+} crystal

Ion	C', at. -%	C_0, at. -%	K
Tm^{3+}	0. 589	1.0	0. 589
Yb^{3+}	0. 294	0. 5	0. 588

Segregation Coefficient

Figure 5 shows the energy-dispersive spectroscopy (EDS) diagram of the as-grown $NaY(MoO_4)_2$:Yb^{3+}/Tm^{3+} crystal, which confirmed that the crystal was mainly composed of six elements: oxygen, molybdenum, yttrium, sodium, thulium, and ytterbium. Table I shows the atomic percent of the above six elements.

The segregation coefficients *K* of Tm^{3+} and Yb^{3+} in $NaY(MoO_4)_2$:Yb^{3+}/Tm^{3+} crystal were calculated by equation 4:

$$K = C'/C_0 \quad [4]$$

C' and C_0 are the concentrations of rare earth ions in the crystal and raw material, respectively. Table II shows the results of $NaY(MoO_4)_2$:Yb^{3+}/Tm^{3+}. The separation coefficient represents the extent to which the dopant occupies the host ion lattice, which depends on the difference of the charge, radius, and properties between the doped and host ions. The closer the separation coefficient is to 1, the more uniform the concentration within the grown crystal.

In this paper, the segregation coefficients of Tm^{3+} and Yb^{3+} ions in $NaY(MoO_4)_2$:Yb^{3+}/Tm^{3+} single crystal are 0.589 and 0.588, respectively, indicating that the concentrations of dopants in different parts during the crystal growth are not uniform. It is reasonable to calculate the spectral parameters using the average concentration of doped ions.

Absorption Spectra of $NaY(MoO_4)_2$ Crystal Co-Doped by Yb^{3+} and Tm^{3+} Ions

Figure 6 shows the absorption spectrum of the annealed $NaY(MoO_4)_2$:Yb^{3+}/Tm^{3+} crystal sample at room temperature. The spectrum ranging from 500 to 2000 nm consisted of the absorption bands near 692, 798, 1220, and 1753 nm, which were corresponding to the transitions from the ground state $^3H_6$ to the excited states $^2F_{2/3}$, $^3H_4$, $^3H_5$, and $^3F_4$ of Tm^{3+}, and near 866 nm was corresponding to the transitions from the ground state $^2F_{7/2}$ to the excited state $^2F_{5/2}$ of Yb^{3+}.

It can be seen from Figure 6 that the absorption of Yb^{3+} ions forms an absorption band between 856 and 1022 nm, which is because in the $NaY(MoO_4)_2$ crystal, the Stark splitting of the crystal field, $^2F_{5/2}$ and $^2F_{7/2}$ of Yb^{3+}, form the upper and lower two-state clusters, namely the upper-state cluster $^2F_{5/2}$ and the lower-state cluster $^2F_{7/2}$, in which the energy level difference is approximately 10,000 cm^{-1}.

The absorption cross section of rare earth ions is very important for analyzing the performance of solid-state lasers and amplifiers doped with rare earth ions. We can calculate the absorption cross section by the measured optical absorption *OD*(λ) (7):

$$\sigma_{abs}(\lambda) = \frac{2.303\ OD(\lambda)}{L \times N_C} \quad [5]$$

where σ_{abs}(λ) is the absorption cross-section, *OD*(λ) is the optical density, *L* is the thickness of sample and N_c is the density of Tm^{3+} (2.83×10^{21} cm^{-3}) or Yb^{3+}(1.43×10^{21} cm^{-3}). The wavelengths of the observed absorption peaks and

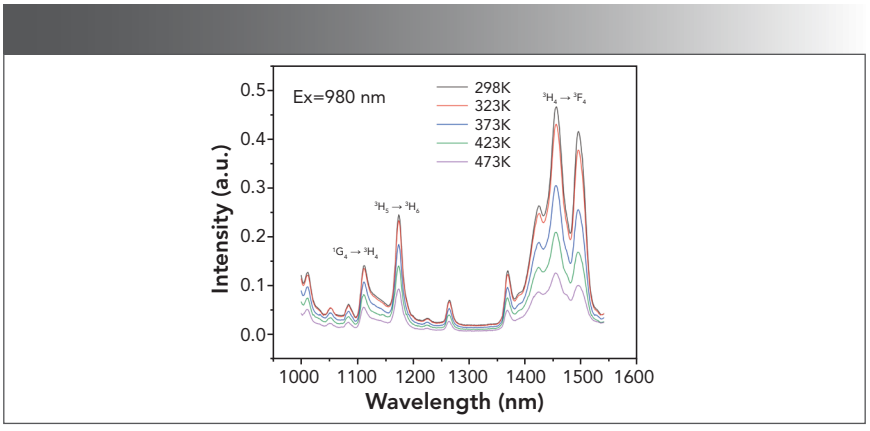

FIGURE 7: Temperature-dependent emission spectra of the annealed $NaY(MoO_4)_2:Yb^{3+}/Tm^{3+}$ crystal.

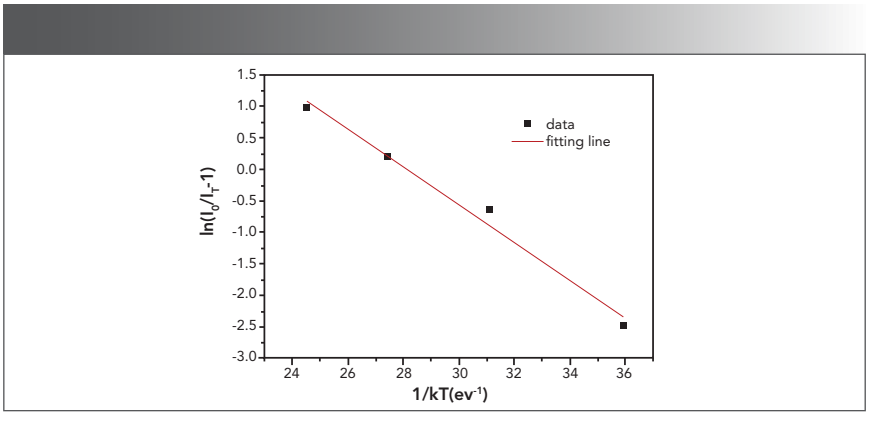

FIGURE 8: A $\ln[I_0/I_T) - 1]$ vs. 1/kT activation energy graph for the thermal quenching of $NaY(MoO_4)_2:Yb^{3+}/Tm^{3+}$ crystal.

TABLE III: Absorption parameters of Yb^{3+} and Tm^{3+} ions in $NaY(MoO_4)_2$ crystal

Transition		λ, nm	σ_{abs}×10^{-20}, cm^2
$Tm^{3+}\ {}^3H_6\rightarrow$	$^2F_{2,3}$	692	4.10
	$^3H_4$	798	9.74
$Yb^{3+}\ {}^2F_{7/2}\rightarrow$	$^3H_5$	1220	4.02
	$^3F_4$	1753	4.73
	$^2F_{5/2}$	941	4.90

the corresponding absorption cross-sections are listed in Table III.

Temperature-Dependent Emission Spectra and Cross-Section

The thermal emission stability of the crystal is an important aspect in the NIR laser field. To investigate the temperature-dependent emission spectra of the $NaY(MoO_4)_2:Yb^{3+}/Tm^{3+}$ crystal at different temperatures, the annealed $NaY(MoO_4)_2:Yb^{3+}/Tm^{3+}$ crystal was excited by a 980 nm LD laser in the range of 298–473 K. The emission intensity of the crystal gradually increased from 473 to 373 K, and sharply increased from 373 K to room temperature, which could be observed from 1000 to 1600 nm in Figure 7.

Under the 980 nm excitation, $NaY(MoO_4)_2:Yb^{3+}/Tm^{3+}$ contains three additional emission bands near 1112, 1174, and 1455 nm, which are corresponding to $^1G_4(Tm^{3+})\rightarrow{}^3H_4(Tm^{3+})$ transition, $^3H_5(Tm^3+)\rightarrow{}^3H_6(Tm^{3+})$, and $^3H_4(Tm^{3+})\rightarrow{}^3F_4(Tm^{3+})$, respectively. As shown from Figure 7, the emission peak intensity at 1455 nm is close to that at 1495 nm, and the intense emission peaks are centered at 1455 nm.

To explain the temperature dependent photoluminescence, activation energy was calculated through the Arrhenius equation 6 (33):

$$I_T = \frac{I_0}{1+c\ exp\left(-\frac{\Delta E}{KT}\right)} \qquad [6]$$

where I_0 is the emission intensity at room temperature; I_T is the emission intensity at measurement temperature; c is a constant; K is the Boltzmann constant (8.617 × 10^{-5} eV/K); and ΔE is the activation energy for thermal quenching. The fitting line of $\ln[I_0/I_T-1]$ versus 1/kT is illustrated in Figure 8. The ΔE of $NaY(MoO^4)^2$ co-doped by Yb^{3+} and Tm^{3+} ions was calculated to be 0.301 eV. Compared to our previous work, where the ΔE of $NaY(MoO_4)_2:Er^{3+}$ co-doped by Tm^{3+} was calculated to be 0.234 eV (10), the thermal emission stability of the $NaY(MoO_4)_2:Yb^{3+}/Tm^{3+}$ crystal increased.

When the temperature rose, the carriers, which were fixed in the traps, were released to the emitting center (Yb^{3+}, Tm^{3+}). Therefore, the electron-phonon interaction was the main one, exciting Yb^{3+}, and the Tm^{3+} luminescence center was activated by the interaction of the phonon, which was obtained by the cross release between the excited state and the ground state. Therefore, as the temperature rose, the emission intensity of the crystal decreased. Therefore, the crystal exhibited a non-radiative transition (27). The emission cross section is an important parameter for evaluating the possibility of laser action. A larger emission cross section means a higher light output. The emission cross section σ_{em} was calculated by the Füchtabauer-Ladeburg (F-L) formula (34):

$$\sigma(\lambda) = \frac{\lambda^5}{8\pi n^2 c}\frac{1}{\tau}\frac{I(\lambda)}{\int \lambda I(\lambda) d\lambda} \quad [7]$$

where τ is the decay time; n is the refractive index, which can be calculated by the following formula: $n^2 = 3.8770 + 62950/(\lambda 2 - 42981)$ (35); λ is the wavelength; $I(\lambda)$ is the relative fluorescence intensities as a function of wavelength; and c is the velocity of light. The peak value of fluorescence cross-sections calculated by equation 7 is 1.97×10^{-20} cm^2 for NaY$(MoO_4)^2$:Yb^{3+}/Tm^{3+} crystal at 1455 nm. The emission cross-section of Yb^{3+} and Tm^{3+} co-doped NaY$(MoO_4)_2$ calculated from equation 7, which is compared with the NaGd$(MoO_4)_2$ crystal, is listed in Table IV.

The electronic configuration is [Xe]4f^{12}, and its ground state spectrum item is $^3H_4$. Furthermore, its spectrum items were ^3H, ^3F, and ^1G; through spin-orbit coupling, each spectrum branch item was formed. Under the excitation of 980 nm, the NaY$(MoO_4)_2$:Yb^{3+}/Tm^{3+} crystal has a strong emission band at 1453 nm, which corresponded to the transition from $^3H_4$ (Tm^{3+}) to $^3F_4$ (Tm^{3+}). It can be seen from Figure 8 that the intensity of the emission peak at 1453 nm was close to the intensity of the emission peak at 1496 nm, so 1453 and 1493 nm in the NaY$(MoO_4)_2$:Yb^{3+}/Tm^{3+} crystal can better overlap to form ultra-wide NIR luminescence.

Energy Transfer and Fluorescence Decay Curves

Tm^{3+} ions formed an absorption band between 1187~1216 nm and 1701~1800 nm under the pump of 980 nm LD. First, the Yb^{3+} ion absorbed a photon through ground state absorption (GSA) to generate the $^2F_{7/2} \rightarrow {}^2F_{5/2}$ transition, and then the excited Yb^{3+} ion transferred its energy to the $^2F_{5/2}$ energy level. Through mass transfer (ET) to Tm^{3+}, the ground state $^3H_6$ level was excited to the $^3H_5$ level through ground state absorption (GSA). The $^3H_5$ and $^3F_4$ energy levels were similar (the difference is approximately 2000 cm^{-1}). Because the difference between the $^3F_2$ and $^3F_4$ energy levels of Tm^{3+} is similar to the $^2F_{5/2}$ energy of Yb^{3+}, the excited state Tm^{3+} at the $^3F_4$ energy level transitions to the $^3F_2$ energy level through excited state absorption (ESA), and $^3F_{2,3}$ then relaxes through multi-phonon relaxation (MR) and returns to the $^3H_4$ level. At the $^3H_4$ excited state energy level, Tm^{3+} can continue to transition to $^1G_4$ energy level through ESA, or it can return to the ground state $^3H_6$ and emit a photon with a wavelength of approximately 795 nm. Tm^{3+} in the excited state $^1G_4$ produces a 692 nm up-conversion

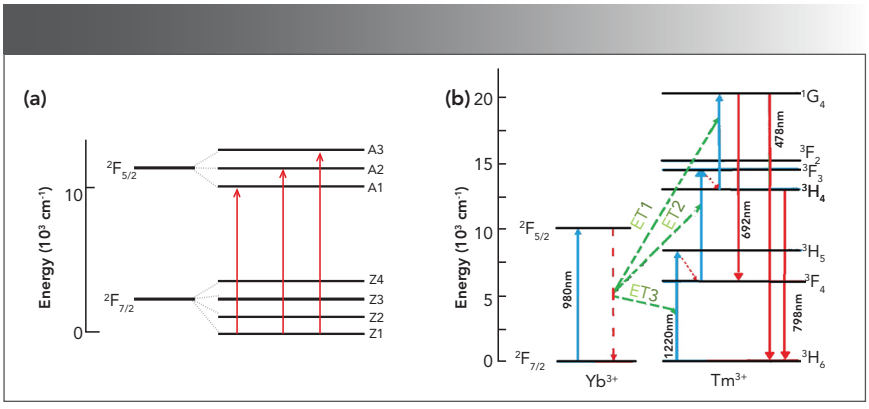

FIGURE 9: (a) Stark level splitting of Yb^{3+} energy level diagram, and (b) possible up-conversion luminescence mechanism of Yb^{3+} and Tm^{3+} co-doped NaY$(MoO_4)_2$ crystal.

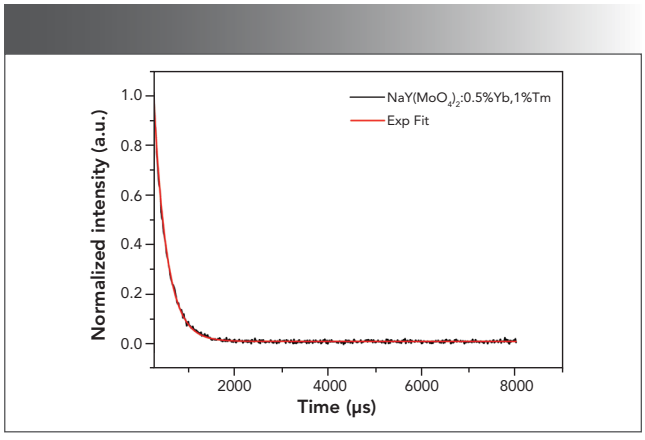

FIGURE 10: The fluorescence decay curves of $NaY(MoO_4)_2$:Yb^{3+}/Tm^{3+} fitted using exponential functions at room temperature.

TABLE IV: Emission parameters of Yb^{3+}/Tm^{3+} co-doped $NaGd(MoO_4)_2$ and $NaY(MoO_4)_2$ crystals

Crystal	λ_{em}, nm	σ_{em}×10^{-20} cm^2	Reference
$NaGd(MoO_4)_2$:Yb^{3+}/Tm^{3+}	1015	1.66	(7)
$NaY(MoO_4)_2$:Yb^{3+}/Tm^{3+}	980	1.97	This work

red light rare earth ion up-conversion luminescence through a radiation transition to $^3F_4$. Figure 8b shows the energy level diagram and possible up-conversion transition process of the Yb^{3+} and Tm^{3+} co-doped sample under 980 nm excitation. According to the energy matching mechanism, the transitions that produce red light $^1G_4 \rightarrow {}^3F_4$ and NIR light $^3H_4 \rightarrow {}^3H_6$ can be explained as follows:

$$Yb^{3+}(^2F_{7/2}) + a\ photon \rightarrow Yb^{3+}(^2F_{5/2}) \quad (GSA) \quad ①$$
$$Yb^{3+}(^2F_{5/2}) + Tm^{3+}(^3H_6) \rightarrow Yb^{3+}(^2F_{7/2}) + Tm^{3+}(^3H_5) \quad (ET1) \quad ②$$
$$Tm^{3+}(^3H_5) \rightarrow Tm^{3+}(^3F_4) + phonons \quad (MR) \quad ③$$
$$Tm^{3+}(^3F_4) + a\ photon \rightarrow Tm^{3+}(^3F_3) \quad (ESA) \quad ④$$
$$Yb^{3+}(^2F_{5/2}) + Tm^{3+}(^3F_4) \rightarrow Yb^{3+}(^2F_{7/2}) + Tm^{3+}(^3F_3) \quad (ET2) \quad ⑤$$
$$Tm^{3+}(^3F_3) \rightarrow Tm^{3+}(^3H_4) + phonons \quad (MR) \quad ⑥$$
$$Tm^{3+}(^3H_4) + a\ photon \rightarrow Tm^{3+}(^1G_4) \quad (ESA) \quad ⑦$$
$$Yb^{3+}(^2F_{5/2}) + Tm^{3+}(^3H_4) \rightarrow Yb^{3+}(^2F_{7/2}) + Tm^{3+}(^1G_4) \quad (ET3) \quad ⑧$$
$$Tm^{3+}(^3H_4) \rightarrow Tm^{3+}(^3H_6) + hv\ (798\ nm) \quad ⑨$$
$$Tm^{3+}(^1G_4) \rightarrow Tm^{3+}(^3F_4) + hv\ (692\ nm) \quad ⑩$$

where h is the Planck constant and v is the frequency. Because the energy difference between the transition between Yb^{3+}:$^2F_{5/2} \rightarrow {}^2F_{7/2}$ and Tm^{3+}: $^3H_6 \rightarrow {}^3H_5$, $^3F_4 \rightarrow {}^3F_2$, $^3H_4 \rightarrow {}^1G_4$ does not match, the ET between Yb^{3+} and Tm^{3+} is a rope assist energy transfer. It can be seen from the above that the up-conversion near-infrared light ($^3H_4 \rightarrow {}^3H_6$ transition) is a two-photon absorption process. Up-converting blue light ($^1G_4 \rightarrow {}^3H_6$ transition) and red light ($^1G_4 \rightarrow {}^3F_4$ transition) are three-photon absorption processes, and up-converting blue light is not reflected in the figure. In addition, the energy levels of $^3H_5$ and $^3F_{2,3}$ are very short-lived. The ions in these energy levels can quickly and non-radiatively transit to the $^3F_4$ and $_3H_4$ energy levels, making reverse energy difficult to perform because of the processes ②,④,⑧. The process has high energy transfer efficiency. Therefore, the Yb^{3+} and Tm^{3+} co-doped NaY(MoO^4)^2 crystal can produce strong near infrared light emission (798 nm) under the excitation of 980 nm LD pump, which is consistent with the transition mechanism in Figure 9.

The fluorescence attenuation curve of the $NaY(MoO_4)_2$:Yb^{3+}/Tm^{3+} crystal after annealing was measured as shown in Figure 10. The curve of the crystal can be calculated by fitting an exponential function:

$$I = I_0 + I_1 e^{-t/\tau} \quad [8]$$

where I_0 is the initial spectral intensity and τ is the decay time constant of the emission. Hence, the decay time from the emission line $^3H_4 \rightarrow {}^3F_4$ at 1455 nm of the $NaY(MoO_4)_2$:Yb^{3+}/Tm^{3+} crystal after annealing is fitted to be 166.67 μs. The fluorescence lifetime of co-doped sample was shorter, which was mainly because of the energy transition between ions in a shorter time.

Conclusion

The $NaY(MoO_4)_2$ crystal co-doped by Yb^{3+} and Tm^{3+} ions have been grown by the vertical Bridgman method using spontaneous crystallization. The grown doped $NaY(MoO_4)_2$ crystal appeared dark brown in color, and the PXRD pattern confirms that the crystal structure was tetragonally symmetric with $I4_{1/a}$ space group. The $NaY(MoO_4)_2$ co-doped crystal enriches the emission band in the near-infrared region, and improves the pump energy absorption efficiency at 980 nm. In addition, as the temperature dropped from 473 K to room temperature under 980 nm LD laser excitation, the emission intensity increased. Therefore, $NaY(MoO_4)_2$:Yb^{3+}/Tm^{3+} crystal as a NIR laser crystal has a strong potential application prospect in optics and photonic devices.

Acknowledgments

This work was sponsored by National Natural Science foundation of China (No. 61875096 and 61775108).

References

(1) L. Dai, Y. Shao, C. Liu, R. Chen, X. Han, and S. Yang, *Opt. Mater.* **95,** 109193 (2019).

(2) J. Pisarska, R. Lisiecki, W. Ryba-Romanowski, G. Dominiak-Dzik, and W.A. Pisarski, *J. Alloys Compd.* **451,** 226–228 (2008).

(3) R. Soulard, J.L. Doualan, A. Braud, M. Sahli, A. Benayad, G. Brasse, A. Hideur, A. Tyazhev, R. Moncorgé, and P. Camy, *Opt. Mater.* **72,** 578–582 (2017).

(4) G. Jiang, X. Wei, Y. Chen, C. Duan, and M. Yin, *J. Rare Earths* **31,** 27–31 (2013).

• Continued on Page 82

NEW!

PIKE TECHNOLOGIES

MIRacle Peltier

By PIKE Technologies

A new temperature control option for your ATR accessory.

Retrofit your existing MIRacle or configure a new ATR

Take advantage of the perks that the MIRacle Peltier element offers:

- Sub-ambient measurements to 10 °C without a refrigerated liquid circulator, up to 90 °C.
- Fast heating and cooling rates, 10 °C/min and 5 °C/min, respectively.
- Temperature stability, even at room temperature.

To learn more about PIKE Technologies' latest MIRacle Peltier, visit our website, piketech.com or contact us at info@piketech.com.

www.piketech.com | info@piketech.com | 608.274.2721 | Madison, WI 53719

PEER-REVIEWED RESEARCH
Spectroscopy papers have undergone a double-blind peer review process and are available on our open-access website.

Optical Properties of the Suwannee River Fulvic Acid Complexation with Thorium Using 3D Fluorescence Spectroscopy

Xiao Long Sun, Xiangshu Ma, Liu Leng, and Yichuan Fang

The relationship between the complexation amount of thorium (Th) and Suwannee River fulvic acid (SRFA) and the changes in Th concentration and pH were studied using differential spectroscopy and 3D excitation-emission matrix fluorescence spectroscopy (3D EEM). Experiments were performed at different Th concentrations and pH values. In the differential spectra at different concentrations, four bands of aromatic components appeared, and thorium was complexed with the carboxyl groups in SRFA. The 3D EEM spectra showed a fulvic acid-like fluorescence region, a visible-light fulvic acid region, and the blueshift phenomenon. The fluorescence intensity decreased with increasing thorium concentration and increased with increasing pH. The results showed that the amount of complexation of thorium and SRFA increased with increasing thorium concentration, and high pH was not conducive to the complexation of thorium and SRFA.

Thorium, associated with the migration of disposed nuclear waste from solid to water phases, has increasingly been studied because of its safe characteristics, including low-level radioactivity and chemical toxicity. Natural organic matter (NOM) plays an important role in the surface water environment, and is involved in physical, chemical, and biological reactions. NOM affects the migration, transformation, and potential toxicity of heavy metals because of ion exchange, adsorption, and chelation (1–3). Because thorium is widely distributed on Earth, the study of the behavior between thorium and NOM is key in controlling radionuclide pollution in the environment.

Research on thorium and NOM adsorption has received considerable attention. Reiller (4) studied the Th(IV) and humic acid (HA) adsorption on hematite and goethite; in the pH range of 3.5–9.5, HA easily complexed with hematite surface sites, and the adsorption of Th(IV) decreased. Chen (5) investigated the removal behavior of Th(IV) in multi-component systems containing silica (SiO_2) in the presence of HA and FA, and found that humic substances (HS) could enhance Th(IV) sorption at low pH. Moreover, Th(IV) sorption was reduced at intermediate and high pH values according to the relationships $\equiv MOH+H^+ \leftrightarrow \equiv MOH_2^+$ in acidic media and $\equiv MOH \leftrightarrow \equiv MO^- + H^+$ in alkaline solutions. In experiments without or with soil FA/HA, the sorption of Th(IV) on TiO_2 strongly depended on pH, but weakly depended on the ionic strength, and the presence of HA enhanced the sorption of Th(IV) onto TiO_2 (6). Alpatova thought that low metal rejection in the absence of HS at higher pH proved an effect of the HS–metal complexation on the metal rejection (7). We tested the complexation between different types of NOM and lead, and investigated their binding properties (8). However, the chemical formulas that describe the complexation between NOM and heavy metals are seldom discussed.

Regarding the binding of Th^{4+} with HA, Th^{4+} bound to carboxylate sites on gray HA only form a 1:1 complex, and the binding constant increases with the degree of ionization and the pK_a of the HA (9). Thorium and soil organic matter can form stable thorium-organic complexes, and HA can enhance the complexation adsorption of free thorium ions with humic materials (10).

The UV spectroscopy of HS can obtain information about chromophores, and differential absorbance spectroscopy can be used to quantify the protonation and site specificity of FA in situ (11). Differential absorbance spectroscopy has high sensitivity and can detect subtle chemical changes in NOM, and the complexation effect of humic acid on metal ions was quantified (5,12). Fluorescence

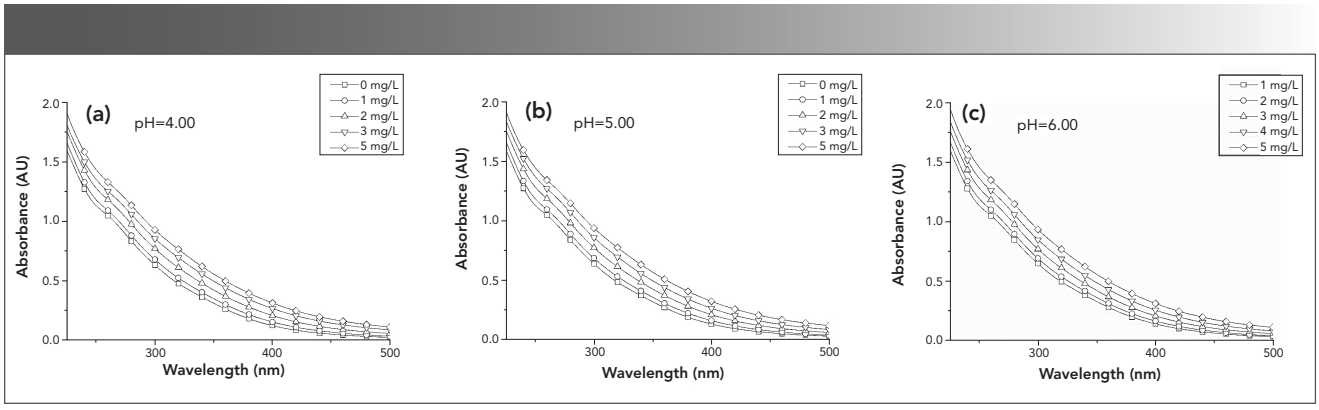

FIGURE 1: Effect of pH on the absorbance spectra of complexation between SRFA and thorium; SRFA=5.0 mg/L; Th=0, 1, 2, 3 and 5 mg/L. (a) pH = 4.0; (b) pH = 5.0; (c) pH = 6.0.

spectroscopy can determine the binding characteristics between metal and humus (13). When metals and humus are combined, pH and metal form can cause changes in the fluorescence intensity that can be used to determine the binding characteristics of humus components and trace metals (14,15). Here, fluorescence spectrometry and differential absorbance spectra were used to track the complexation between thorium and SRFA, detect the behavior of fluorescence spectra-based parameters, and quantify their associations with the Th concentration and pH value.

Materials and Methods

Reagents and Solutions

Thorium(IV) perchloric acid with a concentration of 1,001 ±5 mg/L was obtained from Inorganic Ventures, Inc. The HA was standard Suwannee River fulvic acid (SRFA, the International Humic Substance Society). SRFA was diluted to 50 mg/L to obtain a concentrated stock. Dissolved organic carbon (DOC) was analyzed by a Shimadzu TOC-VCSH carbon analyzer.

A concentrated stock of 0.1 mol/L $NaClO_4$ was prepared to dilute solutions to a background ionic strength of 0.01 mol/L.

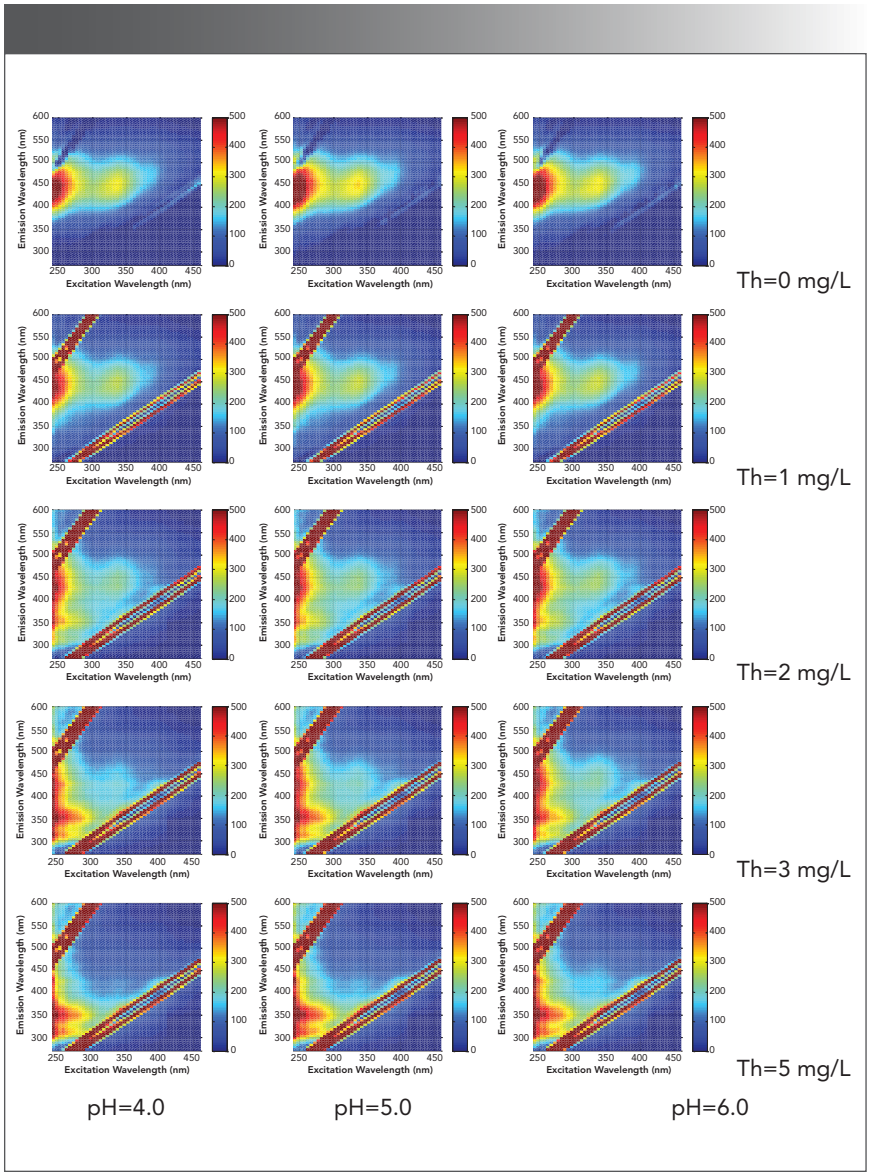

FIGURE 2: 3D EEM spectra of the complexation between thorium and SRFA. (Rows 1 through 5) Thorium concentrations from 0 mg/L to 5 mg/L; and (Columns 1 through 3) pH at 4.0, 5.0, and 6.0.

NaOH and $HClO_4$ (1.00 mol/L, 0.10 mol/L, and 0.01 mol/L) were prepared to adjust the pH of the solutions.

Experimental

Three milliliters of 0.1 mol/L $NaClO_4$, 3 mL of 50 mg/L (DOC) SRFA and different amounts of Th were added to a beaker, and the solution was diluted to 30 mL. The $NaClO_4$ concentration was 0.01 mol/L, the DOC was 5 mg/L, and the pH of the solution was adjusted to 4.00, 5.00, and 6.00. UV spectroscopy (Perkin-Elmer Lambda 18 UV/vis spectrophotometer with a 5-cm cell) and 3D excitation-emission matrix fluorescence spectroscopy (3D EEM) (LS-50B fluorometer) were used to assess the solutions of each pH. Solutions of 0.0, 0.05, 0.1, 0.2, 0.3, 0.4, 0.6, 0.8, 1.0, 2.0, 3.0, and 5.0 mg/L Th were analyzed with UV spectroscopy, and solutions of 0.0, 1.0, 2.0, 3.0, and 5.0 mg/L Th were analyzed with 3D EEM. The pH adjustment reaction lasted 5–10 min. UV and 3D EEM measurements were then performed for solutions with different pH values and Th concentrations. Each concentration solution was repeated three times, and the mean value was used as the final result of spectral analysis. The free thorium concentration was analyzed through differential pulse voltammetry (DPV, Shanghai Chenhua Electrochemical Workstation CHI760E) with a hanging mercury drop electrode (HMDE).

Results

UV Spectroscopy of Thorium and SRFA

Figure 1 shows the absorbance spectra for complexes between SRFA and thorium at varying thorium concentrations. In Figure 1, the absorbance spectra have a consistent and monotonic increase from 500 nm to 225 nm, and increase with the thorium concentration because of various light-absorbing components in NOM (16). However, there was little difference between the different pH absorbance spectra before data processing, and the UV spectra are mainly affected by carboxylic groups at pH <7 (11). The curves of the absorbance spectra for thorium and SRFA complexation were smooth and did not exhibit characteristic absorption peaks because of the vast array of potentially dissimilar aromatic constituents in FA. The spectra exhibit featureless shape characteristics with increasing thorium concentration.

HSs are typically closely linked to the adsorption and chelation of heavy metal ions because of their aromatic groups, and adsorption occurs at the carboxylic and phenolic groups. The characteristic changes in C-H, C-O and C=O groups, according to UV spectroscopy, are an effective tool to indicate humic structural changes caused by the adsorption reaction. However, from Figure 1, the bands of the absorbance spectra have little difference, and the only detectable trend based on the analysis of the raw absorbance spectra was that increasing thorium concentration was accompanied by a consistent and monotonic increase in absorbance at all wavelengths. This effect was attributed to the deprotonation of chromophores and possible conformational changes in the FA molecules (17).

3D EEM of Thorium and SRFA

There are functional groups such as aromatic carboxylic groups, phenolic groups, and unsaturated fatty acids in SRFA, so fluorescence spectroscopy techniques can be used to assess humic structures (18,19). Because paramagnetic metal ions produce fluorescence quenching of dissolved organic matter (DOM), the fluorescence intensity decreases because of quenching, and the fluorescence spectra can be used to check the ligand effects between paramagnetic metal ions and NOM (20,21). The fluorescence spectra of SRFA with thorium are shown in Figure 2.

Figure 2 shows the typical EEM spectra of SRFA with and without thorium (SRFA = 5.00 mg/L; ionic strength = 0.01 mg/L $NaClO_4$). The spectra are characterized by two peaks at excitation/emission (Ex/Em) values of <240/440 nm (P1) and 335/450 nm (P2), which are common in the EEM spectra of terrestrial and organic matter. Peak P1 is in the range of 220–240 nm Ex and 410–450 nm Em, which has been previously classified as the UV fulvic-like region, and peak P2 is in the range of 330 nm–370 nm Ex and 420 nm–460 nm Em, which has been classified as the visible fulvic-like region (22–24).

In Figure 2, the EEM spectrum of SRFA with 1.0 mg/L thorium has the same peaks, and only P1 has a blueshift from <240/440 nm to <240/425 nm (Ex/Em), while P2 remains essentially unchanged. When the thorium concentration increases to 2.0 mg/L, P1 remains at 240/425 nm, and P2 shifts to 335/425 nm. The emergence of the blueshift shows a decrease in the number of organic aromatic rings, a decrease in molecular weight, or a reduction of polar groups in solution, such as the carboxyl, amino, and hydroxyl groups (25,26).

Discussion

UV Spectroscopic Analysis of Thorium and SRFA

From Figure 1, differential absorbance spectra ($\Delta A_{Th}[\lambda]$) are calculated as follows:

$$\Delta A_{Th}(\lambda) = A_{Th}(\lambda) - A_{Th\_ref}(\lambda) \quad [1]$$

where $A_{Th}(\lambda)$ and $A_{Th\_ref}(\lambda)$ are the absorbance spectra at the wavelength measured at a certain thorium concentration and at Th = 0.0 mg/L.

For example, the differential absorbance spectra at pH 4.0 in Figure 3 contain four bands: a band at 235–265 nm with a relatively sharp peak at 247 nm; a band at 265–300 nm with a peak at 280 nm; a band at 300–350 nm with a peak at approximately 320 nm; and a band below 320 nm with a peak at approximately 380 nm. Similar peaks appeared in the studies of Yan, Chen, and Dryer, which indicates that these peaks represent the aromatic composition and absorbance of chromophore (11,27,28). Among chromophores, carboxylic chromophores overwhelmingly contribute to absorbance changes in the pH range of 3–5, and the differential spectra were dominated by a prominent peak near 280 nm; in contrast, phenolic

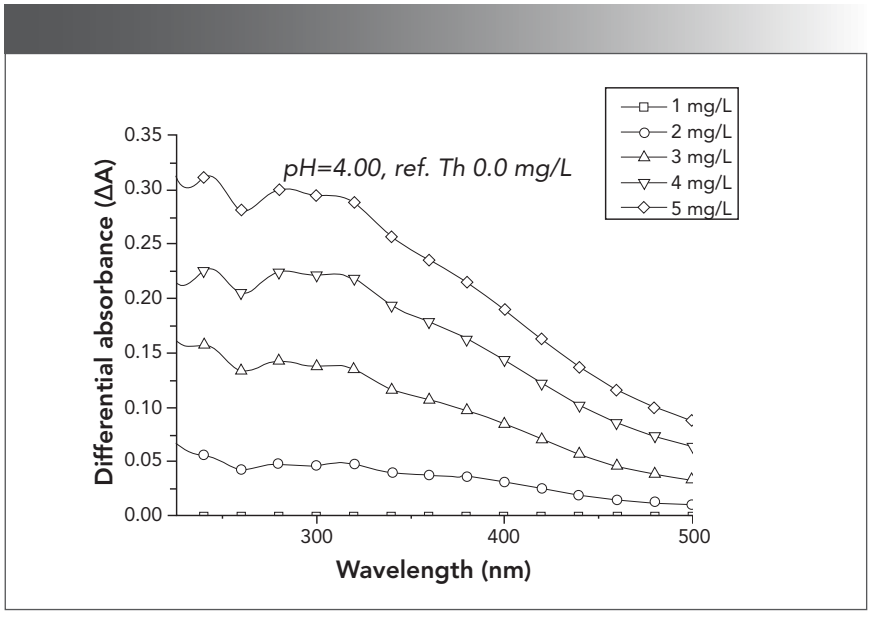

FIGURE 3: Differential absorbance spectra of the complexation between SRFA and thorium relative to a reference spectrum of Th = 0.0 mg/L.

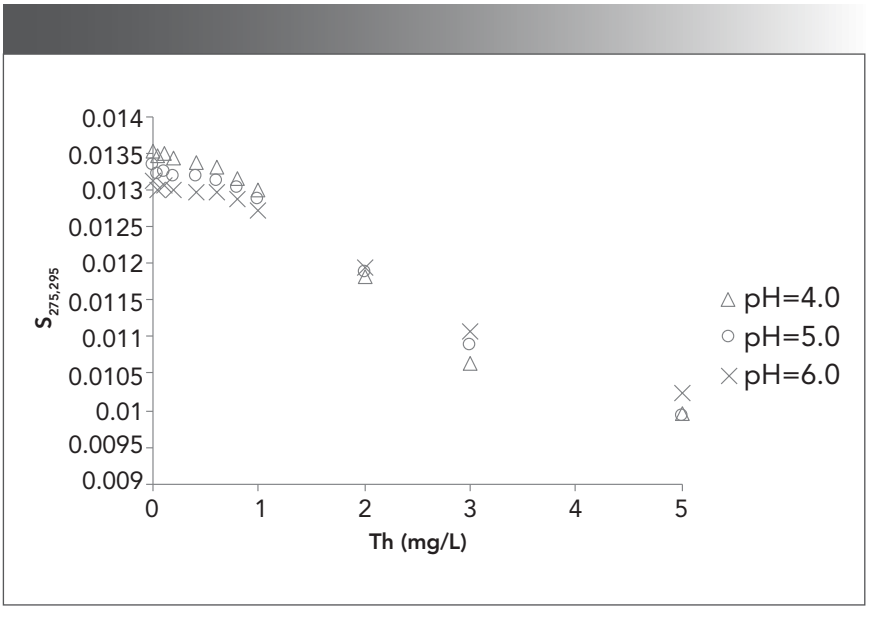

FIGURE 4: Spectral slope parameters with respect to the thorium concentration and pH.

chromophores predominated at pH >8, and exhibited a peak near 390 nm (11,29). According to Figure 3, the changes among different thorium concentrations decrease when the thorium concentration increases; for example, the difference between 5 mg/L and 3 mg/L thorium was less than that between 3 mg/L and 2 mg/L thorium. If the absorbance is because of complexation between thorium and SRFA, the absorbance increases with the thorium concentration, and the complexation amount would approach the amount of SRFA if the SRFA concentration was fixed. However, in the complex of SRHA with rare earth ions, with the increase in concentration, the absorbance decreases at 260 nm and increases at 320 and 387 nm, while the absorbance of Pahokee Peat humic acid (PPHA) decreases because of the interaction of Eu^{3+} (12,28). The change in aromatic groups in SRFA in the presence of metal was because of the unshared electron pairs or π electron pairs in the SRFA functional groups (30). Thorium complexation with carboxylic chromophores in SRFA displaces the electrons and enhances the aromaticity of SRFA, and the absorbance at 280 nm and 390 nm was increased.

The DOM absorption spectrum follows the equation $A_\lambda = A_{\lambda 0} \times exp\ (-S \times [\lambda - \lambda 0]) + K$. In the equation, λ is the wavelength (nm); λ_0 is the reference wavelength (400 nm); A_λ and $A\lambda_0$ are the absorbances at λ and λ_0, respectively; S is the spectral slope; and K is the residual scattering or residual noise offset. The spectral slope (S) values of a narrow wavelength range (275–295 nm) are recommended as indicators of the molecular weight (MW), source, and photobleaching of chromophoric dissolved organic matter (CDOM) (31–33).

In Figure 4, the changes in $S_{275–295}$ exhibit a striking relationship, and the spectral slope (S) decreases with the thorium concentration. The $S_{275–295}$ curve gently changes at low concentrations (0.0–1.0 mg/L) and high concentrations (3.0–5.0 mg/L) and has S-curve characteristics. Helms (31) proposed that the 275–295-nm slope was routinely reported in future DOM studies, since it could be measured with high precision and appeared to be a good proxy for DOM MW, where $S_{275–295}$ is negatively correlated with DOM MW. In Figure 4, $S_{275–295}$ decreases when the thorium concentration increases, so the average MW increases when the thorium concentration increases. This result may indicate the thorium ion complexation with SRFA molecules, and many SRFA molecules gather into larger FA molecules. $S_{275–295}$ hardly varies with respect to pH except at 0.0 mg/L thorium, indicating that the thorium concentration (0.0–5.0 mg/L) has a greater impact than pH (4–6) on the spectral slope, and thorium is the main factor that changes the UV spectral results.

3D EEM Analysis of Thorium and SRFA

In Figure 4, after thorium was added to the SRFA solution, the SRFA molecules gathered into larger FA molecules, and

there was no redox reaction in solution, so the blueshift was because of a reduction in the polar groups. Therefore, the thorium complexation with SRFA occurred on carboxyl or hydroxyl groups, and similar studies have shown that carboxyl and hydroxyl groups participate in the complexation of heavy metal ions (34). After the thorium concentration increased to 3.0 mg/L, P2 gradually decreased, and there was a new peak at <240/345 nm (P3). The outermost electron arrangement of Th(IV) was saturated 6d26p6, which is identical to the structure of noble gas, so Th(IV) is a diamagnetic ion, which can change the structure of organic ligands into the rigid planar structure, and make organic ligands show strong fluorescence. The addition of Al^{3+} to fulvic acid by Kelly also proves the change in structure of organic ligands (35); thus, P3 belongs to the ligand of SRFA and thorium. In most cases, the fluorescence intensity of complexation between SRFA and thorium decreases when the thorium concentration increases. Because the peak blueshift and fluorescence intensity change, the carboxyl and hydroxyl groups in SRFA can complex with thorium when the thorium concentration increases, and the decrease in fluorescence intensity can be related to thorium binding to SRFA.

The fluorescence intensities at P1 and P2 are listed in Figure 5. From Figure 5a, the fluorescence intensity overall has a downward trend in the UV fulvic-like (P1) region, but its variation trend is not obvious. First, the fluorescence intensity decreases from 0.0 mg/L to 1.0 mg/L thorium, increases at 2.0 mg/L thorium, and finally decreases again when the thorium concentration increases to 3.0 mg/L and 5.0 mg/L. In Figure 5b, the fluorescence intensity decreases when the thorium concentration increases with a maximum at 0.0 mg/L thorium and a minimum at 5.0 mg/L thorium. This is similar to the fluorescence intensity when SRHA is complexed with rare earth ions Eu^{3+} and Tb^{3+}, and there is a certain correlation between the amount of complexation and the fluorescence intensity (12). When the concentration of $Cr_2O_7^{2-}$ increases, the fluorescence intensity begins to decrease, and the conformation and function of HA will change (12,36).

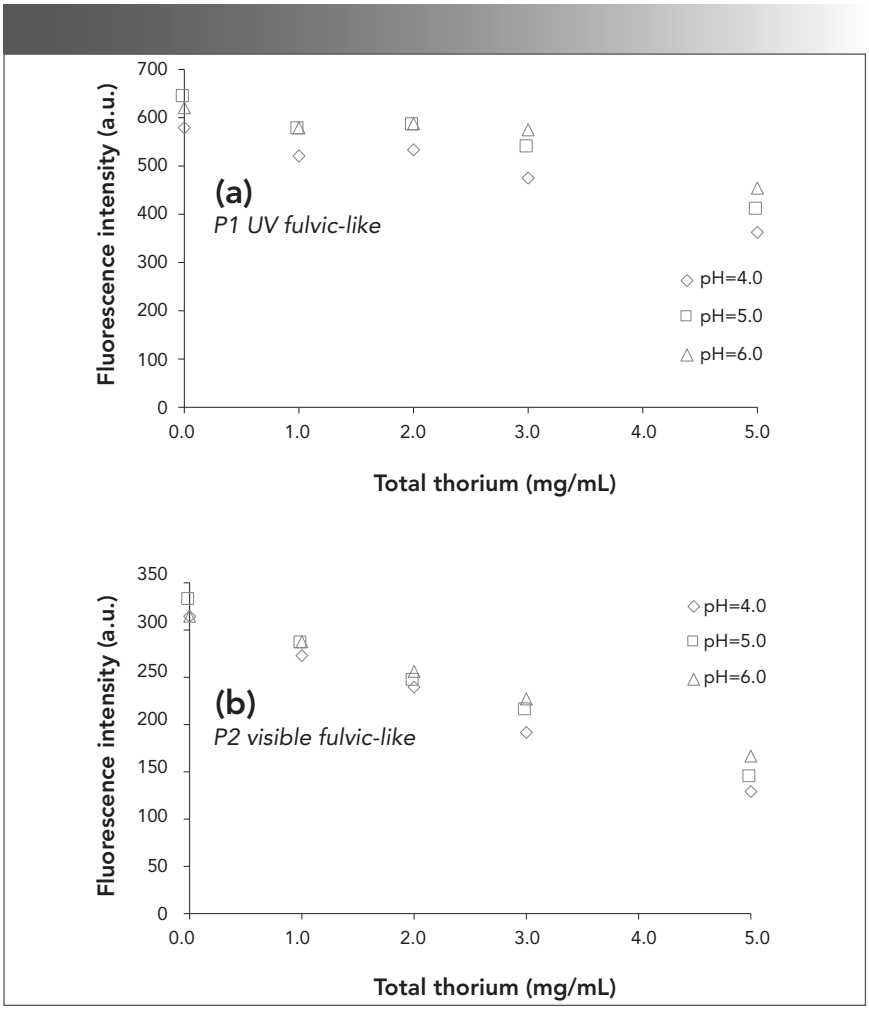

FIGURE 5: Fluorescence intensity at (a) 240/440 nm (P1); and (b) 335/450 nm (P2) with different thorium concentrations and pH values.

In particular, the fluorescence intensity at different thorium concentrations increases with pH. This result indicates that the complexation between SRFA and thorium decreases with pH, and thorium has difficulty combining with SRFA at higher pH.

Optical Characteristics of Complexation Between Thorium and SRFA

The Visual Minteq database has been proven to be a reasonable and effective tool to simulate the amount of complexation between SRFA and metal ions (12,37). The above data suggest that thorium addition causes SRFA molecules to gather into larger FA molecules. A comparison of $S_{275–295}$ and the fluorescence intensity at P1 (UV fulvic-like) is shown in Figure 6.

In Figure 6, the complexation amount of Th and SRFA calculated by Minteq increases with increasing Th concentration; $-1 \bullet S_{275–295}$ is also proportional to the concentration of Th, but $S_{275–295}$ is inversely proportional to the amount of complexation (Figure 6b), which shows a significant negative linear relationship with $R^2 > 0.9$. $S_{275–295}$ can be used to measure the change in MW: when the concentration of Th increases, the amount of complexation increases, the MW increases, and the spectral slope monotonically decreases. This relationship shows that the aromaticity of SRFA is enhanced, and there was a negative correlation between spectral slope and aromaticity (38). The $-1 \bullet S_{275-295}$ and complexation amount of each pH are shown as pH 6 >

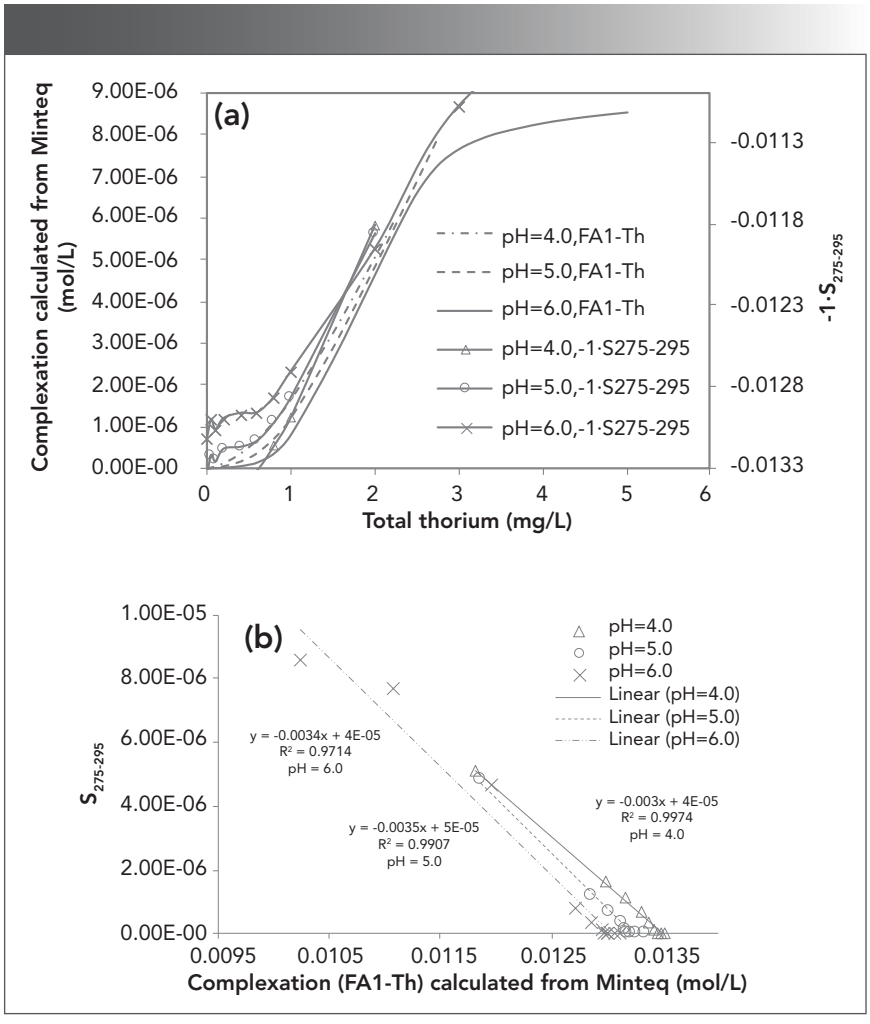

FIGURE 6: Relationships between (a) the thorium concentration and calculated complexation, and (b) spectral slope for calculated complexation vs. $S_{275-295}$.

pH 5 > pH 4. These results indicate that high pH will hinder the complexation of FA with Th. When the pH value increases, the concentration of OH^- increases, the ability to compete with FA is strengthened, and the amount of FA1-Th complexation decreases (39). A change in pH will affect the charge of humus, and an electric field will affect the complexation (40).

In this study, the fluorescence intensity of 0.0 mg/L thorium was used as a reference, and the *Q* values of FA and HA were calculated as follows:

$$Q = 1 - I_{con(Ex,Em)}/I_{0(Ex,Em)} \quad [2]$$

The *Q* values according to the total thorium concentration are listed in Figure 7. *Q* has an inverse relationship with the fluorescence intensity (*I*). In Figure 7a, *Q* increases with the thorium concentration in most of the UV fulvic-like region. In Figure 7b, *Q* monotonically increases in the visible fulvic-like region. The MW of FA in the visible-light region is larger than that in the UV region, and the coordination ability is stronger, so the *Q* value in Figure 7b increases faster with the total thorium amount (41). The *Q* value at pH 5.0 is similar to that at pH 4.0, and greater than that at pH 6.0. The *Q* value is related to the complexation between SRFA and thorium. When the pH value is low, thorium easily complexes with SRFA. In contrast, a higher pH value will make the molecular form of FA more open and present a linear structure, which reduces the *Q* value (42).

Conclusion

In complexes with the carboxyl and hydroxyl groups of SRFA, when the Th concentration increases, complexation increases, the MW increases, the spectral slope decreases, the fluorescence intensity decreases, and the aromaticity of SRFA increases. There are FA-like fluorescent regions and visible-light FA fluorescent regions. $S_{275-295}$ can measure the change in MW. High pH will hinder the complexation of FA and Th. The complexation of Th and SRFA decreases with increasing pH. The *Q* value at pH 5.0 is similar to that at pH 4.0 and greater than that at pH 6. The *Q* value is related to complexation between SRFA and thorium. When the pH value is low, thorium is easily complexed with SRFA. In contrast, a higher pH value will make the molecular form of FA more open and present a linear structure, which reduces the *Q* value.

Funding

This study was sponsored by the Scientific Research Fund of Yunnan Provincial Education Department, China (Grant number 2022J0524) and the General Project of The National Natural Science Foundation of China (31860126).

References

(1) A. Nebbioso and A. Piccolo, *Anal. Bioanal. Chem.* **405**(1), 109–124 (2013).
(2) A. Philippe and G. E. Schaumann, *Environ. Sci. Technol.* **48**(16), 8946–8962 (2014).
(3) L. Wang, Y. Liu, X. Shu, S. Lu, X. Xie, and Q. Shi, *PloS One* **14**(9), e0218742 (2019).
(4) P. Reiller, V. Moulin, F. Casanova, and C. Dautel, *Appl. Geochem.* **7**(12), 1551–1562 (2002).
(5) C. Chen and X. Wang, *Appl. Radiat. Isot.* **65**(2), 155–163 (2007).
(6) X. Tan, X. Wang, C. Chen, and A. Sun, *Appl. Radiat. Isot.* **65**(4), 375–381 (2007).
(7) A. Alpatova, S. Verbych, M. Bryk, R. Nigmatullin, and N. Hilal, *Sep. Purif. Technol.* **40**(2), 155–162 (2004).
(8) T.M. Filella, *Sci. Total Environ.* **300**(1–3), 143–154 (2002).
(9) A.A. Helal, *J. Radioanal. Nucl. Chem.* **274**(3), 575–580 (2007).
(10) P. Guo, T. Duan, X. Song, J. Xu, and H. Chen, *Talanta* **77**(2), 624–627 (2008).

(11) D.J. Dryer, G.V. Korshin, and M. Fabbricino, *Environ. Sci. Technol.* **42**(17), 6644–6649 (2008).

(12) Y. Chen, M. Fabbricino, M.F. Benedetti, and G.V. Korshin, *Water Res.* **68,** 273-281 (2015).

(13) H. Ma, L. Huang, J. Zhang, D. Shi, and J. Yang, *Environ. Pollut.* **242**(part A), 760–768 (2018).

(14) Y. Yamashita and R. Jaffe, *Environ. Sci. Technol.* **42**(19), 7374–7379 (2008).

(15) F. Wu, Y. Cai, D. Evans, and P. Dillon, *Biogeochemistry* **71**(3), 339–351 (2004).

(16) W. Chen and H-Q. Yu, *Water Res.* **190,** 116759 (2020).

(17) M. Grassi and M. Rosa, *Inorg. Chim. Acta* **363**(3), 495–503 (2009).

(18) E.M. Carstea, A. Baker, M. Bieroza, and D. Reynolds, *Water Res.* **44**(18), 5356–5366 (2010).

(19) N. Patel-Sorrentino, S. Mounier, and J.Y. Benaim, *Water Res.* **36**(10), 2571–2581 (2002).

(20) T. Ohno, A. Amirbahman, and R. Bro, *Environ. Sci. Technol.* **42**(1), 186–192 (2008).

(21) S.L. Zhang Xiao, W. Zhao-qun, S. Bi-quan, L.Hai-su, and X. Zi-yan, *Spectroscopy* **35**(S5), 32–38 (2020).

(22) F.U. Ping-Qing and L. Cong-Qiang, *Spectroscopy and Spectral Analysis* **25**(12), 2024–2028 (2005).

(23) A. Baker, *Water Res.* **36**(1), 189–195 (2002).

(24) F. Wu and E. Tanoue, *Environ. Sci. Technol.* **35**(18), 3646–3652 (2001).

(25) T. Zhang, J. Lu, J. Ma, and Z. Qiang, *Chemosphere* **71**(5), 911–921 (2008).

(26) J. Świetlik and E. Sikorska, *Water Res.* **38**(17), 3791–3799 (2004).

(27) M. Yan, J. Ma, and G. Ji, *Water Res.* **93(**Apr. 15), 84–90 (2016).

(28) Y. Chen, M. Fabbricino, V. Luongo, and G.V. Korshin, *Chemosphere* **235,** 96-103 (2019).

(29) G.V. Korshin, M.M. Benjamin, H.S. Chang, and H. Gallard, *Environ. Sci. Technol.* **41**(8), 2776–2781 (2007).

(30) D. Hernández, C. Plaza, N. Senesi, and A. Polo, *Environ. Pollut.* **143**(2), 212–220 (2006).

(31) J.R. Helms, A. Stubbins, J.D. Ritchie, E.C. Minor, D.J. Kieber, and K. Mopper, *Limnol. Oceanogr.* **53**(3), 955–969 (2008).

(32) Y. Zhang, M.A.V. Dijk, M. Liu, G. Zhu, and B. Qin, *Water Res.* **43**(18), 4685–4697 (2009).

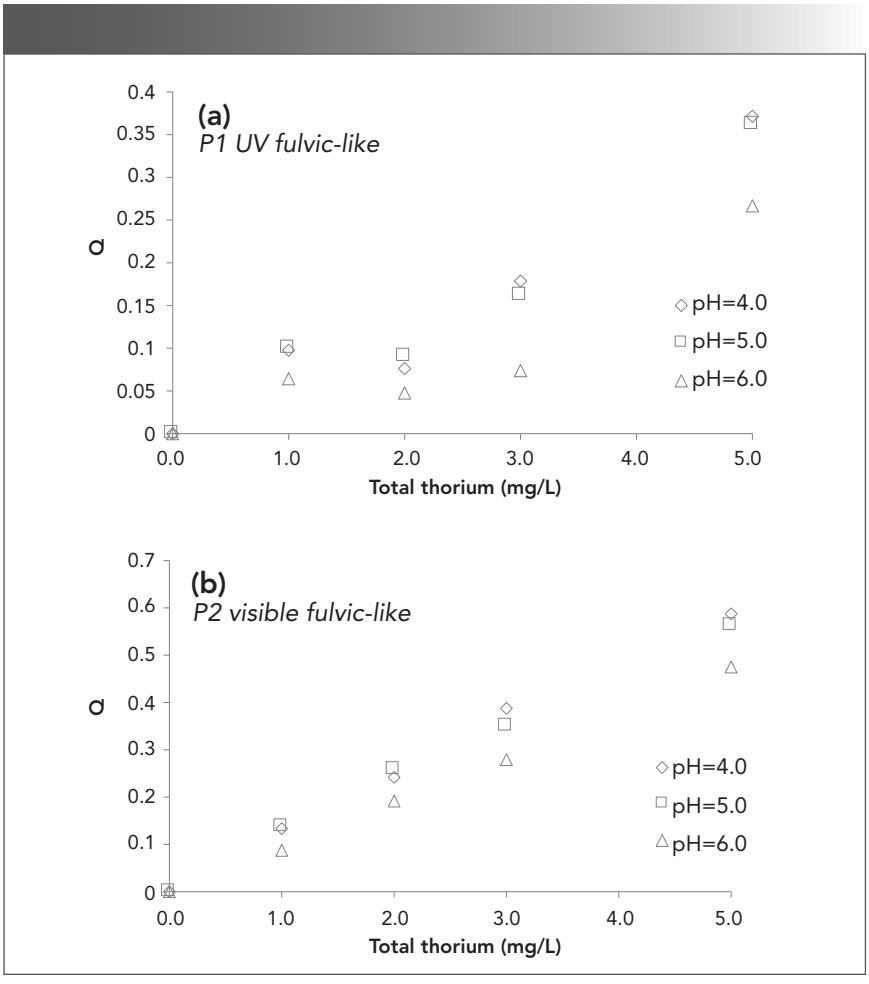

FIGURE 7: *Q* **calculated from the fluorescence intensity at (a) 240/440 nm (P1); and (b) 335/450 nm (P2) with different thorium concentrations.**

(33) C.G. Fichot and R.Benner, *Limnol. Oceanogr.* **57**(5), 1453–1466 (2012).

(34) A. Piccolo and J.F. Stevenson, *Geoderma* **27**(3), 195–208 (1982).

(35) K.M. Elkins and D.J. Nelson, *J. Inorg. Biochem.* **87**(1–2), 81–96 (2001).

(36) Y.L. Gu, M.X. Yin, H.M. Zhang, Y.Q. Wang and J.H. Shi, *Spectrochim. Acta, Part A,* **136**(2), 1702–1709 (2015) .

(37) C.J. Milne, D.G. Kinniburgh, and E. Tipping, *Environ. Sci. Technol.* **35**(10), 2049–2059 (2003).

(38) N.V. Blough and S. Green, in *Role of Nonliving Organic Matter in the Earth's Carbon Cycle, R.G. Zepp and C. Sonntag, Eds.* (John Wiley & Sons, New York, NY, 1995) pp. 23–45.

(39) S. Abalikmu, A. Ilahong, T. Turhong, and A. Aubri, *Xinjiang Agricultural Sciences* **49**(9), 1701–1706 (2012).

(40) M.A. Ramos, S. Fiol, R. López, J.M. Antelo, and F. Arce, *Environ. Sci. Technol.* **36**(14), 3109–3113 (2002).

(41) W. Kaifeng, P. Na, H. Jiang, W. Libin, and L. Siwu, *Environ. Sci. Technol.* **40**(10), 151–156 (2017).

(42) S.d.C. Saab, E.R. Carvalho, R. Bernardes Filho, M.R.d. Moura, L. Martin-Neto, and L.H.C. Mattoso, *J. Braz. Chem. Soc.* **21**(8), 1490–1496 (2010).

Xiao Long Sun, Xiangshu Ma, Liu Leng, and **Yichuan Fang** are with the Wetland College of Southwest Forestry University and the National Plateau Wetland Research Center, in Kunming City, China. Direct correspondence to Xiao Long Sun at sunxl.96@qq.com ●

Nine Tips for Successful TGA-IR Measurements

Jenni Briggs, PIKE Technologies

With its high-precision balance and furnace, a thermogravimetric analyzer (TGA) monitors sample weight loss caused by volatilization and degradation as a function of temperature. Typical samples include polymers, epoxies, fibers, and laminates for applications such as investigating deformulation, determining thermal stability, or conducting comparative material studies. A TGA only measures the mass loss caused by evolved gas events. By coupling a TGA with a Fourier transform infrared (FT-IR) instrument, unique spectroscopic data of the evolved gases may now be obtained.

Hardware Requirements

A TGA-IR accessory consists of two major components: a heated gas cell for your FT-IR sampling compartment and a heated transfer line connecting the TGA furnace assembly to the gas cell. **Tip 1:** Before embarking on TGA-IR experiments for evolved gas analysis, your TGA system must have a take-off port to interface with the heated transfer line.

Connecting a low-flow vacuum pump downstream of the gas cell will aid in moving the gases through the system. **Tip 2:** Aim for a vacuum pump flow rate of roughly 20–30 mL/min, while not exceeding the total flow rate of the TGA purge. **Tip 3:** To avoid surpassing the temperature limitation of the vacuum pump, place coiled copper tubing between the gas cell exit port and the pump to reduce the temperature of the gas.

Tip 4: Although not required, you may wish to consider an external sample module, which uses the external beam of your FT-IR instrument, for TGA-IR experiments. This creates a second sample compartment off to the side of your FT-IR instrument reserved for the TGA-IR accessory and leaves your main IR sample compartment available for routine measurements.

FT-IR Software and Collection Parameters

Tip 5: To make your data collection and analysis considerably easier, use time-based data collection software, an optional module for most FT-IR instruments. The software allows spectra to be collected in series and creates a Gram-Schmidt (G-S) plot—this will let you determine when a "gas event" is passing through the IR cell. From there, you can simply co-add spectra across a G-S band and correlate the resulting IR spectrum to TGA weight loss data (Figure 1).

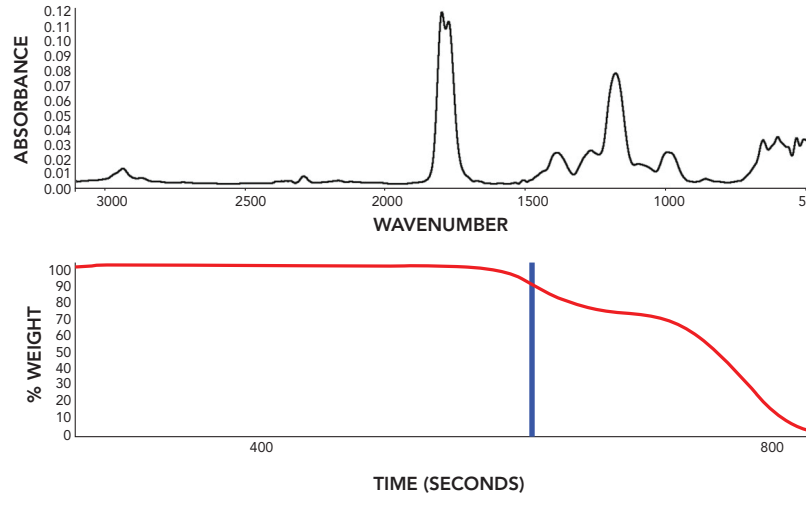

FIGURE 1: TGA weight loss trace of ethylene vinyl acetate (red) and corresponding FTIR spectrum (black) of acetic acid.

Tip 6: To speed data collection time when using a deuterated triglycine sulfate (DGTS) detector, consider using a resolution of 8 cm^{-1}. Higher resolution (<8 cm^{-1}) and longer collection time may result in the gas event spectra being diluted where the collective measurement reflects the sample and possibly the purge gas flowing in front of and behind the evolved gas.

TGA-IR Accessory Maintenance

Tip 7: It is good practice to check the energy throughput of your gas cell periodically to determine the transmittance of the windows and to detect possible contamination on the window surfaces. **Tip 8:** When using ZnSe windows in the gas cell, it is important to keep the temperature of the two TGA-IR accessory components at less than 250 °C because ZnSe will oxidize at higher temperatures.

Released gases from some samples during TGA heating may be dirty and clog the transfer line. **Tip 9:** For easy cleaning, thread a guitar string through the transfer line and pull the string back and forth to loosen the obstruction.

Conclusion

Coupling a TGA and an FT-IR instrument is a relatively straightforward sampling setup. By integrating these tips, you will be on your way to successful TGA-IR measurements. You can find a variety of useful tips across all sampling techniques on the PIKE Technologies' YouTube channel. Tips are posted weekly, and all questions are welcome.

PIKE TECHNOLOGIES

How to Characterize Tungsten Diselenide Layers with Cryogenic Raman Imaging

Thomas Dieing*, Patrick Altmann†, Jan Englert*, Damon Strom*, and Mirko Bacani†

***WITec GmbH**
†attocube systems AG

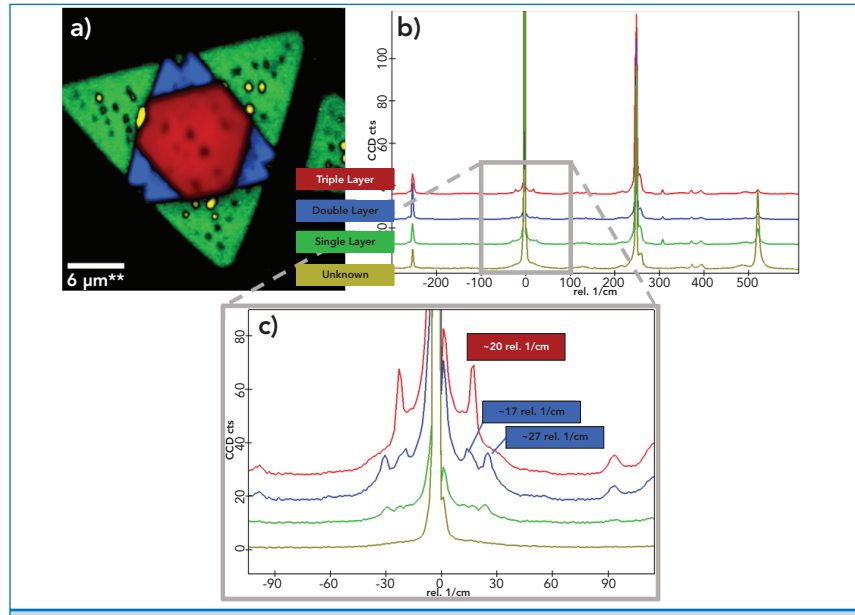

FIGURE 1: (a) Confocal Raman image of WSe_2 of various layer numbers at 120K. (b) Combined false-color image showing the location of the different numbers of layers. Raman spectra of the layers in the corresponding colors and (c) zoom-in of the spectra around the Rayleigh peak.

Raman microscopy at cryogenic temperatures is an analytical method that is growing in prominence and utility. Though the primary driver of its application was initially the carbon nanotubes and graphene community, a recent wave of cryogenic Raman studies has been dominated by research on transition metal dichalcogenides.

In order to address both existing and emerging market requirements, cryoRaman was jointly developed by low-temperature specialists attocube systems and Raman microscopy pioneer WITec GmbH. It is an advanced cryogenic Raman imaging microscope that offers excitation wavelengths from the visible to the near infrared with optimized spectrometers, 1.8K to 300K operating temperatures, cryogenic Raman-specific objectives, and an exceptionally precise piezoelectric scan stage.

In a demonstration of the cryoRaman system's low-temperature capabilities, a tungsten diselenide flake on Si/SiO_2 was examined and its numbers of layers were determined.

The Experiment

To investigate the WSe_2, a 532 nm laser was used for excitation and a RayShield coupler was employed that allowed detection of Raman bands down to ~±10 rel. 1/cm. The experimental setup also included a UHTS 300 spectrometer optimized for detection in the visible range with an 1800 g/mm grating and a back-illuminated CCD camera.

The cryostat cooled the sample to 120K. An LT-APO 532-RAMAN objective with a numerical aperture of 0.82 and piezoelectric positioners controlled through the Control FIVE software were used. The acquired data set was evaluated with the Project Plus software package using the cosmic ray removal tool as well as background subtraction before TrueComponent Analysis was employed to automatically identify the sample components by layer number.

Images of the tungsten diselenide that show different numbers of layers were acquired and combined in the false color image shown in Figure 1a. It is color coded according to the Raman spectra shown in Figure 1b. The image is 30 × 30 µm² in size with 400 × 400 pixels and was created with an integration time of 150 ms per spectrum. A zoom-in image, Figure 1c, shows the low-wavenumber area with the most prominent peaks for the double and triple layers as labeled. The presence of the single, double, and triple layers could be clearly identified by the peaks present. The unknown phase shows in part the features of the single layer, but with an enhanced intensity of the Si-peak near 520 rel. 1/cm.

Summary

The cryoRaman microscopy system offers researchers an integrated and powerful tool for examining transition metal dichalcogenide samples and determining their numbers of layers at very low temperatures. As layer number affects the physical and electronic properties of these materials, this capability will be of great use as research on 2D materials and TMDs continues.

Reference

Extracted and adapted from the whitepaper: Cutting-edge Cryogenic Raman Microscope https://bit.ly/cryoRaman_whitepaper

PEER-REVIEWED RESEARCH
Spectroscopy papers have undergone a double-blind peer review process and are available on our open-access website.

Terahertz Spectroscopic Analysis of Co-Crystallized Mixtures in an L-threonine Diastereomer System

Ruonan Zeng, Yujing Bian, Xun Zhang, Zhenqi Zhu, and Bin Yang

Terahertz (THz) resonance absorption originates from intermolecular interactions, which are suitable for identifying amino acids with multiple isomers. L-threonine and L-allo-threonine are diastereomers with two characteristic peaks in the effective spectrum range of 1.0–2.3 THz, which are located at 1.42 and 2.14 THz for L-threonine (L-thr) and 1.63 and 2.16 THz for L-allo-threonine (L-allo-thr). Based on the density functional theory (DFT) of the crystal structures of L-thr and L-allo-thr, the vibration frequencies of 1.56, 1.87, 2.16 THz, and 2.22 THz were obtained, corresponding to the THz characteristic peaks. Through vibration model analysis, it was found that lattice and skeleton vibrations mediated by intermolecular hydrogen bonds play a crucial role in the THz response. Studying the experimental absorption spectra of different proportions co-crystallized mixtures and 1:1 physical mixture of L-thr and L-allo-thr, it was found that the characteristic peaks of the physical mixture include the characteristic peaks of the two diastereomers in the THz band, while amino-acid co-crystallized mixtures formed their own characteristic peaks depending on the proportion. The results show that the co-crystallized mixture composition of diastereomers can be quantitatively analyzed by THz time-domain spectroscopy (THz-TDS).

As one of the eight essential proteinogenic amino acids, L-threonine (L-thr) is required for body growth, uric acid metabolism, and the immune system. L-allo-threonine (L-allo-thr) is used as a starting material in the chemical synthesis of lysobactin, which displays strong antibiotic activity (1). L-thr and L-allo-thr are diastereomers and the molecular formula is $C_4H_9NO_3$, but the molecule configuration is different. The main difference between the two isomers is that the chirality of the center carbon atom C_3 can be interchanged through the chiral conversion of the C_3 atom (2,3). Another characteristic of the two isomers is that they can also be completely miscible to form a continuous set of co-crystallized mixtures (4,5). L-thr and L-allo-thr have the same functional groups (amino, carboxyl, and side-chain hydroxyl), and the same type of hydrogen bonds. Among them, proton donors, such as -OH and -NH_2, and proton acceptors, such as oxygen and nitrogen atoms, can form not only intramolecular hydrogen bonds but also intermolecular hydrogen bonds. Therefore, the three structures of L-thr, L-allo-thr, and L-thr-L-allo-thr all have similar "framework" characteristics comprised of hydrogen bonds.

A *terahertz (THz) wave* refers to electromagnetic wave with frequencies in the 0.1–10 THz frequency band. The intermolecular and intramolecular interaction energies of many polar macromolecules are in tune with photons of frequencies in the THz band. For compounds with similar molecular structures and the same functional groups, their infrared (IR) spectroscopies are similar or the same, whereas THz can distinguish intermolecular hydrogen bonds, which is mainly because the IR resonance absorption originates from intramolecular vibrations. The molecular arrangement and intermolecular interactions of these compounds are different where most of the THz resonance absorption originates. Therefore, THz spectroscopy is more suitable for identifying such substances than IR spectroscopy (6,7). The 20 basic amino acids that comprise various proteins in organisms, except for glycine (the α-carbon atoms of other amino acids), are all chiral carbon atoms. Therefore, amino acids are isomers of various configurations. For various amino acids, the vibrational and torsional motions of groups of atoms, hydrogen bondings, van der Waals forces, and lattice vibrations have strong resonance absorption in the THz band, and they have their own distinct characteristic peaks,

CANNABIS SCIENCE CONFERENCE

AN MJH life sciences BRAND

September 14-16, 2022

Baltimore Convention Center
Baltimore, MD

Join us at the world's largest scientific & medical cannabis event!

- Canna Boot Camp
- Exciting Keynotes
- Huge Exhibit Floor
- Cultivation Gurus
- Analytical/Scientific Experts
- Medical/Wellness Professionals
- Networking Mixers
- Global KOLs
- and much more!

Educational Tracks

Analytical Science | Medical Science | Cultivation Science | Hemp Science | **NEW!** Psychedelic Science

Make your plans today to attend and/or exhibit!
Learn More at **CannabisScienceConference.com**

TABLE I: Comparison of theoretical characteristic absorption frequency and experimental characteristic absorption frequency of L-thr and L-allo-thr crystals and the vibration mode at the characteristic absorption frequency

Amino Acid	Experimental Result (f/THz)	Theoretical Calculation (f/THz)	Mode Assignment
L-thr	1.42	1.56	Mainly from v $(NH^{3+})^{+}$ v(COO^{-}) along the *z*-axis
	2.14	2.16	Mainly from V(COO-)+V(C_4H_3)
L-allo-thr	1.63	1.87	Collective v (L-allo-thr) along the *x*-axis
	2.16	2.22	Mainly from V(R)+V(C_4H_3-C_3-H_5)

which can form a unique THz "fingerprint" spectra (8–10). For biomolecules with a large number of weak molecular interactions (such as hydrogen bonds), low-frequency vibration strongly affects their structure, conformation, and function because of the complexity of this type of vibration; the analysis of the THz spectrum lacks the corresponding molecular vibration model. Currently, solid density functional theory (DFT) simulation is considered to be an effective way to connect the predicted vibration mode and molecular structure. *Simulated spectrum calculation* refers to modeling with the aid of quantum mechanics calculation software to obtain a theoretical spectrum. Combined with experimental data and related visualization software, the vibration mode of absorption peaks can be identified, and the source of these absorption peaks can be explained.

In recent years, DFT has been well applied to simulate the THZ spectrum of threonine molecules. In 2009, Wang and others used THz time-domain spectroscopy (THz-TDS) and Raman spectroscopy to test L-thr (11), compare THz absorption and Raman spectroscopy, and then combine them with quantum chemistry calculations to analyze threonine. In 2019, Li Wei and others studied the THz absorption spectra of three configurations of single molecule, dimer, and unit cell of L-thr samples (12) before comparing them with the calculated THz spectra of single molecule and dimer configurations. Their study determined that the calculated THz spectra of crystal cell configurations are in good agreement with the experimental spectra, indicating that the unit cell is the smallest structure that is more consistent with the sample structure and maintains the physical properties of threonine. The results showed that the use of THz spectroscopy could achieve rapid and accurate identification of L-thr and a better theoretical interpretation of its low-frequency vibration mode. Therefore, to understand how the configuration of the hydrogen bond network affects the low-frequency vibrations of the diastereoisomers L-thr and L-allo-thr, we further used THz spectroscopy and solid-state DFT calculations to compare their low-frequency vibration characteristics. For this study, it was helpful to comprehensively understand the diastereomer system of L-thr-L-allo-thr.

Currently, studies on binary solid solution systems formed by different amino acids roughly includes L-valine–L-isoleucine (L-val-L-ile) (13,14), L-val-L-leucine (L-leu) (15), L-ile-L-leu and L-ala-L-ser (16), and L-thr-L-allo-thr (1,4), where the similarity of sizes and shapes of these amino acid molecules indicates that they can form solid solutions in their mixtures. However, most of them are nonequimolar discrete heterocompounds and limited solid solutions in the vicinities of pure components, whereas in the L-thr-L-allo-thr study system exists the phenomenon of the continuous isomorphic miscibility of the components, which is rarely found in chiral systems. In addition, in the synthesis or purification process of L-amino acid products, many impurities are often encountered, including pure compounds, physical mixtures, intermediate compounds, or co-crystallized mixtures. Therefore, a fast and accurate method is needed to determine whether a pure monomer or eutectic is formed (4,8,17). The THz absorption spectra is sensitive to the structural changes of diastereomers, taking L-thr and L-allo-thr as the research objects and analyzing the THz absorption of threonine and allo-threonine. The low-frequency vibration mode of them is calculated by using DFT, and the effects of intermolecular hydrogen bonds on different cell configurations and various low-frequency vibration modes in amino acid molecules are analyzed. To understand this process, it is helpful to further understand the molecular interaction of the co-crystallized mixtures L-thr-L-allo-thr.

Experimental Methods and Sample Preparation

Experimental System

This experiment used the transmission TDS system produced by Daheng Optoelectronics. The THz emission source was a light guide antenna, and the THz detector was zinc telluride (ZnTe). The center wavelength was 800 nm, the laser pulse width was 100 fs, and the repetition frequency was set at a 84 MHz pulse. The effective THz spectral range was 0.2–3.0 THz. The sample was placed in a sample chamber filled with nitrogen, and the relative humidity was less than 1%, which was measured at room temperature.

A powder X-ray diffraction (PXRD) system from ThermoARL was used in this experiment. The working voltage was 40 kV. The working current was 40 mA. The scanning range was 5–50°. The scanning speed was 0.2°/step.

IR spectroscopy was performed using a Nicolet 5700 Fourier transform IR (FT-IR) spectrometer under the conditions of a pressure of 15 MPa and a temperature of room temperature. The scanning range was 400–4000 cm^{-1}, the number of scanning was 32 times, and the resolution was 4 cm^{-1}.

Sample Preparation

L-thr (CAS: 72-19-5, purity >99%) and L-allo-thr (CAS: 1509-34-08, purity >98%) were purchased from Aladdin. The samples used in the experiment were not purified further. The sample and polyethylene (PE) were mixed thoroughly at a ratio of 1:5. Then, the mixture was compressed into pellets with a diameter of 13 mm and a thickness of approximately 1 mm at room temperature under a pressure of 10 MPa for 3 min.

Theoretical Method

The theoretical calculations in this study were all performed using Castep-20.11 software (18). The generalized gradient approximation method (GGA) based on the plane wave was used for the calculation, and the exchange correlation functional used was the typical Perdew-Burke-Ernzerhof (PBE) functional method. The mass calculated by the energy was ultrafine, and the plane-wave cutoff energy was 750 eV. The total energy converges to 5.0×10^{-6} eV/atom, and the maximum forces between atoms were less than 0.01 eV/Å. The crystal structure data of L-thr (identifier: 128538) and L-allo-thr (identifier: 1061093) come from the Cambridge Crystallographic Data Center (CCDC). The space group of L-thr and L-allo-thr is p212121 ($Z = 4$), and the corresponding lattice parameters are $a = 13.628$ Å; $b = 7.618$ Å; $c = 5.110$ Å, α, β, γ = 90° (19,20), and $a = 13.71$ Å, $b = 7.74$ Å, $c = 5.14$ Å, α, β, γ =90° (4,21), respectively. The crystal structures of L-thr and L-allo-thr are shown in Figure 1.

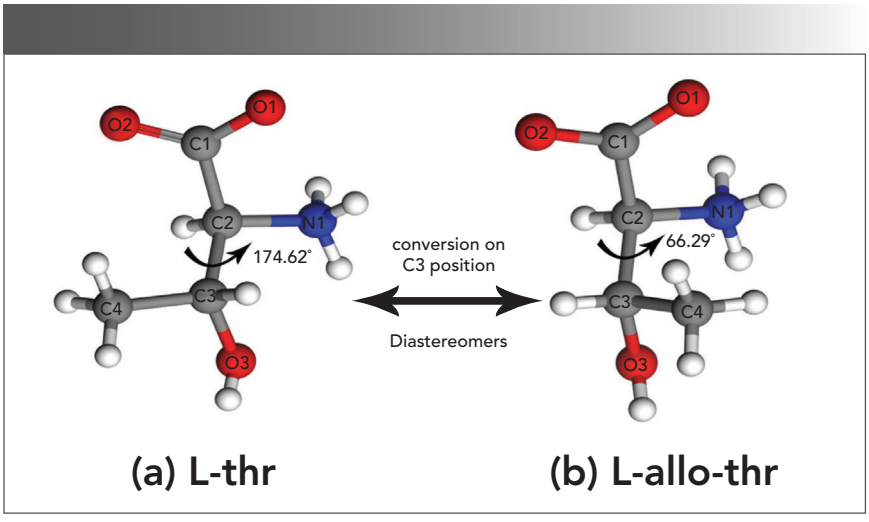

FIGURE 1: The molecular structure of (a) L-thr (a) and (b) L-allo-thr.

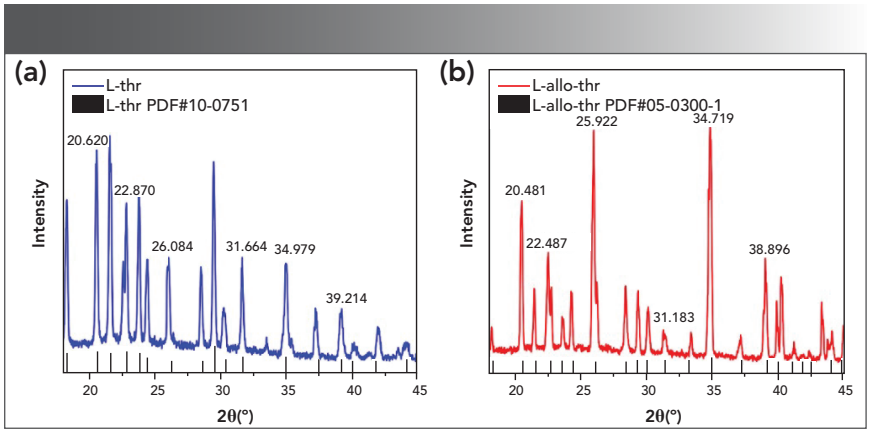

FIGURE 2: XRD patterns of (a) L-thr and (b) L-allo-thr.

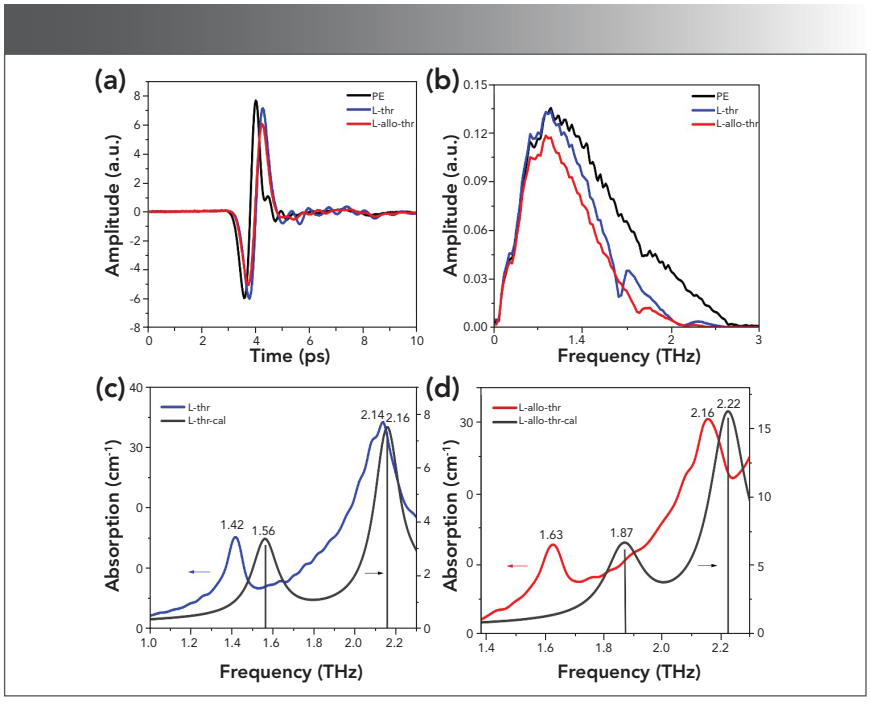

FIGURE 3: (a) Time domain spectra and (b) frequency domain spectra of reference PE and amino acid samples. Experimental and theoretical THz absorption spectra of (c) L-thr and (d) L-allo-thr.

TABLE II: Comparison of XRD and theoretical crystal structure data and hydrogen bonds of L-thr and L-allo-thr

Amino Acid	L-thr		L-allo-thr	
	CCDC	Optimization	CCDC	Optimization
a(Å)	13.63	13.543	5.142	5.401
b(Å)	7.753	7.779	7.741	8.199
c(Å)	5.162	5.116	13.711	13.564
v(Å3)	545.486	538.976	545.756	600.652
$O_2\cdots H_3$-N_1	1.91	1.741	1.906	1.711
$O_3\cdots H_2$-N_1	2.264	2.1	2.066	1.925
$O_1\cdots H_6$-O_3	1.948	1.637	1.85	1.701

Experimental Results and Discussion

XRD Analysis of L-thr and L-allo-thr

To confirm the crystal structure of the amino acid samples in this experiment, PXRD technology was used, and the results are shown in Figure 2. The measured main peak positions are in good agreement with the spectra matched by the Jade 6.0 standard PDF library (L-thr (PDF #10-0751), L-allo-thr (PDF #05-0300)). The agreement shows that the quality of the samples used in this experiment was higher. The XRD spectrum of L-thr was different from that of L-allo-thr, which was caused by the different crystal structures of the two amino acids.

THz Spectral Analysis and Cell Simulation Calculation of L-thr and L-allo-thr

PE has almost no absorption of the THz waves and can be used as the reference. The time domain spectra and frequency domain spectra of the reference and experimental samples are shown in the Figure 3a and 3b. Compared with the pure PE signal, the THz time-domain signal of samples containing amino acids have time delay and amplitude attenuation. The time delay is mainly because the refractive index of the THz wave passing through sample is larger than the reference, and the time delay increases with the increase of sample thickness. Meanwhile, the attenuation of signal intensity is caused by the absorption and random scattering of the THz wave by the samples. Using Matlab software, fast Fourier transform was performed on the THz time-domain spectra of the samples, and the THz frequency domain spectra can be obtained. Compared with PE, the frequency domain spectra of the L-thr and L-allo-thr samples not only has corresponding amplitude attenuation, but also has several distinct and unique characteristic absorption bands.

Figure 3 also shows the experimental and theoretical THz absorption spectra of L-thr (Figure 3c) and L-allo-thr (Figure 3d), respectively, with significant differences in the frequency range of

1.0–2.3 THz. The characteristic peaks of L-thr are located at 1.42 and 2.14 THz (11,12,22,23), and the characteristic peaks of L-allo-thr are located at 1.63 and 2.16 THz. It shows that L-thr and L-allo-thr can be distinguished by a THz fingerprint, which is consistent with the THz spectral results of L-thr in other literatures. Currently, there are no reports on the spectral studies of L-allo-thr. In addition, theoretical simulations can link the calculated vibration patterns to the molecular structure. The experimental and theoretical characteristic peaks of these two amino acids obtained by DFT crystal structure calculation based on GGA-PBE are listed in Table I. The theoretical characteristic peaks of L-thr are 1.56 and 2.16 THz, which corresponded to the experimental results of 1.42 and 2.14 THz. The theoretical characteristic peaks of L-allo-thr are 1.87 and 2.22 THz, corresponding to the experimental results of 1.63 and 2.16 THz. The two amino acids simulation peaks are blue shifted relative to the experimental characteristic peaks, and the largest error is that L-allo-thr is blue shifted 0.24 THz at 1.63 THz. According to the comparison of XRD data of L-thr and L-allo-thr and the optimized intermolecular hydrogen bonds in Table II, it can be seen that the intermolecular hydrogen bond lengths in their crystal cells are shortened. These shortened bond lengths further resulted in the increase of vibration frequency, the change of electron orbital density of amino acid molecules, and the internal structure reorganization. Thus, blue shift would be triggered (24,25). On the other hand, the DFT calculates the absorption frequency at the temperature of 0 K, whereas the experimental spectra are all measured at room temperature, and the difference of temperature will also cause blue shift (26–28).

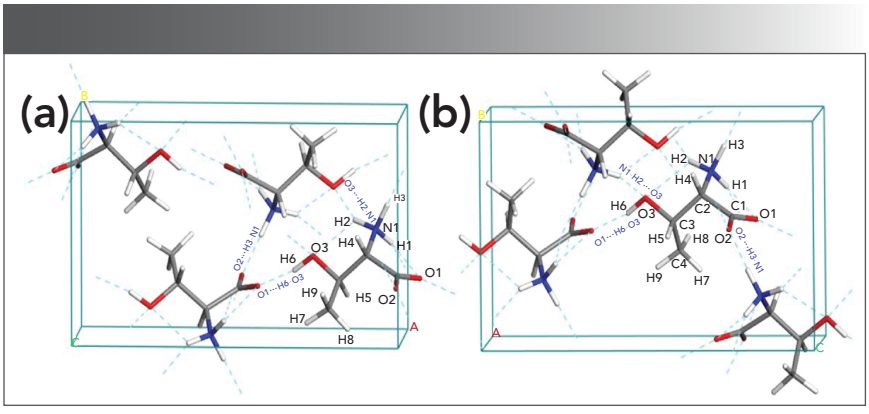

FIGURE 4: The crystal structure of unit cells of (a) L-thr and (b) L-allo-thr.

Hydrogen Bond Network Structure Analysis and Vibration Mode Attribution of L-thr and L-allo-thr

Figure 4 shows the hydrogen bond network structure in unit cell of L-thr (Figure 4a) and L-allo-thr (Figure 4b), respectively. L-thr and L-allo-thr have the same atoms and number of atoms, forming three identical hydrogen bond types, namely O_2···H_3-N_1, O_3···H_2-N_1 and O_1···H_6-O_3, respectively. The threonine molecules in the crystal exist in the form of zwitterions, where two hydrogen bonds come from NH_3^+ and one hydrogen bond from COO- (29). Both of them are all hydrogen bond networks formed between carbonyl, carboxyl, and amino groups through O···H-N and O···H-O, connecting with neighboring molecules (7,30–32). However, L-thr and L-allo-thr are diastereomers of each other, and there are certain differences in the hydrogen bond interaction between them. Between cells, L-thr requires three threonine molecules to form a three-dimensional (3D) hydrogen bond network, whereas L-allo-thr requires four allo-threonine molecules.

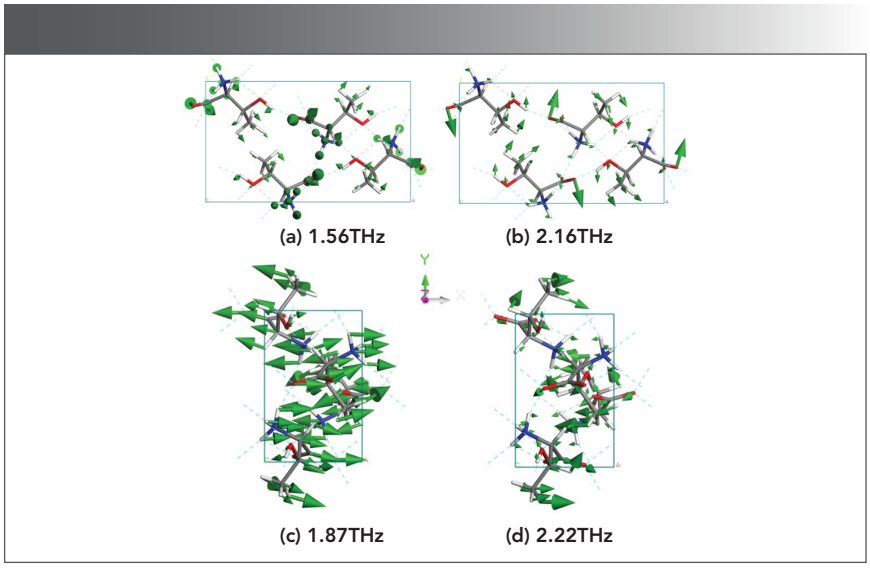

FIGURE 5: The vibration modes of the crystal structure calculated by L-thr at (a) 1.56 THz and (b) 2.16 THz, and L-allo-thr at (c) 1.87 THz and (d) 2.22 THz, respectively.

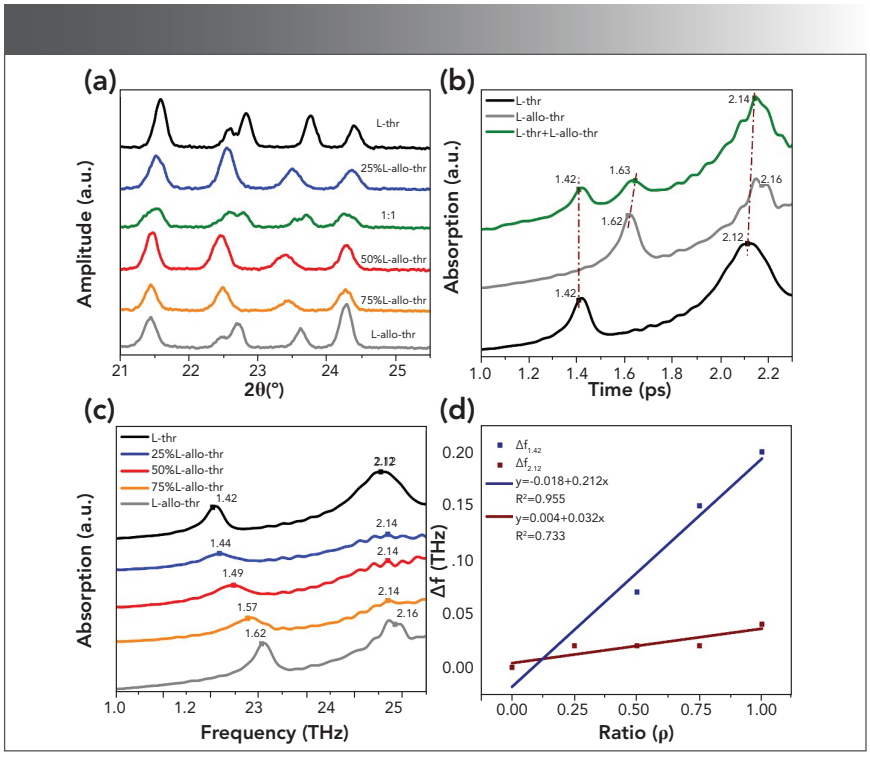

FIGURE 6: (a) The XRD patterns of co-crystallized mixtures and physical mixture, (b) THz spectra of L-thr, L-allo-thr and their physical mixture, (c) THz spectra of cocrystallized mixtures (L-thr, 25%, 50%, 75%, L-allo-thr), (d) the correlation between the frequency offset of the co-crystallized mixtures' characteristic peaks (Δf, relative to the characteristic peaks at 1.42 and 2.14 THz of L-thr at zero) and the composition ratio of L-allo-thr.

Figure 5 shows the calculated crystal structure vibration modes of L-thr at 1.56 (Figure 5a) and 2.16 (Figure 5b), and the structural modes of THz and L-allo-thr at 1.87 (Figure 5c) and 2.22 (Figure 5d) THz, respectively. A variety of vibration modes exist in the 1–2.3 THz region mainly because of the hydrogen bond interaction, leading to the specific structure in the crystal and resulting in the specific vibration behavior of different characteristic peaks in the THz frequency band (6). There are certain differences in the location of the THz characteristic peak and corresponding vibration modes between L-thr and L-allo-thr, which are mainly attributed to the deviation of their cell parameters, including the length of hydrogen bonds and the volume of the unit cell (33). It can be seen from Table I that the volume of the unit cell of L-allo-thr after optimization is much larger than that of L-thr. The reduction in the distance between the nitrogen and oxygen atoms in adjacent molecules in a unit cell leads to the enhancement of intermolecular interactions, especially the short-range force of hydrogen bonds. Small differences in the structure of molecules will cause changes in the hydrogen bond energy and bond length (7,33,34). Therefore, compared with L-allo-thr, the crystal structure of L-thr is denser, the noncovalent interaction is stronger, and the intermolecular motion is stronger. The detailed description of the calculated vibration modes of L-thr and L-allo-thr is shown in Table I. At 1.56 THz, L-thr is reflected in the swinging vibration of the amino and carboxyl groups connected with hydrogen bonds along the *z*-axis. The vibration mode at 2.16 THz was the carboxyl group in-plane swing vibration and the collective swing vibration of C_4H_3, whereas the vibration mode of L-allo-thr at 1.87 THz was mainly because of the collective swing vibration of all atoms along the *x*-axis. The absorption peak at 2.22 THz was the rocking vibration in the base plane of R and the collective swing vibration of C_4H_3-C_3-H_5. It can also be seen from Figure 5 that the group connected with hydrogen bond in the crystal cell vibrates significantly. Therefore, within the effective THz frequency range, the vibration mode between L-thr and L-allo-thr molecules were mainly swing vibration modes centered on intermolecular hydrogen bonds.

Qualitative and Quantitative Analysis of the Co-crystallized Mixtures of L-thr and L-allo-thr

The L-thr and L-allo-thr powders were mixed in a fixed ratio and completely dissolved in deionized water, recrystallized in a vacuum oven at 50 °C, and formed a new phase. In addition, a 1:1 physical mixed tablet of L-thr and L-allo-thr was prepared. The two solid drugs were simply mixed together and pressed into tablets. To further determine the formation of co-crystallized mixtures, we also used PXRD technology to characterize the structure of these samples. The crystal structure changes after co-crystallized can be clearly seen from Figure 6a. The diffraction patterns of L-thr and L-allo-thr in Figure 6 have similar configurations; for the physical mixtures, the diffraction patterns contain most of the diffraction peaks of the two groups of pure enantiomers. For co-crystallized mixtures, their diffraction peaks tend to be wider and not as sharp as those measured by the pure components. Moreover, the total diffraction peaks are gradually biased to the pure L-allo-thr with the increase of the L-allo-thr component. The results show that L-thr and L-allo-thr form co-crystallized structures through noncovalent bonding successfully, especially driven by strong intermolecular hydrogen bonds, whereas the mixtures do not involve such hydrogen bonds or other noncovalent interactions (35).

Figure 6b shows the THz absorption spectra of L-thr, L-allo-thr, and their 1:1 physical mixture. Figure 6c shows the THz absorption spectra of co-crystallized mixtures with different proportions. The THz spectra of the physical mixture has three characteristic peaks: one of the absorption peaks at 2.14 THz was relatively strong, and the other two absorption peaks at 1.42 THz and 1.63 THz were relatively weak because the spectra at 2.14 THz was affected by the common absorption of two amino acids (36). As a result, the absorbance was slightly improved. The results showed that the measured absorption peaks of the physical mixture corresponded to the experimental absorption peaks of the two pure diastereomeric components L-thr and L-allo-thr. However, the THz spectra of the eutectics contained two characteristic peaks. One of the weaker absorption peaks was located at 2.14 THz, and the other characteristic peaks of cocrystallized mixtures were respectively located at 1.44, 1.49, and 1.57 THz for 25%, 50% and 75% L-allo-thr. With the gradual increase of L-allo-thr components in co-crystallized mixtures, their characteristic peaks are closer to those of pure L-allo-thr (4). The significant difference here can be used for identifying co-crystallized mixtures in different proportions. The co-crystallized mixtures with different crystal structures have their own characteristic peaks, and the difference in the characteristic absorption peaks of the 1:1 physical mixture and co-crystallized mixtures was because of the THz experimental spectra caused by the collective low frequency vibration mode of the molecules (16).

In addition, Figure 6d is a linear fitting between the frequency offset of the co-crystallized mixtures characteristic peaks (Δf) and the composition ratio of L-allo-thr, which was relative to the characteristic peaks of L-thr at 1.42 and 2.14 THz. The results show a blue–red straight line, in which the fitting equation of $\Delta f_{1.42}$ is $y = -0.018 + 0.212x$, $R^2 = 0.955$ (1), and the fitting equation of $\Delta f_{2.12}$ is $y = 0.004 + 0.032x$, $R^2 = 0.733$ (2), where *y* represents the relative frequency offset, *x* represents the composition ratio of L-allo-thr, R^2 is the correlation coefficient of linear fitting, where the R^2 of the blue line is greater than the R^2 of the red line, indicating that the fitted line between $\Delta f_{1.42}$ and the composition ratio of L-allo-thr is in good agreement with the experimental data because with the increase of the absorption coefficient of the THz spectrum in the high-frequency region, the signal-to-noise (S/N) ratio decreases. This relationship enabled us to quickly determine the composition ratio of L-thr and L-allo-thr in co-crystallized mixtures according to the frequency offset of characteristic peaks (8,17,37,38).

Conclusion

The absorption spectra of the L-thr and L-allo-thr diastereomers were studied by THz-TDS, and the results calculated by DFT were in good agreement with the measured characteristic peaks. The cell configurations of L-thr, L-allo-thr, and the differences between various low-frequency vibration modes were analyzed from the perspective of hydrogen bond configurations. It was found that the hydrogen bond between the amino group, carboxyl group, and the side hydroxyl group between the cell molecules was the main cause of the molecular skeleton vibration. The THz spectra of the 1:1 physical mixture and co-crystallized mixtures of L-thr and L-allo-thr showed that the THz absorption characteristics of the physical mixture included the absorption characteristics of the two pure diastereomers, and the co-crystallized mixtures comprised of diastereomers in different proportions had their own distinct characteristic peaks. It was indicated that the THz-TDS technique provided a feasible method for the quantitative analysis of the co-crystallized mixtures formed by diastereomers L-thr and L-allo-thr.

References

(1) N. Taratin, H. Lorenz, D. Binev, et al., *Cryst. Growth Des.* **15**(1), 137–144 (2015).

(2) H. Zhao, K. Hamase, A. Morikawa, et al., *J. Chromatogr. B Analyt Technol. Biomed. Life Sci.* **810**(2), 245–250 (2004).

(3) X. Xu and Z. Lin, *J. Mol. Struct.: Theochem.* **962**(1–3), 23–32 (2010).

(4) D. Binev, N. Taratin, E. Kotelnikova, et al., *Cryst. Growth Des.* **14**(1), 367–373 (2014).

(5) E.N. Kotelnikova, A.I. Isakov, L.Y. Kryuchkova, and A.A. Zolotarev, in *Processes and Phenomena on the Boundary between Biogenic and Abiogenic Nature* (Springer, Berlin, Germany, 2020), pp. 695–719.

(6) C. Song, W.-H. Fan, L. Ding, et al., *Sci. Rep.* **8**(1), 8964 (2018).

(7) L.-j. Huang, X. Zhang, G. Wang, et al., *Spectrosc. Spect. Anal.* **37**(8), 2462–2466 (2017).

(8) T. Zhou, Y. Wu, J. Cao, et al., *Appl. Spectrosc.* **71**(2), 194–202 (2017).

(9) L. Xu, Y. Li, Q. Zhou, et al., *Spectrochim. Acta A.* **224**, 117468 (2020).

(10) Z. Wu, Z. Zhu, C. Cheng, et al., *Spectrochim. Acta A.* **225**, 117509 (2020).

(11) W.-N. Wang, *Acta Physica Sinica.* **58**(11), 7640–7645 (2009).

(12) W. Li, F. Yan, Z.-c. Wang, et al,. *Spectrosc. Spect. Anal.* **40**(7), 2054–2058 (2020).

(13) A.I. Isakov, E.N. Kotelnikova, S. Muenzberg, et al., *Crys. Growth Des.* **16**(5), 2653–2661 (2016).

(14) E.N. Kotelnikova, A.I. Isakov, and H. Lorenz, *Crystengcomm.* **19**(14), 1851–1869 (2017).

(15) A.I. Isakov, H. Lorenz, A.A. Zolotarev, Jr., et al,. *Crystengcomm.* **22**(5), 986–997 (2020).

(16) E. Kotelnikova, R. Sadovnichii, L. Kryuchkova, et al., *Crystals* **10**(7), 618 (2020).

(17) M. Yamaguchi, F. Miyamaru, K. Yamamoto, et al., *Appl. Phys. Lett.* **86**(5), (2005).

(18) S.J. Clark, M.D. Segall, C.J. Pickard et al., *Z. Kristallogr.* **220**, 2567–2570 (2005).

(19) D.P. Shoemaker and B.G. Bergman, *J. Am. Chem.* **72**(12), 5793(1950).

(20) D.Z.J. Janczak and P. Luger, *Acta Crystallogr. C Cryst. Struct. Commun.* **C53,** 1901–1904 (1997).

(21) P. S. Swaminathan, *Acta Cryst.* **B31**, 217–221 (1975).

(22) W.-N. Wang, H.-Q. Li, Y. Zhang, et al., *Acta Physico-Chimica Sinica.* **25**(10), 2074–2079 (2009).

(23) Z.-f. Tang, H.-t. Lin, X.-w. Chen, et al., *Spectrosc. Spec. Anal.* **29**(9), 2351–2356 (2009).

(24) Q. Cai, J. Xue, Q. Wang, et al., *J. Mol. Struc.* **1153**, 170–178 (2018).

(25) P. Hobza and Z. Havlas, *Chem. Rev.* **100**(11), 4253–4264 (2000).

(26) S. Zong, G. Ren, S. Li, et al,. *J. Mol. Struct.* **1157**, 486–491 (2018).

(27) J. Liang, X. Zhang, N. Wang, et al., *Spectrochim. Acta A Mol. Biomol. Spectrosc.* **228**, 117591 (2020).

(28) Z. Zhu, G. Ren, C. Cheng, et al., *Chin. J. Lasers* **46**(6), 0614017 (2019).

(29) M.T. Ruggiero, J. Sibik, J.A. Zeitler, et al., *J. Phys. Chem. A.* **120**(38), 7490–7495 (2016).

(30) Y. Li, L. Xu, Q. Zhou, et al., *Spectrochim Acta A Mol. Biomol. Spectrosc.* **214**, 246–251 (2019).

(31) T.B. Issa, F. Sayari, H. Ghalla, et al., *J. Mol. Struct.* **1178**, 436–449 (2019).

(32) Y. Li, L. Xu, H. Li, et al., *J. Mol. Struct.* **1180**, 636–641 (2019).

(33) Z. Wu, Z. Zhu, C. Cheng, et al., *Spectrochim. Acta A Mol. Biomol. Spectrosc.* **225**, 117509 (2020).

(34) M. Ge, H. Zhao, W. Wang, et al., *J. Biol. Phys.* **32**(5), 403–412 (2006).

(35) B. Xwa, C. Yw, D. Jx, et al., *Spectrochim. Acta A.* **234,** 118265 (2020).

(36) F. Huang, S. Zhuang, W. Liu, et al., *Spectrochim. Acta A Mol. Biomol. Spectrosc.* **248**, 119277 (2021).

(37) Y. Du, Y. Xia, H. Zhang, et al., *Spectrochim. Acta A Mol. Biomol. Spectrosc.* **111**, 192–195 (2013).

(38) H. Yan, W. Fan, X. Chen, et al., *Spectrochim. Acta. A Mol. Biomol. Spectrosc.* **258**, 119825 (2021).

Ruonan Zeng, Yujing Bian, Xun Zhang, Zhenqi Zhu, and Bin Yang are with the College of Materials and Textiles at Zhejiang Sci-Tech University, in Zhejiang, China. **Yang** is also with the Key Laboratory of Advanced Textile Materials and Manufacturing Technology of Ministry of Education at Zhejiang Sci-Tech University, in Zhejiang, China. Direct correspondence to: yangbin5959@zstu.edu.cn ●

Savillex

Savillex C-Flow Nebulizers

Consistent Nebulizer-to-Nebulizer Performance.

The C-Flow's unique, two-piece design is made possible by Savillex's expertise in fluoropolymer injection molding, allowing for precise manufacturing and higher, more consistent performance than any other PFA nebulizer.

Don't Settle for Less.

Savillex
10321 West 70th St. | Eden Prairie, MN USA | Phone: 952.935.4100
www.savillex.com

Key Steps to Follow in a FRET Experiment

W. Russ Algar

Förster resonance energy transfer (FRET) is a versatile part of the toolbox of fluorescence methods. This through-space, photon-less energy transfer process between a donor fluorophore and an acceptor chromophore is perhaps most famous for its utility as a "molecular ruler" that can resolve nanometer-scale distances. FRET is also a popular and advantageous basis for biomolecular assays and sensors.

One of the most attractive features of the Förster resonance energy transfer (FRET) mechanism is that it can be measured with the simplest of fluorimeters up through to the most advanced single-molecule fluorescence systems. However, this relative simplicity sometimes belies careful considerations that must be taken into account in most FRET experiments. As the user base for FRET and the scope of its applications continues to grow, it is important to understand how to design an optimized and rigorous FRET experiment. This article provides a brief overview of the key considerations, most of which are linked to Figure 1. A much more detailed and broader scope of guidance can be found in the literature (1), and readers are encouraged to review the fundamental FRET theory in the literature (2,3).

Know the Limits of Common Theory

Although basic FRET theory can be found in numerous publications and on a multitude of websites, these basics are not always sufficient. For example, the classic equation (shown in Figure 1a) for FRET efficiency (the probability of FRET occurring) applies to a uniform ensemble of discrete one donor–one acceptor pairs. This equation must be modified if multiple acceptors interact with a common donor, and will often be a poor approximation if multiple donors interact with a common acceptor, if a system is highly heterogeneous in its donor–acceptor combinations, or if different FRET pathways compete with one another. Such non-classic systems will need to be modeled using analyses that compare the rates of the various FRET pathways against one another and the rates of other excitation and relaxation processes (4).

Furthermore, many sources present the equation for the FRET-relevant spectral overlap integral (between donor emission and acceptor absorption) without specifying units for the quantities, which must be correct for downstream estimation of the Förster distance, R_0 (Figure 1b). Units should thus be confirmed in a reference source or assessed by dimensional analysis. Most estimations of a Förster distance will also assume a "dynamic averaging regime" with an orientation factor of $\kappa^2 = 2/3$ between donor and acceptor (Figures 1b, 1c). A recent perspective has addressed potential challenges from this assumption in detail (5). Adopting $\kappa^2 = 2/3$ or another "special" value (such as, for example, static averaging regime) is not necessarily a bad

Spectroscopy

SOLUTIONS FOR MATERIALS ANALYSIS

More learning tools for **spectroscopists** exclusively online

Webcasts

View our educational webcasts **live or on demand** in topics such as ICP methods, raman fundamentals, atomic spec, microplastics, and many more!

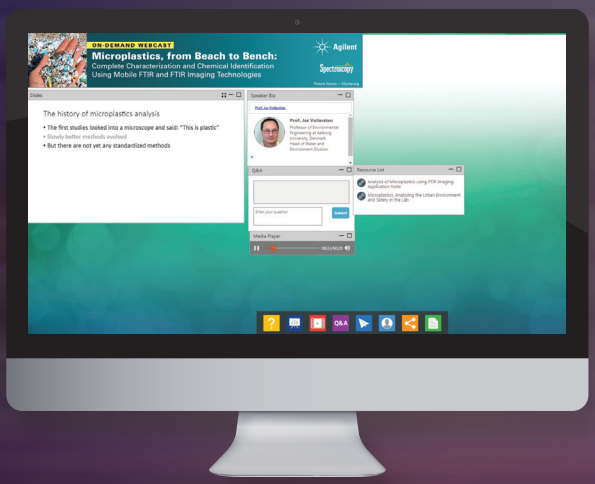

eBooks

Choose from topics such as food safety, sample prep, raman imaging, atomic absorption and more!

Visit spectroscopyonline.com today!

AN MJH life sciences™ BRAND

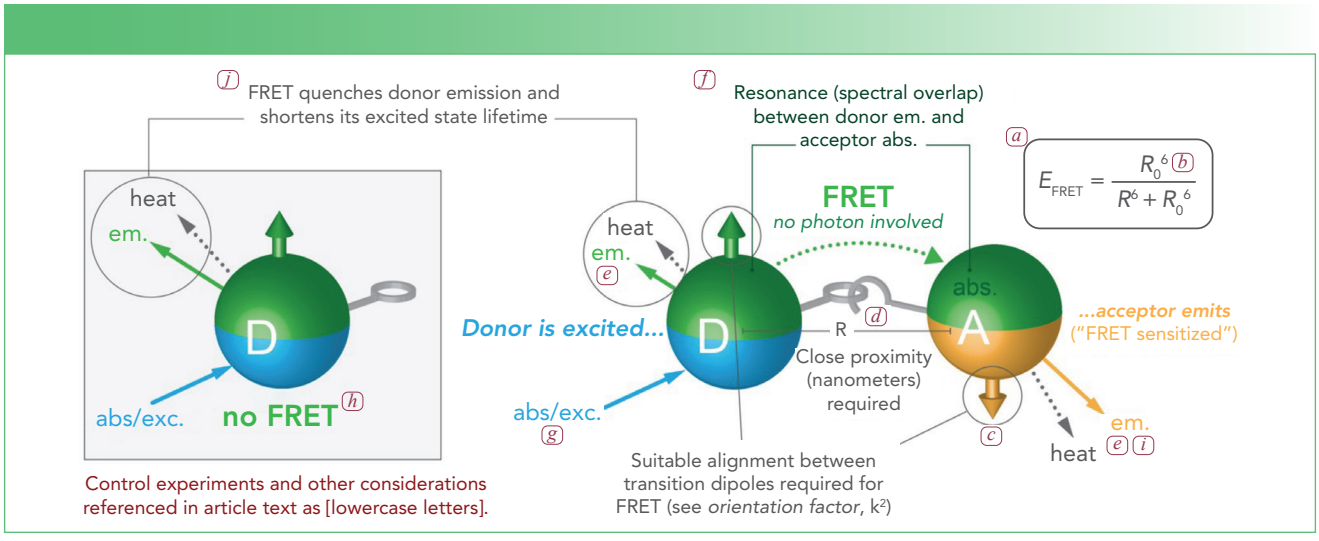

FIGURE 1: Conceptual illustration of FRET. Parts of this illustration are linked to the discussion in the text through lowercase letter labels (a–j).

practice, provided the uncertainties associated with this assumption are factored into drawing conclusions from an experiment—a conclusion predicated on an accurate and precise value for κ^2 is usually not a solid conclusion.

Define the Mechanism of Donor-Acceptor Proximity

An essential requirement of FRET is close proximity between donor and acceptor, usually within 10 nm, but up to approximately 15 nm in special cases. A rigorous FRET experiment will rationally design or, at minimum, understand the origin of donor-acceptor proximity (Figure 1d). Common approaches include having the donor and the acceptor attached to the same macromolecular scaffold, and also having molecules that are separately labeled with donor and acceptor interacting through specific binding, aggregation, or assembly on a common scaffold or surface.

Match the Measurement Modality and FRET Metric to the Objective and Limitations of the Experiment

FRET is famously useful as a "molecular ruler" because the energy transfer efficiency can be used to measure the nanometric distance between donor and acceptor. For such measurements, it is important that the FRET efficiency has maximum variation around the distance of interest. This means avoiding too close an approach to the plateaus in FRET efficiency near 0 and 100%. A mathematical model of FRET efficiency versus distance for a hypothetical system will indicate a range over which efficiency is approximately linear with distance, although the overall relation is sigmoidal.

FRET is also a useful mechanism for sensors. For this application, it is often preferred that the FRET efficiency switches between a negligible value (~0%) and a significant value upon detection of the target analyte (or otherwise maximizes the relative change in the measured FRET signal). This signal change also has a role in determining the concentration of FRET probe that should be used. For example, if it is possible to detect the switch in FRET efficiency for one probe out of 100, then the concentration of probe should not exceed 100-fold of the lowest concentration of target analyte to be detected.

A FRET measurement must also be designed around the available technical capabilities. Important considerations are as follows: whether the metric for assessing FRET will be based on fluorescence intensity or lifetime; whether this metric will be measured for the donor, the acceptor, or both (as applicable); and whether resolution of donor and acceptor emission will be via emission filters or spectrally via monochromator (Figure 1e). For the latter, spectral measurements allow more robust correction of overlapping donor and acceptor fluorescence emission and may thus accommodate a wider array of potential donor–acceptor pairs. Crosstalk between detection channels (wavelengths or filters) for donor and acceptor emission is common and should be checked for, and may require mathematical correction to avoid skewing the value of the chosen FRET metric.

Ensemble FRET efficiency is best reserved as a metric for homogeneous systems. The apparent ensemble efficiency for heterogeneous systems is a function of both the real FRET efficiencies and fractions of whatever subpopulations are in the system. Thus, the ensemble efficiency for a heterogeneous system loses meaning without independent knowledge of the sub-populations. For example, sensing applications detect initially unknown concentrations of the analyte and are better suited to a metric such as donor intensity or lifetime, acceptor intensity, or an acceptor–donor intensity ratio.

Donor and acceptor fluorescence intensities are simple and versatile metrics, but have the drawbacks of being sensi-

A New Compact, Powerful, FTIR Spectrometer

Introducing the FT/IR-4X

The latest in a very long line of IR instruments dating back to the 1950s, the innovative 4X compact FTIR spectrometer has many new features for simplified operation and a long life, including:

- Completely sealed aluminum interferometer (with humidity sensor) protecting the source, beam-splitter, and diode laser
- Great for routine operation in the mid-IR, with options for near- to mid-IR and from mid- to far-IR
- Integrated broad-range monolithic diamond ATR, with wavenumber range sensing
- Large sample compartment compatible with virtually all legacy accessories

Spectra Manager™ Suite 2.5 has many new features for user automation to get better data, faster.

Visit our website to find out more or to book a 15 minute online demonstration.

www.**jasco**inc.com/4X

JASCO

tive to the concentration of the FRET pair, measurement volume, and drift or fluctuation in instrumentation. The acceptor–donor intensity ratio and donor fluorescence lifetime are more robust metrics because they are approximately insensitive to sample volume and concentration over whatever range the donor–acceptor proximity is unaffected by concentration. An acceptor–donor intensity ratio and donor fluorescence lifetime are also either self-correcting or less affected by many forms of instrumental drift or fluctuation. Many interesting applications of FRET have a biological system as the gatekeeper of a number of FRET probes being measured (not well-controlled by the experimentalist), making this advantage significant.

Another consideration is whether an ensemble measurement is satisfactory or if single-molecule measurements are necessary. Single-molecule measurements are most informative when heterogeneity or asynchronous processes within a sample are of interest, but are beyond the scope of this short article.

Choose an Optimum Donor–Acceptor Pair

The first and best-known criterion for a good donor–acceptor pair is substantial overlap between the donor emission spectrum and the acceptor absorption spectrum (Figure 1f). However, the considerations do not stop here. The magnitude of the Förster distance must be commensurate with the experimental objective and the mechanism of donor–acceptor proximity. Moreover, the labeling chemistries, solubility, charges, and sizes of the donor and acceptor should also be good matches to the mechanism of proximity. For a FRET pair where both donor and acceptor are fluorescent, it is also preferable that there is an excitation wavelength for the donor at which direct excitation of the acceptor is negligible (Figure 1g). The choices of donor and acceptor must also align with available technical capabilities (such as satisfactory excitation wavelengths and emission filters, suitable resistance to photobleaching). For all of the foregoing, there are pros and cons for the many candidate donor and acceptor materials available, which range from organic dyes to fluorescent proteins to various nanoparticles. One should go into a FRET experiment anticipating that multiple FRET pairs may need to be tried to achieve optimum results.

Implement Control Samples

Some general challenges with fluorescence include the potential sensitivity of the fluorescence intensity of a dye to its local microenvironment (such as viscosity or other restriction of movement, solute concentrations, and more), the lack of a standardized unit for fluorescence intensity, and potentially large differences in brightness between different fluorophores. Consequently, control experiments that ensure that changes in donor and acceptor emission arise from FRET and not from other processes are essential. With only a few exceptions, experimental samples and control samples must usually be measured under the same instrument and with the same settings.

The minimum control sample is a no-FRET reference state (Figure 1h) with only the donor, but more control samples would be beneficial. For example, reabsorption of the donor emission by an acceptor could give the appearance of donor quenching and acceptor sensitization, but is not actually FRET. A control experiment that has a combination of donor and acceptor but with disrupted proximity (Figure 1d) will guard against such trivial energy transfer via reabsorption. If the mechanism of proximity is sufficiently robust, consistent FRET metrics over a range of dilutions may also be a guard against trivial energy transfer.

For a fluorescent acceptor, another important control is a sample with only an acceptor to distinguish between FRET-sensitized acceptor emission and directly-excited acceptor emission (Figure 1i). Potential brightness differences mean that the latter cannot be reliably assumed to be negligible simply from qualitative inspection of an absorption spectrum.

It is also good practice to ensure that two metrics yield similar FRET efficiencies for samples expected to have maximum FRET. Commonly, the decreases in donor intensity and lifetime (relative to a no-FRET reference state) are compared (Figure 1j). Commensurate values will tend to indicate an absence of trivial energy transfer. Even when not the preferred metric for all the experiments, a one-time measurement of lifetime may help to confirm FRET. Alternatively (or in addition), quantitative comparison of a measured FRET metric to a predicted one can be diagnostic, as a large discrepancy may indicate something other than FRET (or a poor model of an actual FRET system).

Summary

Ensemble FRET measurements are both powerful and accessible to a broad array of experimentalists. Although it surprisingly easy to be fooled into a false observation of FRET, it does not take much additional effort or resources to safeguard against false observations. Again, this article is intended to be a starting point—there are certainly details and special cases beyond the scope of this text. Nevertheless, the above guidance is a solid foundation for many applications of FRET.

References

(1) W.R. Algar, N. Hildebrandt, S.S. Vogel, and I.L. Medintz, *Nat. Meth.* **16**, 815–829 (2019).

(2) N. Hildebrandt, C.M. Spillmann, W.R. Algar, T. Pons, M.H. Stewart, E. Oh, K. Susumu, et al, *Chem. Rev.* **117**, 536–711 (2017).

(3) B.W. van der Meer, in *FRET – Förster Resonance Energy Transfer*, I.L. Medintz and N. Hildebrandt, Eds. (Wiley-VCH Verlag GmbH & Co., Weinheim, Germany, 2013), pp. 23–62.

(4) M. Massey, H. Kim, E.M. Conroy, and W.R. Algar, *J. Phys. Chem. C* **121**, 13345–13356 (2017).

(5) B.W. van der Meer, *Meth. Appl. Fluoresc.* **8**, 030401 (2020).

W. Russ Algar is with the Department of Chemistry at the University of British Columbia, in Vancouver, British Columbia, Canada. Direct correspondence to: algar@chem.ubc.ca

Understanding the Fundamental Components of Sample Introduction for ICP-OES and ICP-MS

Simon Nelms and Daniel Kutscher

Analytical techniques based on inductively coupled plasma (ICP) are commonly used for analyzing the elemental composition of a sample and are widely applied in analytical testing laboratories. Particularly for larger laboratories, analysis time and throughput are essential performance indicators, which can be severely impacted if sample analysis needs to be repeated because of insufficient stability or quality control (QC) failures. However, such failures are, in many cases, avoidable by selecting the right configuration of the sample introduction system of the instrument. This tutorial explains the most critical components of the sample introduction system of modern ICP-optical emission spectroscopy (OES) and ICP-mass spectrometry (MS) instruments, providing analysts with a guide for initial configuration settings and recommended maintenance intervals for reliable daily operation.

Inductively coupled plasma (ICP), when combined with optical emission spectroscopy (OES) and mass spectrometry (MS), is a well-established tool for elemental analysis. Continued technological development has led to significant increases in sensitivity and interference removal (for common polyatomic as well as other types of interferences). However, the technology surrounding sample introduction has remained comparable over the years.

Many of the challenges analysts face today, such as signal suppression, drift, or even failure of quality control (QC) checks can be related to the sample introduction system setup. In many cases, incorrect configuration or errors during routine maintenance are the root cause for these issues.

Unexpected Contamination: Sample Vials and Tubing

Techniques such as ICP-OES and ICP-MS provide the high sensitivity required to analyze the concentrations of toxic metals at trace and ultra-trace levels. However, high sensitivity makes both techniques susceptible to problems associated with unintended contamination, such as increased background levels, elevated detection limits, or over and underestimated results. There are multiple ways in which a sample can become contaminated, including, but not limited to, sample preparation, workplace cleanliness, and the purity of reagents used (that is, acids used in digestion or dilution steps). However, in most cases, the impact of plasticware used in the laboratory is underestimated. Plasticware comprised of perfluoroalkoxy (PFA) polymers is known to be available in high purity, whereas vials that are used for sample storage are often made from polypropylene (PP) or polyethylene (PE), which have lower purity.

Before starting an analysis, it is good practice to look at the quality of all materials and reagents used in the sample preparation process. Contamination can arise from the surrounding laboratory environment (even in areas dedicated to trace metal analysis) where sporadic and unexpected contamination can occur. Usually, this contamination can be attributed to residues in the plasticware used, such as vessels or peristaltic pump tubing. Many laboratories refrain from switching suppliers of sample tubes because it can potentially introduce contamination because of differences in the manufacturing processes and materials. Although most tubes are fairly clean, experience has shown that vial caps can be a significant source for metal contamination, particularly aluminum, zinc, nickel, and copper. The extent of contamination can be significantly reduced

TABLE I: Appropriate configuration of the sample introduction system for different sample types in ICP-OES

Configuration	TDS > 0.5%	TDS > 3%	TDS > 10%	Organic
Nebulizer	Glass concentric nebulizer	Glass concentric nebulizer	Parallel path nebulizer	V-Groove
Spray chamber	Glass cyclonic	Glass cyclonic	Baffled spray chamber	Baffled spray chamber
Center tube	Normal bore (1.5 or 2.0 mm i.d.)		Large bore (>2.5 mm i.d.)	Narrow bore (1.0 mm i.d.)
Torch	Quartz	Quartz/ ceramic	Ceramic torch	Ceramic torch
Other	N/A	Online addition of internal standard using a T-piece can reduce plasma load	Addition of a sheath gas prior to the torch can help improve stability	Consider spray chamber temperature, addition of compressed air or oxygen to improve plasma stability

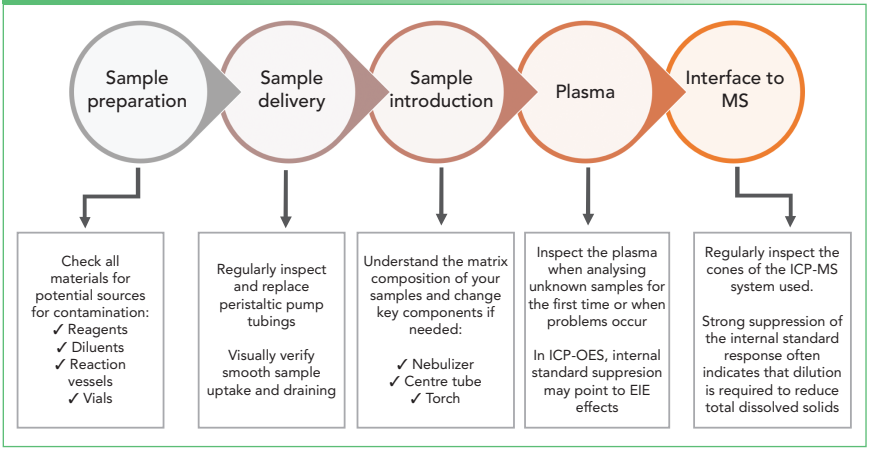

FIGURE 1: The route to success in managing the analysis of previously unknown sample types.

by rinsing vials and caps with dilute nitric acid prior to use. The same considerations may apply to peristaltic pump tubing (typically made from polyvinyl chloride [PVC]). A brief cleaning or conditioning with an acidic solution (a few minutes is sufficient) can wash out any unwanted traces of metals before they can be introduced into the sample analysis.

Sample Consumption and Handling: Peristaltic Pump, Nebulizer, and Spray Chamber

Problems with an incorrect sample delivery to the plasma often express themselves in a secretive manner. An important parameter to be checked during the daily performance check is the short-term stability of the system, or percent relative standard deviation (%RSD), of the signal determined over a period of 10 min. Some laboratories or methods require continuous monitoring of the signal stability in each run, where data showing a %RSD greater than 2–3% must be discarded. In many cases, instabilities observed either during set up of the instrument or the sample analysis are related to the sample delivery to the plasma. The most common source of instability is related to the peristaltic pump delivery speed, the worn out peristaltic pump tubing, or the uneven draining of the spray chamber. When signal variation appears to be periodic (a similar pattern repeating every few seconds), sample delivery is most often found to be the source of the problem.

If increased signal fluctuation is only observed for a subset of analytes, the root cause can sometimes be found in the preparation of the sample. Elements, such as aluminum or iron, need to be stabilized in an acidic environment. If they are not, they may form colloid species like hydroxides, which can lead to unstable signals in both ICP-OES and ICP-MS. This problem can be observed with samples having a pH value of approximately 4, where additional acid is needed to lower the pH further to improve the stability of the signal.

When Problems Become Visible in ICP-OES: Torch

Have you ever noticed the central channel of your plasma turn orange when running an analysis? The orange glow is emission from excited sodium atoms and is a sign that your sample contains high levels of dissolved solids (typically dissolved salts of mainly sodium, potassium, magnesium, and calcium). In addition, the presence of organic solvents is immediately visible in an incorrectly configured system. In the latter case, the plasma exhibits a green emission followed by an orange glow from the carbon deposited at the sample cone tip, with the plasma often extinguishing after a short time. All instruments available on the market allow at least a visual observation of the plasma using a window. Certain instruments allow direct observation of the plasma directly on the control PC by means of a camera. In either case, a close look at the plasma when challenges are observed may help to identify issues with the analysis. In many cases, problems related to the analysis of difficult sample types, such as brine or organic solvents, can be overcome by selecting a different configuration of the sample introduction system configuration. Table I contains a few recommendations for analysis carried out using an ICP-OES instrument. ICP-MS is generally able to handle samples containing completely dissolved solids of up to 0.2% (m/v). Higher total dissolved solids can be handled by an ICP-MS instrument, but it would require a special configuration using argon gas from the

instrument as a diluent that is introduced to the sample flow at the spray chamber. If the samples contain hydrofluoric acid (HF), then all components of the sample introduction system need to be exchanged for HF-resistant versions.

More Than Just an Interface: The Role of Cones in ICP-MS

Although ICP-OES and ICP-MS have a lot in common when looking at the general setup of the sample introduction system, they differ significantly when it comes to the most important sample types. ICP-OES is able to analyze high matrix-containing samples such as brines and wastewater. On the other hand, ICP-MS is preferably applied for sample types that contain less problematic matrices or those that have undergone thorough cleanup procedures to remove the matrix components. The main reason for this distinction is that in ICP-MS, ions need to be transferred into the high vacuum of the mass spectrometer, whereas the emission of light can be viewed at an ambient atmosphere (residual air needs to be removed inside the optical system though to avoid emission signal absorption, particularly for wavelengths in the UV range of the spectrum). The ion extraction is accomplished in the interface with a set of two narrow orifices (less than 1 mm diameter) kept at an intermediate pressure level of less than 2 mbar. The interface cones of an ICP-MS can typically handle up to 0.2% (m/v) dissolved solids entering the plasma. Above this level, blocking of the orifices at the interface will occur, particularly on the skimmer cone where its cooler temperature makes it more prone to clogging from the buildup of accumulated solids. As mentioned previously, sample analysis with a higher matrix load by ICP-MS is possible with the introduction of argon gas as a diluent between the spray chamber and the torch. Although no manual dilution with a liquid is made, the sample flow is reduced, thus reducing the amount of matrix introduced. Lower sample flow results in a reduction in sensitivity of the system, but the impact on the method detection limits (MDL) is often not noticeable compared to a manual or automated liquid dilution. The direct analysis of samples (without prior manual dilution) is attractive as less diluents are used, reducing cost, labor, and the risk of errors or contamination. However, this approach is less flexible, with the dilution factor remaining constant for all the samples in a batch and samples containing less challenging matrix being analyzed under the same conditions (that is, reduced sample flow) as the more challenging samples. In addition, automated adjustment of the dilution factor (based on the concentration found in a sample relative to the calibrated range) is not possible as this causes a mismatch between the calibration solution signal response and the diluted (with a different dilution factor, that is not exactly calculated under argon gas dilution conditions) sample signal response.

Problems at the interface region can often be recognized by checking the response of the internal standards.

• Continued on Page 62

ICP-MS: Key Steps to Control Contamination and Achieve Low Detection Limits

Bert Woods and Ed McCurdy

Inductively coupled plasma–mass spectrometry (ICP-MS) instruments can perform low-level elemental analysis in a wide range of sample types, from high-purity chemicals to high matrix digests. But achieving consistently low detection limits requires good control of elemental contamination, as well as spectral interferences. A clean working area, careful selection of reagents, and good sample handling techniques are key to successful trace and ultra-trace elemental analysis. In this article, we provide five practical tips for controlling contaminants and minimizing detection limits.

Inductively coupled plasma-mass spectrometry (ICP-MS) instruments offer high sensitivity and low random background, which enables the technique to provide ng/L (ppt) level trace element analysis. However, routinely achieving low detection limits requires more than just a sensitive instrument. In industries such as semiconductor manufacturing, experienced analysts develop working practices that minimize the potential for contamination to affect results. The following practical suggestions can be implemented in any laboratory and will help ensure data quality is not compromised by contamination that could have easily been prevented.

Consider Whether the Laboratory Environment is Suitable for Your Analysis

Analytical laboratories doing trace element analysis in industries such as environmental monitoring, food safety, pharmaceutical manufacturing, and clinical research do not need a special clean laboratory environment to achieve the method detection limits (DLs). However, even a normal trace element laboratory should be designed and constructed in a way that minimizes sources of elemental contamination.

In the semiconductor manufacturing and process chemical industries, trace elements are routinely measured at ppt and sub-ppt levels, so laboratories in these industries often install a dedicated cleanroom. Cleanrooms are classified according to the number of particles of various sizes between 0.1 and 5 micrometers per unit volume of laboratory air. For example, an International Organization for Standardization (ISO) Class 3 laboratory (equivalent to the earlier US Federal Standard 209E [FS209E] Class 1) can contain a maximum of 8 particles of 1 µm and 1000 particles of 0.1 µm per cubic meter of air. An ISO Class 7 laboratory (FS209E Class 10,000) may contain up to 83,200 particles of 1 µm per cubic meter.

However, ISO Class 1 to 4 cleanrooms are expensive to build and maintain, and only retain their rated classification through strict control of access and working practices. A lower cost alternative is to install the ICP-MS in a small Class 10 enclosure located inside a Class 10,000 laboratory or normal trace element laboratory. Another option is to place just the autosampler in a clean enclosure, such as a high efficiency particulate air (HEPA) filtered laminar flow hood. Preparation of samples and standards can also be performed in a similar hood to avoid contamination of vials and solutions while they are open on the bench.

Limit Sources of Particulate Contamination

In a typical laboratory, one of the most problematic sources of sample contamination is airborne particulate material. Consider where contamination may come from, and try to eliminate particulate sources from the laboratory.

Common sources of particles in the laboratory include air conditioning units (especially those with overhead vents), corroded bare metal surfaces, printers and personal computers (PCs), and recirculating water chillers, particularly where a fan is used in an air-cooled heat exchanger. Contamination can also arise from dirt and dust brought into the laboratory on people's shoes, clothing, and personal belongings. Simple steps can remove or reduce the contribution from these sources; for example, by placing the water recirculator in an adjacent service room, or printing to a remote device in a neighboring office. Sticky mats by entrance doors can significantly reduce the amount of dust brought into the laboratory on people's shoes.

Using appropriate materials during laboratory-based activities can also help to reduce contamination. Gloves are routinely used for safety reasons when handling potentially corrosive acids, and powder free nitrile gloves will help minimize particle contamination.

With a little thought and attention to the way laboratory services, equipment, and personnel are managed, particulate contamination in the laboratory can be minimized without the high costs of installing and operating a dedicated cleanroom.

Avoid Glass! Use Plastic Labware to Minimize Elemental Backgrounds

The following recommendations are appropriate for laboratories that analyze typical ICP-MS sample types prepared and stabilized in dilute acid solutions. If other solvents are used, the details of the cleaning and rinsing protocols will need to be adjusted as appropriate.

Sample vials, pipette tips, and other labware that comes into contact with the sample solution can be a significant source of contamination. Acidic solutions should not be prepared or stored in glassware, even if it has been precleaned, as the acid will extract metal contaminants from the glass. Alkaline solvents such as ammonium hydroxide and tetramethylammonium hydroxide (TMAH) will also extract metals from glass containers. Plastic labware is much cleaner than glass, but brands that contain pigments made with metal additives should be avoided where possible. Clear plasticware made of materials such as polypropylene (PP), low density polyethylene (LDPE), polyethylene terephthalate (PET), or fluoropolymers (PTFE, FEP, and PFA) are recommended for the best chemical resistance and lowest levels of contamination. New labware should be acid rinsed to remove surface contamination and manufacturing residues prior to use.

Polypropylene sample vials and centrifuge tubes (15 mL or 50 mL) from brands such as DigiTube, Corning, or Nalgene are inexpensive, largely free from metal contamination, and are Class A graduated so they can be used for volumetric sample preparation. Many laboratories prepare standards and do sample dilution by weight. Conical base DigiTubes are available with a skirt to allow them to stand upright on the balance or bench, without needing to be held in an autosampler rack.

Implement Effective Procedures for Cleaning, Storage, and Use of Labware

If the laboratory's workflow and sample throughput allow, it is good practice to soak sample vials and tubes before use in a covered, clear plastic tank containing ultrapure water (UPW) or dilute acid (for example 0.1% HNO_3), as shown in Figure 1. These plastic containers can be purchased at relatively low cost from a normal hardware store. This sort of precleaning approach will help remove manufacturing residues such as mold release agents, which can contain metals, including Al and Zn. More aggres-

FIGURE 1: Clear plastic containers of various sizes used for cleaning and storage of sample tubes and other consumables.

FIGURE 2: ICP-MS sample introduction components are cleaned and stored in separate containers for different kits (for example, standard quartz and PFA inert kit components).

sive cleaning may be required to achieve the lowest background levels for ultratrace analysis. Vials and containers should be rinsed three times in UPW prior to use.

The same sort of precleaning approach can also be used for soaking pipette tips before use, although clear tips supplied in a covered container will be dust free and do not usually require precleaning, except for when ultralow level analysis is required. The rinse baths should not become significantly contaminated, and can usually be used for a year or more before the UPW or acid needs to be changed.

Similar clear plastic storage containers can be used to clean and store ICP-MS sample introduction components, ideally with separate containers for different components, such as standard and inert kits (Figure 2). Sample introduction parts such as the quartz spray chamber and torch can be soaked in an acid bath, then dried before use. Interface cones can be sonicated in UPW or a dilute laboratory cleaning agent such as Citranox, then dried and stored in a sealed container. For very contaminated cones, a fine abrasive polishing powder and a pointed Q-tip can be used, followed by sonication in UPW.

Use Reagents of Appropriate Quality for the Analysis

Good quality deionized water (18 MΩ.cm) is essential to maintain the low background levels required for trace level analysis, particularly for common contaminants such as Na, Al, and Fe. The elements B and Si are more difficult for ion exchange systems to remove, so pay particular attention to the background levels for these elements. An increase in B or Si backgrounds may indicate that the ion exchange cartridge of your ultrapure water system needs to be replaced.

The quality of reagents such as acids should be appropriate for the levels of trace elements being measured, but, in general, using better quality acids will reduce the time you have to spend dealing with errors due to contamination. A viable alternative to high purity acids is to purchase reagent grade acids and purify them in the laboratory using sub-boiling distillation.

When using concentrated high purity acids to prepare samples, calibration standards, and quality control standards (QCS), a small volume of acid should be decanted into a micro beaker or the acid bottle lid before pipetting into the sample or standard vials. This will help avoid contaminating the acid in the bottle.

Once empty, the perfluoroalkoxy alkanes (PFA) bottles that high purity acids are supplied in can be rinsed and dried, and will then be excellent metal-free containers for subsequent use. These bottles can be used to prepare and store diluents, and can even be used for low-level standard addition analysis with the spikes being added directly into the sample in the reused acid bottle.

Summary

These practical tips from experienced ICP-MS analysts have been demonstrated to reduce errors because of contamination. By implementing a few simple procedures and ensuring reagents and consumables are suitable for the intended analysis, ICP-MS users can minimize the possibility of data quality being compromised by trace element contamination.

Bert Woods and **Ed McCurdy** are with Agilent Technologies, Inc. Direct correspondence to: ed_mccurdy@agilent.com ●

Valuable Techniques for Repeatable Absorbance Measurements

Derek Guenther

Spectroscopy offers a range of available techniques that can be differentiated by the use or omission of reference spectra. This differentiation means that techniques such as Raman or fluorescence typically look at raw intensity outputs, whereas techniques such as transmission or reflectance require some reference scan to calculate those relative outputs. Within the group of referenced spectral techniques, absorbance is easily one of the most common and offers much value because of the concentration dependence of Beer's Law. However, this value is only properly captured when system components and samples are made to be repeatable, both for the reference scans and live acquisitions. This article discusses several useful techniques to establish this repeatability, including proper cuvette and probe handling, component setup, and sample considerations. By optimizing repeatability of the measurement system, the observed concentration values calculated from absorbance outputs are much more accurate and relevant to the sample being measured.

Think back to the first time you baked something, swung a golf club, or typed on a keyboard. How did you do? Were you as good the second time? Were you as good as you are today? Most likely, the answer is "No," because it took some experience to build and understand the techniques needed to perform each activity effectively. Without proper technique, we do not see our efforts result in us reaching our true potential, but without experience, we never have the chance to build those techniques. Spectroscopy is no different, and each spectral method has its own tricks to pull more out of the measurement than would be possible otherwise.

Modern times give focus to more modern spectral techniques, and rightfully so. We now see a rapid democratization of Raman and time-resolved measurements that were once largely restricted by bulky instrument size and high cost, which is fantastic news because it gives more researchers opportunities to push boundaries and open new doors. However, there is also value in remembering traditional techniques and the methods that brought us to where we are today. Whether reflection, transmission, absorbance, fluorescence, or others, these traditional approaches are by no means "done" in their development and deployment; rather, we can always improve old techniques with new considerations.

Absorbance is one technique that stands a bit taller than the rest. The origin of the absorbance concept that we know today began in the early 1700s when French mathematician and scientist Pierre Bouguer expressed curiosity about the transmission of light through his wine when he was on vacation in Portugal. Bouguer's curiosity resulted in him making some measurements to discover that the light attenuation was not linear as the distance (pathlength) increased, but rather followed an exponential trend. More than a century later, German physicist August Beer made a secondary discovery in this same area, noting that the same exponential trend was seen when the concentration of the attenuating species changed and the distance remained constant. Bringing these two observations together under a common relationship gives us the Beer-Lambert law we are all familiar with today:

$$A = \varepsilon l c \qquad [1]$$

where A equals absorbance; ε equals the molar attenuation coefficient; l equals the optical pathlength; and c equals the concentration.

FIGURE 1: To derive meaningful spectral data from optically dense samples, such as dark wines, may require the use of reflectance techniques. The above is an image of wine in bottles during the packaging process.

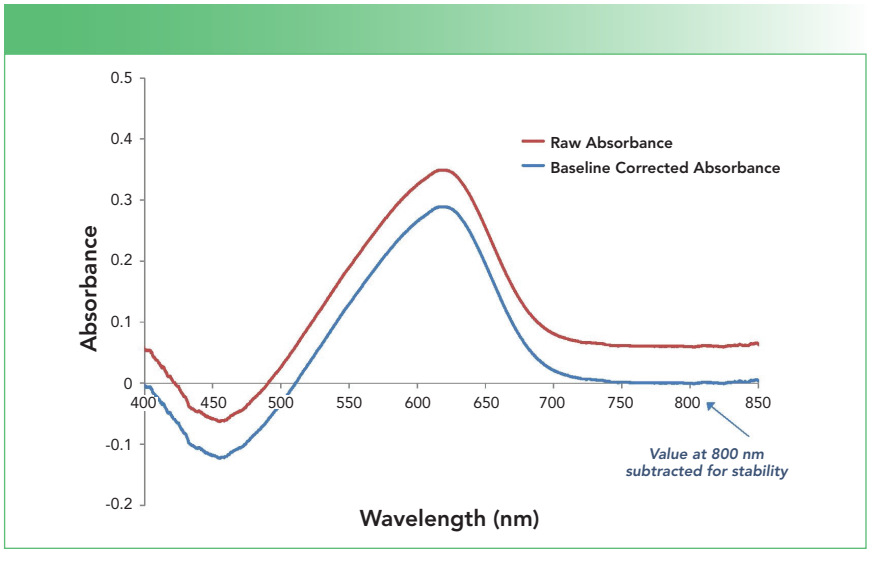

FIGURE 2: Absorbance of pH-responsive dye showing raw (red) and single-point baseline corrected (blue) spectra. Baseline correction of absorbance data can be applied to help mitigate the effects of measurement variability.

The discovery of the Beer-Lambert law was a big deal at the time and remains important today. Beer's law allows us to quickly convert optical signals into meaningful concentration values for all sorts of systems. It lets us shine light on something and know how much light is there. The specific sample being measured determines what "mode" was used to interrogate the sample, which could include transmission, reflection, or in rarer cases, evanescent interactions.

Perhaps the most common mode of absorbance measurement is transmission, and within that, most commonly the transmission of liquids like Bouguer's wine. Transmission is only feasible if the sample is transmissive in the spectral region of interest, though a simple visual check may not be sufficient. It is possible that a crystal-clear sample can be a massive UV-range filter, which would make UV absorbance regressions impossible in transmissive mode. Conversely, you could have something that looks solid and not optically transmissible but may give very usable transmission in the near-infrared (NIR) wavelength range. The more the sample is absorbed, the harder it will be to get meaningful and coherent photons through to the other side. Your two most important tools to help with this process include a stronger light source and a shorter pathlength. More photons at the input will give you more photons at the output, and the less sample the light has to interact with will also allow more light through.

Think back to Bouguer's wine. Compared with a light white wine, a dark red wine would need a stronger light source, a shorter pathlength, or both, to get coherent measurements. However, at some point, the sample may be too thick or optically dense for transmission to work well. In that scenario, it may make more sense to look at the reflective mode (Figure 1). Samples like whole blood or plant extracts can give the same valuable absorbance information, but instead of passing light through the sample, we can bounce the light off the sample surface. A third approach using evanescent interactions could be considered a fusion of these two approaches because the evanescent waves interact "through" the sample but only at the primary surface interface. The specific system you're working with will dictate what makes sense for data acquisition.

When working in transmissive mode, you will likely be using some type of cuvette (or cuvet) and cuvette holder to manage your sample, and there are some key considerations with that setup to make the best measurements possible. When using fiber optics for connecting the various optical components, ensure the fiber connections are threaded tightly and do not have the ability to rotate. Also, it is important to

ensure that the fibers are positioned so that they aren't frequently moved or touched. Fiber movement can be a leading cause of odd absorbance behaviors, so always keep this thought in mind when you plan to work in transmissive mode.

The cuvette should be optically clean on the inside and outside. If being moved between measurements, the cuvette should be placed in the same orientation; cuvettes often have a marker near the top to assist with this step. The cuvette should sit snuggly within the holder, so that there is minimal-to-no play in its movement or resting position. There is often a set screw to tighten the fitting of the cuvette. It is important to be careful not to crack the cuvette when adjusting this, especially with expensive quartz cells. When using the same cuvette for multiple samples, it is also important that you ensure the cell has been sufficiently flushed with the new sample so that you do not see contamination from a previous sample.

Typically, it is more difficult to achieve repeatable absorbance scans in reflective mode than transmissive mode, which is largely because of the more consistent nature of the transmissive hardware we discussed above. Cuvettes are convenient because they snap right into place! Reflective probes and holders often require a greater level of physical sturdiness and placement considerations to get the same results, so taking the time to develop a proper opto-mechanical fixture can make all the difference in the world for this approach. Think about distance and angle, not just of the optical probe versus the stage but versus the sample. For example, if the sample is a powder that may have variable height, think about how the probe could be designed so that it sees a flat portion of the powder at the same distance each time. Sometimes, using a region of the spectrum known to have a good baseline for a sanity check can be valuable in ensuring the system "sees" the sample as it had before (Figure 2).

However, hardware is only half the battle in the world of modern science, where software plays just as (if not more) critical a role in determining the validity and value of our final result numbers. Although this article focuses on absorbance, a key first step of many traditional spectroscopy techniques is determining what sample condition creates the "brightest" scenario or the most photonic signal to the detector. Knowing the sample condition will allow you to complete the full range of acquisitions without saturating the detector and needing to adjust software parameters on the fly.

Set your integration time to approximately 80% saturation, and then adjust your averaging setting to establish the total scan time, which will be the integration time multiplied by the number of averages. Averaging can improve the stability of your output, but it also increases the measurement time. Boxcar, on the other hand, is a pixel-averaging setting that does not affect your total scan time and can be very helpful in cleaning up spectral outputs. The boxcar setting is the number of 2n+1 pixels that are averaged around the center pixel, such that a boxcar of $n = 0$ will treat every pixel independently, whereas a boxcar of 1 will average each pixel with the pixel immediately to the left and to the right of it. Having a boxcar of at least 1 will let the spectrometer function as a coherent system rather than as an array of independent detectors. Many absorbance applications deal with broad peak activities and applying boxcar can significantly help stabilize these broad trends across many scans. However, be careful: the sharper the peak activities, the lower the boxcar setting that should be used.

Taking quality absorbance measurements goes beyond simply dropping liquid into a cuvette; there are multiple considerations around spectral method, hardware setup, and software parameters. With the proper planning on the front end of your tests, you will set yourself up for accurate and valuable results at the output. Whether with spectral measurements or other efforts, you will bring yourself closer to success by knowing the details of the techniques as much as knowing the basics of the technology.

Derek Guenther is a Senior Application Scientist at Ocean Insight. Direct corerspondence to: derek.guenther@oceaninsight.com. •

Avoiding Misunderstanding Self-Absorption in Laser-Induced Breakdown Spectroscopy (LIBS) Analysis

Vincenzo Palleschi

In a recent article published in this journal (1), I discussed seven common errors that may affect the results of laser-induced breakdown spectroscopy (LIBS) analysis. Among these errors, one of the recurring ones is related to misunderstanding the process of self-absorption in LIBS plasmas. Because many people working in LIBS still consider self-absorption as a problem yet to be solved, I am dedicating a full article to this topic. The physics and chemistry of the phenomenon have been well known for many years, and this knowledge can tell us how self-absorption can be not only "corrected," but also tuned to our advantage in analytical applications of LIBS.

Self-absorption occurs in spectrochemistry when part of the radiation emitted by an extended source is re-absorbed before exiting the source and eventually reaching the detector. In LIBS quantitative analysis, the measurement of the radiation intensity determines the number concentration of the emitting analyte. When the effects of self-absorption are negligible, a linear relationship is typically obtained between the measured intensity and the analyte number concentration. Dealing with linear relations makes life easier for the analyst because it allows for the building of (linear) calibration curves from which limits of detection (LOD) and limits of quantification (LOQ) of the analyte being studied can be determined.

In most spectro-analytical techniques, self-absorption effects can be considered negligible; however, in LIBS analysis, we often make measurements involving large concentrations of the analyte (percent level). In this case, the probability for a photon emitted by an atom or ion in the plasma to be reabsorbed by another atom or ion before exiting the plasma could be quite high, and definitely higher than that for the same analyte diluted at sub-ppm concentration in, for example, inductively coupled plasma–optical emission spectroscopy (ICP-OES) analysis.

The result of a strong self-absorption in LIBS is a nonlinear saturation effect, which is observed in the calibration curve; when the number concentration of the analyte increases, the measured intensity of the emission line does not grow proportionally. At large concentrations, the calibration curve saturates; it is well-known in the literature that in a log–log scale, the slope of the calibration curve changes from 1 to ½ with the increase of the analyte concentration and the effect of self-absorption.

Don't Mistake Self-Reversal for Self-Absorption

Two observations should be made at this point, both correlated to frequent analytical errors. The first error that is often made in dealing with self-absorption in plasmas is mistaking this effect with the self-reversal phenomenon. Self-reversal manifests as a narrow dip on top of the emission line. Its presence is related to self-absorption, but self-reversal shows up only in the presence of spatial gradients of the plasma temperature and electron number density, which usually occur at the periphery of the plasma. Therefore, although the presence of self-reversal is an indication that the self-absorption phenomena in the emitting source are not negligible, as well as the spatial inhomogeneities in the plasma, its absence does not mean that self-absorption can be considered negligible.

Understand What Is Really Happening in a "Correction"

The second error that is, in my opinion, more subtle and substantial is associated to the need that some people working in LIBS feel to "correct" the effects of self-absorption. Although the term "correction" can be used at a colloquial level, it is nev-

ertheless important to know that this term does not correspond to the true nature of the phenomenon.

An emitting source is also an absorbing source. There is no problem to be solved unless we insist on using an unrealistic treatment of the emission process in which each emitter is considered independent from the others. Instead, what we could do is take into account the physical processes occurring during the propagation of the radiation in the plasma (spontaneous emission, absorption, and stimulated emission, with the latter being in general negligible). In the approximation of homogeneous plasma in local thermal equilibrium, the number of photons emitted by the laser-induced plasma at a given wavelength along the line of sight of the detector can be easily determined by solving a simple differential equation:

$$\frac{dn_p(\lambda\, x)}{dx} = \varepsilon(\lambda) - \mathrm{k}(\lambda) n_p(\lambda,x) \qquad [1]$$

In the above equation, the ε coefficient is proportional to the number of emitters and to the spontaneous emission coefficient A_{ki} of the transition (see Figure 1). Following the Einstein treatment of the propagation of radiation in a two-level atomic system (the same which is used to model the laser effect), it's easy to demonstrate that the absorption coefficient, *k*, and the emission coefficient, ε, are linked by the relation:

$$B(\lambda)k(\lambda) = \varepsilon(\lambda) \qquad [2]$$

where $B(\lambda)$ is the Planck black body radiation function at the plasma temperature (*T*). The radiation propagation equation can be easily solved, at each wavelength, along the line of sight of the detector.

The shape of the lines emitted by an optically thin plasma ($k(\lambda)l \ll 1$) is usually well approximated by a Lorentzian function, peaked at the wavelength of the transition. However, because the absorption coefficient is proportional to the emission coefficient, the effect of self-absorption is more evident where the emission is stronger (at the peak of the line). This deformation of the shape of the emission lines makes the calculation of their integral intensity slightly more complex, but it can be demonstrated that, at least for low to moderate self-absorption, the integral intensity of the line would be given by:

$$I \cong I_0 \left(\frac{1-e^{-k(\lambda_0)l}}{k(\lambda_0)l}\right)^{\frac{1}{2}} \qquad [3]$$

where $k(\lambda_0)$ is the absorption coefficient calculated at the peak of the emission line, and I_0 is the integrated intensity (total number of photons emitted) that would have been measured on the detector if the plasma was optically thin.

It can also be demonstrated that the full width at half maximum (FWHM) of the self-absorbed line will increase with respect to the corresponding FWHM in optically thin plasma conditions following the same square root behavior:

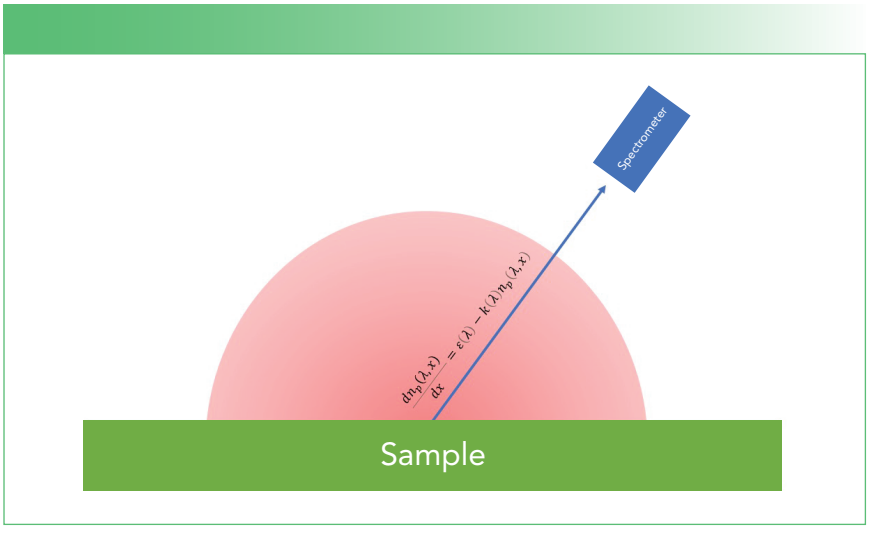

FIGURE 1: Schematic representation of the phenomena occurring within an emitting plasma.

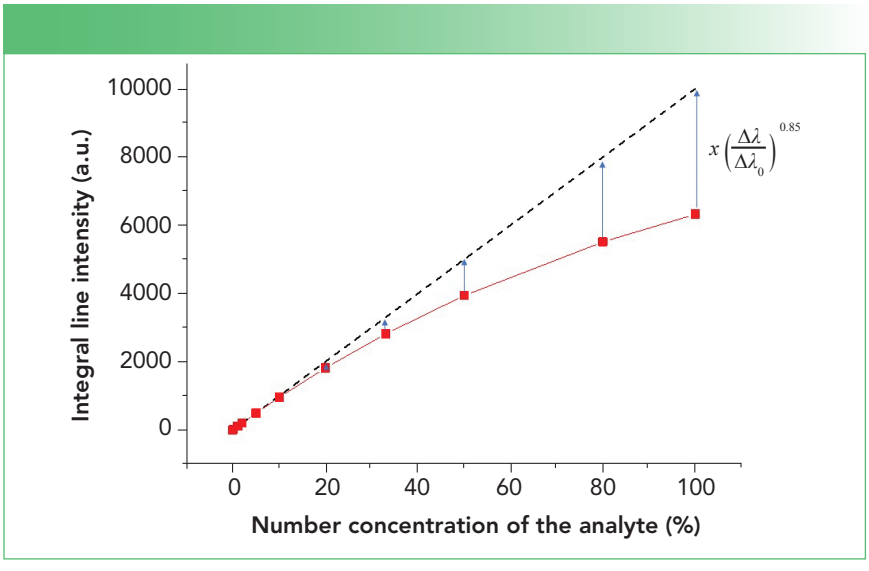

FIGURE 2: Linearization of the calibration curve for a given analyte by multiplying the measured integral line intensity by $(\frac{\Delta\lambda}{\Delta\lambda_0})^{0.85}$. The dotted black line is the optical thin limit, and the dotted red line is the measured intensity.

$$\Delta\lambda \cong \Delta\lambda_0 \left(\frac{1-e^{-k(\lambda_0)l}}{k(\lambda_0)l}\right)^{-\frac{1}{2}} \quad [4]$$

Therefore, if we can estimate the FWHM of the line in the optically thin limit, it would be possible, by measuring the FWHM of the self-absorbed line, to estimate the value of the factor:

$$\left(\frac{1-e^{-k(\lambda_0)l}}{k(\lambda_0)l}\right) \quad [5]$$

Substituting it in the relation for the line intensity, the simple relation is obtained:

$$I_0 \cong I\,\frac{\Delta\lambda}{\Delta\lambda_0} \quad [6]$$

A more precise calculation leads to the formula $I_0 \cong I\,(\Delta\lambda/\Delta\lambda_0)^{0.85}$, which is valid also in case of strong self-absorption. I_0 is, by definition, proportional to the number of emitting atoms or ions in the plasma; therefore, the above equation allows recovering a linear relation between the measured intensity, *I*, and the concentration of the analyte (see Figure 2).

Conclusions

In conclusion, we can safely say that the self-absorption effect in LIBS is not a problem anymore. On the contrary, the simple treatment of the plasma as a homogeneous emitter at a temperature *T* makes it possible to recover the linear dependence between signal intensity and number concentration of the analyte, which characterizes an optically thin plasma. Moreover, knowledge of the physics of the phenomenon contributes to improving the precision of the determination of fundamental plasma parameters as transition probabilities and Stark coefficients of non-optically thin emission lines (2). The numerical simulation of the radiation propagation equation has also demonstrated that the approximation of homogeneous plasma is not critical for the determination of the Stark coefficients of self-absorbed LIBS emission lines (3).

References

(1) V. Palleschi, *Spectroscopy* **34**(8), 16–17 (2019).

(2) S.M. Aberkane, A. Safi, A. Botto, B. Campanella, S. Legnaioli, F. Poggialini, S. Raneri, F. Rezaei, and V. Palleschi. *Appl. Sci.* **10**(14), 4973 (2020). https://doi.org/10.3390/app10144973

(3) V. Palleschi, *J. Quant. Spectrosc. Radiat. Transf.* **271**, 107714 (2021). https://doi.org/10.1016/j.jqsrt.2021.107714

Vincenzo Palleschi is a Senior Researcher at the National Research Council of Italy in Rome, Italy, and a professor with Pisa University in Pisa, Italy. Direct correspondence to: vincenzo.palleschi@cnr.it ●

• Continued from Page 53

Internal standards are elements that are not present (or present at very low levels) in samples. They are added, at a fixed concentration, to all blanks, calibration solutions, and samples, either on-line via a mixing tee or valve port (easy), or off-line, by manual addition (tedious). When a sample contains high concentrations of sodium, potassium, and calcium, the internal standard signals are suppressed compared to what they are in the blank or matrix-free solutions. Many regulated methods specify how much internal standard suppression is permitted in a sample, which is typically between 75–80% of the signal observed in a sample matrix-free blank (usually the first calibration blank in the analysis). In general, if internal standard recovery is less than 75–80% in any sample, dilution and re-analysis is required. The most common reason for internal standard recoveries being greater than 120% is often attributed to the ICP-MS interface not being conditioned properly. *Conditioning* is the process of running a dummy sample containing similar matrix to the samples to be analyzed through the instrument for approximately 30 min before you start the actual analysis, which causes the interface cones to become coated and helps to stabilize ion signals and minimize drift. It remains somewhat unclear as to why cone conditioning helps improve signal stability, but it is a well-documented fact that it does and conditioning in this way is standard practice. Cone conditioning is especially important after cleaning the interface cones or when they are replaced. In general, cleaning the interface cones should only be considered when signs of blockage or unremovable contamination are observed or if the instrument performance has significantly dropped.

Finally, The Route to Success

Finding the right configuration of the sample introduction system for a specific sample type is easy once a few questions are answered up front. The most important questions are related to the sample matrix: is it aqueous or organic? What is the amount of total dissolved solids? And what is the approximate composition?

Figure 1 summarizes a few of the crucial aspects that should be considered when setting up an instrument (either ICP-OES or ICP-MS) for analyzing a new sample type.

If a method is defined and validated but does not perform up to expectations, it is important to know which key areas of the system configuration to focus on and to understand how the different components of the sample introduction system are working together. As a general rule, instability is usually caused by problems upstream of the sample introduction system, whereas drift and suppression are rather caused downstream (injector tube, torch, and interface cones [in the case of ICP-MS]). In some cases, effects that may be attributed to the hardware may also originate from unexpected interferences from the sample, but that is a subject for another tutorial.

Simon Nelms and **Daniel Kutscher** are with Thermo Fisher Scientific. Direct correspondence to: daniel.kutscher@thermofisher.com ●

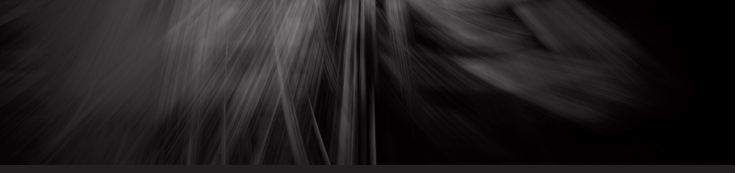

PRODUCT INDEX

Spectroscopy
ONLINE DIRECTORY

SCAN QR CODE TO VIEW


Spectroscopy®
Follow us on social media for more updates on the field of spectroscopy
Join your colleagues in conversation and stay up-to-date on breaking news, research, and trends in the industry.
linkedin.com/company/spectroscopy-media
@SpectroscopyMagazine
@SpectroscopyMag
MJH life sciences™

SPECTROSCOPIC INSTRUMENTATION: SPECTROMETER SYSTEMS

ATOMIC SPECTROSCOPY

ATOMIC ABSORPTION

FLAME AA
Analytik Jena US
(909) 946-3197, (800) 452-6788
PerkinElmer, Inc.
SCP SCIENCE
(514) 457-0701, (800) 361-6820
Shimadzu Scientific Instruments

GRAPHITE FURNACE
Analytik Jena US
(909) 946-3197, (800) 452-6788
PerkinElmer, Inc.
SCP SCIENCE
(514) 457-0701, (800) 361-6820
Shimadzu Scientific Instruments

MERCURY ANALYZERS
Analytik Jena US
(909) 946-3197, (800) 452-6788
Milestone, Inc.
(866) 995-5100
PerkinElmer, Inc.

ZEEMAN
Analytik Jena US
(909) 946-3197, (800) 452-6788
PerkinElmer, Inc.

ATOMIC EMISSION

ICP, AXIAL
Analytik Jena US
(909) 946-3197, (800) 452-6788
Glass Expansion
PerkinElmer, Inc.
Thermo Scientific - CIDTEC

ICP, COMBINED AXIAL/ RADIAL CAPABILITY
Analytik Jena US
(909) 946-3197, (800) 452-6788
Glass Expansion
PerkinElmer, Inc.
Thermo Scientific - CIDTEC

ICP-MS
Analytik Jena US
(909) 946-3197, (800) 452-6788
Glass Expansion
Milestone, Inc.
(866) 995-5100
PerkinElmer, Inc.

Savillex
Email: info@savillex.com
www.savillex.com
(952) 935-4100
See ad on page 45

Shimadzu Scientific Instruments

ICP, RADIAL
Glass Expansion
PerkinElmer, Inc.
Thermo Scientific - CIDTEC

ICP, SEQUENTIAL
Analytik Jena US
(909) 946-3197, (800) 452-6788
Glass Expansion
Thermo Scientific - CIDTEC

ICP, SIMULTANEOUS
Analytik Jena US
(909) 946-3197, (800) 452-6788
Glass Expansion
PerkinElmer, Inc.
Shimadzu Scientific Instruments
Thermo Scientific - CIDTEC

LASER-INDUCED BREAKDOWN SPECTROSCOPY (LIBS)
Analytik Jena US
(909) 946-3197, (800) 452-6788
Avantes
AXT - Scientific Solutions for Industry and Academia
LTB Lasertechnik Berlin GmbH
Ocean Insight
+1 (407) 673-0041

ELEMENTAL MASS SPECTROMETRY

ICP-MS
Analytik Jena US
(909) 946-3197, (800) 452-6788
Glass Expansion
PerkinElmer, Inc.

Savillex
Email: info@savillex.com
www.savillex.com
(952) 935-4100
See ad on page 45

OTHER ATOMIC TECHNIQUES
Analytik Jena US
(909) 946-3197, (800) 452-6788

X-RAY SPECTROMETRY

ENERGY-DISPERSIVE XRF
Applied Rigaku Technologies, Inc.
+1 (512) 225-1796
AXT - Scientific Solutions for Industry and Academia
Malvern Panalytical
Shimadzu Scientific Instruments

HIGH VOLTAGE POWER SUPPLIES
Newport Corporation

TOTAL REFLECTION XRF
AXT - Scientific Solutions for Industry and Academia

WAVELENGTH-DISPERSIVE XRF
AXT - Scientific Solutions for Industry and Academia

X-RAY DIFFRACTION
AXT - Scientific Solutions for Industry and Academia
International Centre for Diffraction Data
Malvern Panalytical
Shimadzu Scientific Instruments

INSTRUMENTS FOR RENT OR LEASE

ATOMIC EMISSION SPECTROMETERS (INCLUDING ICP-OES, ICP-MS, & DCP)
Analytik Jena US
(909) 946-3197, (800) 452-6788
Glass Expansion
Quantum Analytics

INFRARED SPECTROMETERS (INCLUDING FT-IR & NEAR-IR)
DRS Daylight Solutions
NLIR
Quantum Analytics
Spectra Vista Corporation
Thermo Scientific
+1 (800) 532-4752

MASS SPECTROMETERS (INCLUDING GC–MS, LC–MS, & MASS SPECTROMETRY DETECTORS)
Excellims
Exum Instruments
IonSense
Quantum Analytics

OTHER INSTRUMENTS FOR RENT OR LEASE
Quantum Analytics

RAMAN SPECTROMETERS
Nanobase, Inc.
+82 70 8666 0233
Quantum Analytics

UV/VIS SPECTRO-PHOTOMETERS
Excellims

X-RAY DIFFRACTOMETERS
AXT - Scientific Solutions for Industry and Academia
Quantum Analytics

X-RAY FLUORESCENCE SPECTROMETERS
Quantum Analytics

MASS SPECTROMETRY & HYPHENATED TECHNIQUES

GC–MS
Excellims
Quantum Analytics
Shimadzu Scientific Instruments

ICP-MS SYSTEMS
Analytik Jena US
(909) 946-3197, (800) 452-6788
Glass Expansion
PerkinElmer, Inc.
Quantum Analytics
Shimadzu Scientific Instruments

ION MOBILITY
Excellims

IONIZATION MODES

MATRIX ASSISTED LASER DESORPTION IONIZATION (MALDI)
LTB Lasertechnik Berlin GmbH

LC–MS
Analytik Jena US
(909) 946-3197, (800) 452-6788
Excellims
IonSense
Quantum Analytics
Shimadzu Scientific Instruments

MALDI OR MALDI-TOF
LTB Lasertechnik Berlin GmbH
Shimadzu Scientific Instruments

QUADRUPOLE INSTRUMENTS
PerkinElmer, Inc.
Quantum Analytics

SFC-MS
Shimadzu Scientific Instruments

SIMS
Physical Electronics

TOF-MS
AXT - Scientific Solutions for Industry and Academia
Physical Electronics
Shimadzu Scientific Instruments

Spectroscopy
ONLINE DIRECTORY

MISSING FROM THE DIRECTORY?
SCAN THE CODE
TO ADD YOUR LISTINGS.

thermoscientific

The best imager for many applications ...

The only imager for some

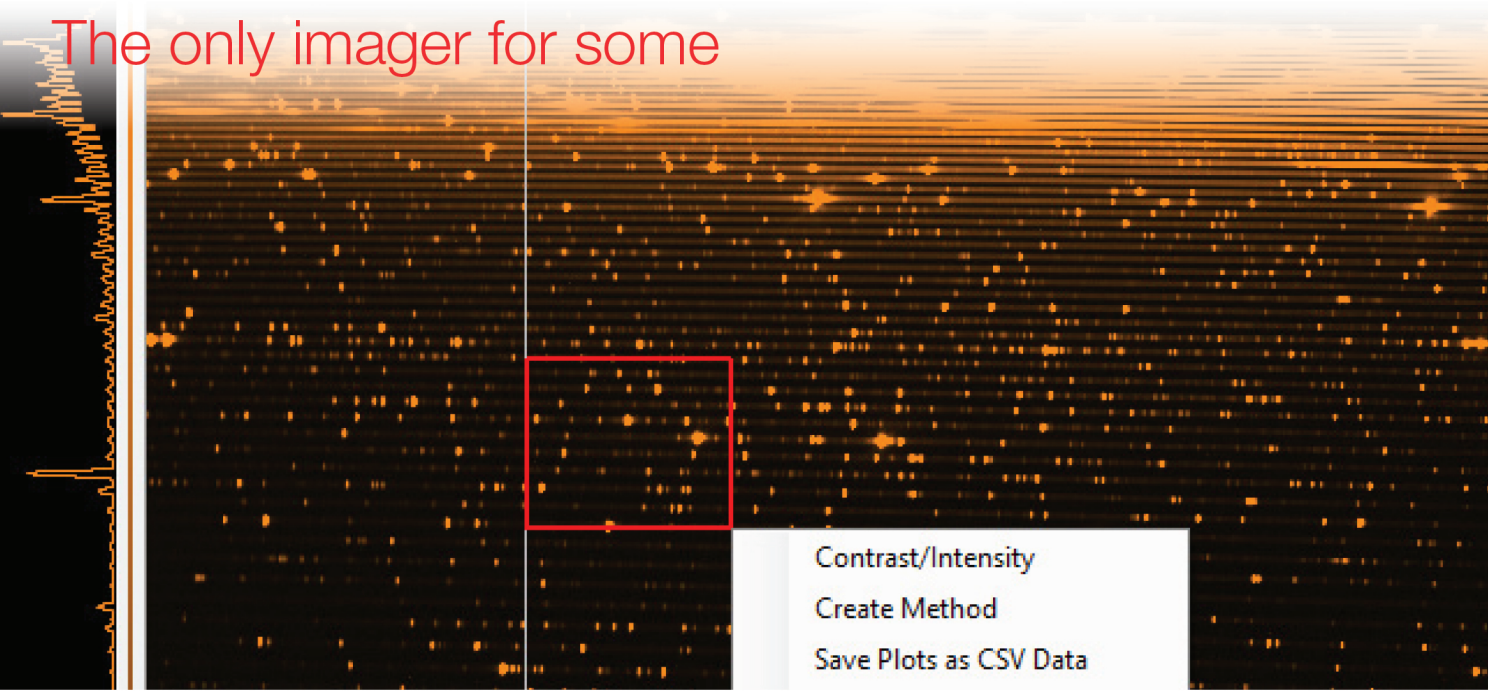

The most advanced CID camera ever developed

Designed specifically for ICP-OES, now available to end users and other OEM applications.
With superior capabilities like true random pixel level addressing, unique non-destructive read-out, and wide spectral response, the SpectraCAM XDR camera offers unprecedented performance.

SpectraCAM XDR with 2,048 x 2048, with 12 micron pixels.
Available FSI, or BSI, in purged, hermetic, or customised OEM housings.

In the United States:
For customer service, call 1-800-888-8761
To fax an order, use 1-315-451-9421
Email: sales.cidtec@thermofisher.com

International:
For customer service, call [01] 315-451-9410
To fax an order, use [01] 315-451-9421
Email: sales.cidtec@thermofisher.com

Learn more at **thermofisher.com/cidtec**

ThermoFisher SCIENTIFIC

MOLECULAR SPECTROSCOPY

FAR-IR/TERAHERTZ

DETECTORS
Edinburgh Instruments
+44 15 06425300
PhaseTech Spectroscopy

SOURCES (LASERS, OTHER)
Edinburgh Instruments
+44 15 06425300

Wavelength Electronics
Email: sales@teamwavelength.com
www.teamwavelength.com
(406) 587-4910

SPECTROMETERS
Analytik Jena US
(909) 946-3197, (800) 452-6788
Edinburgh Instruments
+44 15 06425300
Newport Corporation
PhaseTech Spectroscopy

FLUORESCENCE

FILTER-BASED INSTRUMENTS
Art photonics
+49 30 67798870
JASCO, Incorporated
(410) 822-1220
McPHERSON

FLUORESCENCE LIFETIME
Edinburgh Instruments
+44 15 06425300
HORIBA Scientific

JASCO, Incorporated
Email: sales@jascoinc.com
https://jascoinc.com
(410) 822-1220
See ad on page 49

Lambert Instruments BV
Mad City Labs Inc.
Shimadzu Scientific Instruments

WITec Raman Imaging Solutions
Email: info@WITec.de
https://raman.oxinst.com
+49(0)731 140 700
See ad on page 35

IMAGING
Analytik Jena US
(909) 946-3197, (800) 452-6788
Edinburgh Instruments
+44 15 06425300
HORIBA Scientific
JASCO, Incorporated
(410) 822-1220
Lambert Instruments BV
Mad City Labs Inc.

WITec Raman Imaging Solutions
Email: info@WITec.de
https://raman.oxinst.com
+49(0)731 140 700
See ad on page 35

MICROPLATE READERS
LTB Lasertechnik Berlin GmbH
PIKE Technologies
(608) 274-2721

TIME RESOLVED
Edinburgh Instruments
+44 15 06425300
HORIBA Scientific
Lambert Instruments BV

WITec Raman Imaging Solutions
Email: info@WITec.de
https://raman.oxinst.com
+49(0)731 140 700
See ad on page 35

INFRARED (MID-RANGE)

DISPERSIVE INFRARED
Harrick Scientific Products Inc
JASCO, Incorporated
(410) 822-1220
NLIR

FOURIER TRANSFORM INFRARED (FT-IR)

ABB Measurement and Analytics
Email: contact.center@us.abb.com
https://global.abb
418 877 2944
See ad on page 5

Art photonics
+49 30 67798870
Bruker Optics
+1 (978) 430-2394
Designs & Prototypes, Ltd.
d/b/a D&P Instruments
Harrick Scientific Products Inc

JASCO, Incorporated
Email: sales@jascoinc.com
https://jascoinc.com
(410) 822-1220
See ad on page 49

NeoSpectra by Si-Ware
PerkinElmer, Inc.
Quantum Analytics
Shimadzu Scientific Instruments

GC-IR
PIKE Technologies
(608) 274-2721

IR PROCESS ANALYZERS

ABB Measurement and Analytics
Email: contact.center@us.abb.com
https://global.abb
418 877 2944
See ad on page 5

Art photonics
+49 30 67798870

INFRARED REFLECTANCE/ ABSORBANCE
Art photonics
+49 30 67798870
DRS Daylight Solutions
NeoSpectra by Si-Ware

LC-IR
IonSense

NON-DISPERSIVE/ FILTER-BASED INSTRUMENTS
Edinburgh Instruments
+44 15 06425300

OPEN-PATH/ REMOTE-SENSING IR
ABB Measurement and Analytics
418 877 2944

REACTION MONITORS
Art photonics
+49 30 67798870

MAGNETIC RESONANCE/NMR

NMR IMAGING
AXT - Scientific Solutions for Industry and Academia

NMR PROCESS ANALYZERS
AXT - Scientific Solutions for Industry and Academia

NEAR-IR

FOURIER TRANSFORM-NEAR INFRARED

ABB Measurement and Analytics
Email: contact.center@us.abb.com
https://global.abb
418 877 2944
See ad on page 5

Art photonics
+49 30 67798870
Bruker Optics
+1 (978) 430-2394

JASCO, Incorporated
Email: sales@jascoinc.com
https://jascoinc.com
(410) 822-1220
See ad on page 49

NeoSpectra by Si-Ware
PerkinElmer, Inc.
Quantum Analytics
Shimadzu Scientific Instruments

NEAR-IR REFLECTANCE
Art photonics
+49 30 67798870
Bruker Optics
+1 (978) 430-2394
Metrohm
866-METROHM
NeoSpectra by Si-Ware
Ocean Insight
+1 (407) 673-0041
PIKE Technologies
(608) 274-2721
Spectra Vista Corporation

NEAR-IR TRANSMISSION
Art photonics
+49 30 67798870
Bruker Optics
+1 (978) 430-2394
Metrohm
866-METROHM
Ocean Insight
+1 (407) 673-0041
PIKE Technologies
(608) 274-2721
Spectra Vista Corporation

ON-LINE NEAR-IR ANALYZERS FOR PROCESS ANALYSIS

ABB Measurement and Analytics
Email: contact.center@us.abb.com
https://global.abb
418 877 2944
See ad on page 5

Bruker Optics
+1 (978) 430-2394
Metrohm
866-METROHM

UV/VIS-NEAR-IR ANALYZERS
Art photonics
+49 30 67798870
Metrohm
866-METROHM
PIKE Technologies
(608) 274-2721

RAMAN & RELATED VIBRATIONAL TECHNIQUES

Renishaw
Email: usa@renishaw.com
www.renishaw.com
(847) 286-9953
See ad on page 43

CIRCULAR DICHROISM (VIBRATIONAL)

JASCO, Incorporated
Email: sales@jascoinc.com
https://jascoinc.com
(410) 822-1220
See ad on page 49

COHERENT ANTI-STOKES RAMAN SPECTROSCOPY (CARS)
Coherent, Inc.
Mad City Labs Inc.
McPHERSON

DISPERSIVE RAMAN
Acutech Scientific Inc
Coherent, Inc.
IS Instruments

JASCO, Incorporated
Email: sales@jascoinc.com
https://jascoinc.com
(410) 822-1220
See ad on page 49

McPHERSON
Metrohm
866-METROHM
Ocean Insight
+1 (407) 673-0041

Renishaw
Email: usa@renishaw.com
www.renishaw.com
(847) 286-9953
See ad on page 43

WITec Raman Imaging Solutions
Email: info@WITec.de
https://raman.oxinst.com
+49(0)731 140 700
See ad on page 35

FT-RAMAN

JASCO, Incorporated
Email: sales@jascoinc.com
https://jascoinc.com
(410) 822-1220
See ad on page 49

Renishaw
Email: usa@renishaw.com
www.renishaw.com
(847) 286-9953
See ad on page 43

RAMAN MICROSPECTROSCOPY/ RAMAN IMAGING
Acutech Scientific Inc
Edinburgh Instruments
+44 15 06425300
Endress+Hauser
Harrick Scientific Products Inc
HORIBA Scientific

JASCO, Incorporated
Email: sales@jascoinc.com
https://jascoinc.com
(410) 822-1220
See ad on page 49

LTB Lasertechnik Berlin GmbH
Nanobase, Inc.
+82 70 8666 0233

Renishaw
Email: usa@renishaw.com
www.renishaw.com
(847) 286-9953
See ad on page 43

SPECTROLIGHT, INC.
Wasatch Photonics

WITec Raman Imaging Solutions
Email: info@WITec.de
https://raman.oxinst.com
+49(0)731 140 700
See ad on page 35

REMOTE/ON-LINE RAMAN PROCESS ANALYZERS
Endress+Hauser
IS Instruments
Metrohm
866-METROHM

SURFACE-ENHANCED RAMAN SPECTROSCOPY
Acutech Scientific Inc
Coherent, Inc.
Edinburgh Instruments
+44 15 06425300
HORIBA Scientific
Ionica Sciences

JASCO, Incorporated
Email: sales@jascoinc.com
https://jascoinc.com
(410) 822-1220
See ad on page 49

Mad City Labs Inc.
Metrohm
866-METROHM
Nanobase, Inc.
+82 70 8666 0233
Nikalyte Ltd
Ocean Insight
+1 (407) 673-0041

Renishaw
Email: usa@renishaw.com
www.renishaw.com
(847) 286-9953
See ad on page 43

WITec Raman Imaging Solutions
Email: info@WITec.de
https://raman.oxinst.com
+49(0)731 140 700
See ad on page 35

TIP-ENHANCED RAMAN SPECTROSCOPY
HORIBA Scientific
Mad City Labs Inc.
Nanobase, Inc.
+82 70 8666 0233
Teledyne Princeton Instruments

WITec Raman Imaging Solutions
Email: info@WITec.de
https://raman.oxinst.com
+49(0)731 140 700
See ad on page 35

UV-VIS

CIRCULAR DICHROISM

JASCO, Incorporated
Email: sales@jascoinc.com
https://jascoinc.com
(410) 822-1220
See ad on page 49

DOUBLE-BEAM
JASCO, Incorporated
(410) 822-1220
PerkinElmer, Inc.
Shimadzu Scientific Instruments

MICROPLATE READERS
JASCO, Incorporated
(410) 822-1220
PIKE Technologies
(608) 274-2721

ON-LINE/REMOTE ANALYZERS
PIKE Technologies
(608) 274-2721

POLARIMETERS
JASCO, Incorporated
(410) 822-1220

SINGLE-BEAM
JASCO, Incorporated
(410) 822-1220
McPHERSON
PerkinElmer, Inc.
Shimadzu Scientific Instruments

UV/VIS-NEAR-IR INSTRUMENTS
Analytik Jena US
(909) 946-3197, (800) 452-6788
Edinburgh Instruments
+44 15 06425300
Harrick Scientific Products Inc

JASCO, Incorporated
Email: sales@jascoinc.com
https://jascoinc.com
(410) 822-1220
See ad on page 49

McPHERSON
Metrohm
866-METROHM
Ocean Insight
+1 (407) 673-0041
PIKE Technologies
(608) 274-2721
Shimadzu Scientific Instruments
Spectra Vista Corporation

POINT-OF-MEASUREMENT ANALYZER SYSTEMS

MEDICAL/ IN VIVO DIAGNOSTICS

NEAR-IR
Metrohm
866-METROHM
Newsight Imaging

OTHER MEDICAL/ IN VIVO DIAGNOSTICS
Ionica Sciences
Newsight Imaging

RAMAN
IS Instruments
Metrohm
866-METROHM

UV/VIS
Newsight Imaging

MOBILE/PORTABLE/ ON-SITE/FIELD-BASED ANALYZERS

NEAR-IR
Metrohm
866-METROHM

OTHER MOBILE/PORTABLE/ ON-SITE/FIELD-BASED ANALYZERS
Excellims
Spectra Vista Corporation

RAMAN
Acutech Scientific Inc.
IS Instruments
Metrohm
866-METROHM
Nanobase, Inc.
+82 70 8666 0233

X-RAY
AXT - Scientific Solutions for Industry and Academia

ONLINE/AT-LINE/NEAR-LINE ANALYZERS

NEAR-IR
Metrohm
866-METROHM

OTHER ON-LINE/AT-LINE/ NEAR-LINE ANALYZERS
Applied Rigaku Technologies, Inc.
+1 (512) 225-1796

RAMAN
Acutech Scientific Inc.
IS Instruments
Metrohm
866-METROHM
Nanobase, Inc.
+82 70 8666 0233

X-RAY
Applied Rigaku Technologies, Inc.
+1 (512) 225-1796

REFURBISHED/ PREVIOUSLY OWNED INSTRUMENTS

ATOMIC EMISSION SPECTROMETERS (INCLUDING ICP-OES, ICP-MS, & DCP)
Analytik Jena US
(909) 946-3197, (800) 452-6788
Glass Expansion

INFRARED SPECTROMETERS (INCLUDING FT-IR & NEAR-IR)
Metrohm
866-METROHM
Spectra Vista Corporation
Thermo Scientific
+1 (800) 532-4752

MASS SPECTROMETERS (INCLUDING GC–MS, LC–MS, & MASS SPECTROMETRY DETECTORS)
Analytik Jena US
(909) 946-3197, (800) 452-6788
Elementar Analysensysteme GmbH
IonSense
Quantum Analytics

OTHER
Quantum Analytics

PHOTOMETERS
Edinburgh Instruments
+44 15 06425300

RAMAN SPECTROMETERS
Metrohm
866-METROHM

UV/VIS SPECTROPHOTOMETERS
Analytik Jena US
(909) 946-3197, (800) 452-6788

SURFACE SPECTROSCOPY & MICROANALYSIS

AFM
HORIBA Scientific
Mad City Labs Inc.

WITec Raman Imaging Solutions
Email: info@WITec.de
https://raman.oxinst.com
+49(0)731 140 700
See ad on page 35

AUGER
Physical Electronics

EDS
EDAX
(201) 529-4880
Physical Electronics

ESCA/X-RAY PHOTOELECTRON SPECTROSCOPY
Physical Electronics

NSOM
Mad City Labs Inc.

WITec Raman Imaging Solutions
Email: info@WITec.de
https://raman.oxinst.com
+49(0)731 140 700
See ad on page 35

OTHER MICROANALYSIS/ IMAGING EQUIPMENT
EDAX
(201) 529-4880
Edinburgh Instruments
+44 15 06425300
HORIBA Scientific
Lambert Instruments BV

WITec Raman Imaging Solutions
Email: info@WITec.de
https://raman.oxinst.com
+49(0)731 140 700
See ad on page 35

SEM
AXT - Scientific Solutions for Industry and Academia
EDAX
(201) 529-4880
Physical Electronics

SERS
Edinburgh Instruments
+44 15 06425300
HORIBA Scientific
Mad City Labs Inc.
Metrohm
866-METROHM
Ocean Insight
+1 (407) 673-0041

SIMS
AXT - Scientific Solutions for Industry and Academia
Physical Electronics

TEM
AXT - Scientific Solutions for Industry and Academia
EDAX
(201) 529-4880

OPTICS, ELECTRO-OPTICS, OPTRONICS, FIBEROPTICS, AND RELATED COMPONENTS

DETECTORS & RELATED EQUIPMENT

CCDS
Diffraction Limited
McPHERSON
PerkinElmer, Inc.
Thermo Scientific - CIDTEC

ICCDS
Thermo Scientific - CIDTEC

INGAAS
Princeton Infrared Technologies, Inc.

IR ARRAYS
Princeton Infrared Technologies, Inc.

LASER POWER METERS/PROBES
Newport Corporation

MULTICHANNEL PLATE DETECTORS
McPHERSON

PHOTOMULTIPLIER DETECTORS
McPHERSON

SILICON DIODES/ PHOTOCELLS
McPHERSON

DISPERSIVE COMPONENTS (OEM)

INTERFEROMETERS
NeoSpectra by Si-Ware

MONOCHROMATORS
Newport Corporation
Newsight Imaging
McPHERSON

SPECTROGRAPHS
Coherent, Inc.
McPHERSON

HIGH VOLTAGE POWER SUPPLIES

HIGH VOLTAGE TRANSFORMERS, CUSTOM & STANDARD PRODUCTS
McPHERSON

LAMPS/LIGHT SOURCES

DEUTERIUM
Avantes
McPHERSON
Ocean Insight
+1 (407) 673-0041
REFLEX Analytical Corporation
(201) 444-8958
REFLEX Analytical Corporation
Email: reflexusa@att.net
www.reflexusa.com
(201) 444-8958
See ad on page 82

FIBER OPTIC LIGHT SOURCES
Edinburgh Instruments
+44 15 06425300
ELODIZ Ltd
FiberTech Optica
Newport Corporation
Ocean Insight
+1 (407) 673-0041
SCHOTT North America, Inc. - Lighting and Imaging

HALOGEN
Ocean Insight
+1 (407) 673-0041
REFLEX Analytical Corporation
(201) 444-8958
SCHOTT North America, Inc. - Lighting and Imaging

HOLLOW-CATHODE
McPHERSON
REFLEX Analytical Corporation
(201) 444-8958

KRYPTON
Ocean Insight
+1 (407) 673-0041
REFLEX Analytical Corporation
(201) 444-8958

LAMPS/LIGHT SOURCES
Avantes
Newport Corporation
Ocean Insight
+1 (407) 673-0041

LED LIGHTING
ELODIZ Ltd
Ocean Insight
+1 (407) 673-0041
SCHOTT North America, Inc. - Lighting and Imaging

QUARTZ TUNGSTEN-HALOGEN
Avantes
Light in Motion
Ocean Insight
+1 (407) 673-0041
REFLEX Analytical Corporation
(201) 444-8958

LASERS

ARGON-ION
Coherent, Inc.

CO_2
Coherent, Inc.
Edinburgh Instruments
+44 15 06425300

DIODE/ SEMICONDUCTOR
HÜBNER Photonics - High performance lasers
Email: sales@hubner-photonics.com
https://hubner-photonics.com
+46 854 591 230
See ad on page 7

DIODE-PUMPED SOLID-STATE
Coherent, Inc.
HÜBNER Photonics - High performance lasers
Email: sales@hubner-photonics.com
https://hubner-photonics.com
+46 854 591 230
See ad on page 7
RPMC Lasers Inc

ND: YAG
HÜBNER Photonics - High performance lasers
Email: sales@hubner-photonics.com
https://hubner-photonics.com
+46 854 591 230
See ad on page 7

OPO
HÜBNER Photonics - High performance lasers
Email: sales@hubner-photonics.com
https://hubner-photonics.com
+46 854 591 230
See ad on page 7

OPTICAL MACHINERY
McPHERSON

ULTRA FAST
HÜBNER Photonics - High performance lasers
Email: sales@hubner-photonics.com
https://hubner-photonics.com
+46 854 591 230
See ad on page 7

LASER SAFETY PRODUCTS
Ocean Insight
+1 (407) 673-0041

OPTICAL COMPONENTS/ FIBER OPTICS

ATTENUATORS
Avantes

BEAM SPLITTERS
Avantes
REFLEX Analytical Corporation
(201) 444-8958

CRYSTAL OPTICS
REFLEX Analytical Corporation
(201) 444-8958

FIBER OPTICS, MID-IR (BUNDLES)
Armadillo SIA
Art photonics
+49 30 67798870
FiberTech Optica
Harrick Scientific Products Inc
NLIR
PIKE Technologies
(608) 274-2721

FIBER OPTICS, NEAR-IR (BUNDLES)
Armadillo SIA
Art photonics
+49 30 67798870
FiberTech Optica
SCHOTT North America, Inc. - Lighting and Imaging

HOLOGRAPHIC GRATINGS
McPHERSON
Newport Corporation

FIBER OPTICS, MID-IR (SINGLE FIBERS)
Armadillo SIA
Art photonics
+49 30 67798870
FiberTech Optica
Harrick Scientific Products Inc
NLIR
Ocean Insight
+1 (407) 673-0041
RPMC Lasers Inc

FIBER OPTICS, NEAR-IR (SINGLE FIBERS)
Armadillo SIA
FiberTech Optica
Ocean Insight
+1 (407) 673-0041
RPMC Lasers Inc

FIBER OPTICS, UV (SINGLE FIBERS)
Armadillo SIA
Avantes
FiberTech Optica
Ocean Insight
+1 (407) 673-0041
RPMC Lasers Inc

FIBER OPTICS, UV (BUNDLES)
Armadillo SIA
Art photonics
+49 30 67798870
FiberTech Optica

MIRRORS
McPHERSON

FILTERS/ FILTER WHEELS
McPHERSON

MULTIPLEXERS
Avantes

OPTICAL CHOPPERS
McPHERSON

POLARIZATION OPTICS
Harrick Scientific Products Inc
REFLEX Analytical Corporation
(201) 444-8958

PRISMS
REFLEX Analytical Corporation
(201) 444-8958

OTHER OPTICAL COMPONENTS/ FIBER OPTICS
Armadillo SIA
FiberTech Optica
Ocean Insight
+1 (407) 673-0041
REFLEX Analytical Corporation
(201) 444-8958
SCHOTT North America, Inc. - Lighting and Imaging
Wavelength Electronics
Email: sales@teamwavelength.com
www.teamwavelength.com
(406) 587-4910

UV-IR LENSES
REFLEX Analytical Corporation
(201) 444-8958

WINDOWS
REFLEX Analytical Corporation
Email: reflexusa@att.net
www.reflexusa.com
(201) 444-8958
See ad on page 82

X-RAY OPTICS
McPHERSON
SCHOTT North America, Inc. - Lighting and Imaging

SAMPLING/SAMPLE HANDLING

ANALYTICAL STANDARDS/ REFERENCE MATERIALS

CALIBRATION STANDARDS
ASI Standards
Bruker Optics
+1 (978) 430-2394
Inorganic Ventures
Ocean Insight
+1 (407) 673-0041
PerkinElmer, Inc.
PIKE Technologies
(608) 274-2721
SCP SCIENCE
(514) 457-0701, (800) 361-6820

DILUTION SYSTEMS FOR STANDARD PREPARATION
SCP SCIENCE
(514) 457-0701, (800) 361-6820

LABELED COMPOUNDS
Edinburgh Instruments
+44 15 06425300

REAGENTS
Alpha Resources LLC
SCP SCIENCE
(514) 457-0701, (800) 361-6820

REFERENCE MATERIALS AND CERTIFIED REFERENCE MATERIALS, INORGANIC
Alpha Resources LLC
Bruker Optics
+1 (978) 430-2394
Inorganic Ventures
International Centre for Diffraction Data
PerkinElmer, Inc.
SCP SCIENCE
(514) 457-0701, (800) 361-6820

REFERENCE MATERIALS AND CERTIFIED REFERENCE MATERIALS, ORGANIC
Alpha Resources LLC
Bruker Optics
+1 (978) 430-2394
International Centre for Diffraction Data

CUVETTES/CELLS

CYLINDRICAL CELLS
REFLEX Analytical Corporation
(201) 444-8958

FLOW CELLS
Ocean Insight
+1 (407) 673-0041
REFLEX Analytical Corporation
(201) 444-8958

MICRO CELLS
Ocean Insight
+1 (407) 673-0041
REFLEX Analytical Corporation
(201) 444-8958

MICRO FLOW CELLS
REFLEX Analytical Corporation
(201) 444-8958

SEMIMICRO CELLS
REFLEX Analytical Corporation
(201) 444-8958

STANDARD TRANSMITTANCE
REFLEX Analytical Corporation
Email: reflexusa@att.net
www.reflexusa.com
(201) 444-8958
See ad on page 82

THREADED CAP
REFLEX Analytical Corporation
(201) 444-8958

HPLC/FT-IR INTERFACES
Excellims

IMMERSION PROBES
Bruker Optics
+1 (978) 430-2394
Coherent, Inc.
Metrohm
866-METROHM
Ocean Insight
+1 (407) 673-0041

MISCELLANEOUS PREPARATION DEVICES

EVACUABLE DIES
REFLEX Analytical Corporation
Email: reflexusa@att.net
www.reflexusa.com
(201) 444-8958
See ad on page 82

GRINDERS
REFLEX Analytical Corporation
(201) 444-8958
Verder Scientific Inc

LABORATORY PRESSES
REFLEX Analytical Corporation
(201) 444-8958
Verder Scientific Inc

MILLS
REFLEX Analytical Corporation
(201) 444-8958
Verder Scientific Inc

OTHER MISCELLANEOUS PREPARATION DEVICES
S.T.Japan-Europe GmbH
Verder Scientific Inc

THIN FILM FABRICATORS
REFLEX Analytical Corporation
(201) 444-8958

SAMPLE DIGESTION EQUIPMENT/ELEMENTAL ANALYSIS

MICROWAVE DIGESTION/ EXTRACTION

BLOCK DIGESTION UNITS, PROGRAMMABLE
CEM Corp.
Milestone, Inc.
(866) 995-5100
SCP SCIENCE
(514) 457-0701, (800) 361-6820

CLOSED VESSEL
CEM Corp.
Milestone, Inc.
(866) 995-5100
PerkinElmer, Inc.
SCP SCIENCE
(514) 457-0701, (800) 361-6820

HOTPLATES (HTP)
CEM Corp.
SCP SCIENCE
(514) 457-0701, (800) 361-6820

MICROWAVE-ASSISTED EXTRACTION
CEM Corp.
Milestone, Inc.
(866) 995-5100
PerkinElmer, Inc.
SCP SCIENCE
(514) 457-0701, (800) 361-6820

SIMULTANEOUS DIGESTION SYSTEMS
Milestone, Inc.
(866) 995-5100

SAMPLE HANDLING ACCESSORIES

ATTENUATED TOTAL REFLECTION/INTERNAL REFLECTANCE CELLS
Bruker Optics
+1 (978) 430-2394
PerkinElmer, Inc.
PIKE Technologies
(608) 274-2721
REFLEX Analytical Corporation
(201) 444-8958

CYLINDRICAL INTERNAL REFLECTANCE
REFLEX Analytical Corporation
(201) 444-8958

DIAMOND ANVIL
S.T.Japan-Europe GmbH

DIFFUSE REFLECTANCE CELLS
PIKE Technologies
(608) 274-2721
REFLEX Analytical Corporation
(201) 444-8958

FLOW-THROUGH
REFLEX Analytical Corporation
(201) 444-8958

FT-RAMAN ACCESSORIES
Bruker Optics
+1 (978) 430-2394
S.T.Japan-Europe GmbH
Wavelength Electronics
Email: sales@teamwavelength.com
www.teamwavelength.com
(406) 587-4910

GAS
Bruker Optics
+1 (978) 430-2394
REFLEX Analytical Corporation
(201) 444-8958

HIGH-PRESSURE
Bruker Optics
+1 (978) 430-2394
REFLEX Analytical Corporation
(201) 444-8958

HORIZONTAL ATTENUATED TOTAL REFLECTANCE
PIKE Technologies
(608) 274-2721
REFLEX Analytical Corporation
(201) 444-8958

INTEGRATING SPHERES
Newport Corporation
Ocean Insight
+1 (407) 673-0041
PIKE Technologies
(608) 274-2721

LIQUID
Analytik Jena US
(909) 946-3197, (800) 452-6788
Bruker Optics
+1 (978) 430-2394
REFLEX Analytical Corporation
(201) 444-8958
SCP SCIENCE
(514) 457-0701, (800) 361-6820

MICROSPECTROSCOPY
Coherent, Inc.
S.T.Japan-Europe GmbH

MICROWELL PLATE READERS
Coherent, Inc.

REFLECTANCE
Bruker Optics
+1 (978) 430-2394
Ocean Insight
+1 (407) 673-0041
REFLEX Analytical Corporation
(201) 444-8958

SOLID
REFLEX Analytical Corporation
(201) 444-8958

SPECULAR REFLECTANCE
Ocean Insight
+1 (407) 673-0041
PIKE Technologies
(608) 274-2721
REFLEX Analytical Corporation
(201) 444-8958

TRANSMISSION
Coherent, Inc.
Ocean Insight
+1 (407) 673-0041
PIKE Technologies
(608) 274-2721

REFLEX Analytical Corporation
(201) 444-8958
S.T.Japan-Europe GmbH

VARIABLE TEMPERATURE
BV Thermal Systems
REFLEX Analytical Corporation
(201) 444-8958

Wavelength Electronics
Email: sales@teamwavelength.com
www.teamwavelength.com
(406) 587-4910

SAMPLE INTRODUCTION EQUIPMENT

GRAPHITE TUBES
Alpha Resources LLC

REFLEX Analytical Corporation
Email: reflexusa@att.net
www.reflexusa.com
(201) 444-8958
See ad on page 82

SCP SCIENCE
(514) 457-0701, (800) 361-6820
Verder Scientific Inc

ICP-MS CONES
Glass Expansion
REFLEX Analytical Corporation
(201) 444-8958
SCP SCIENCE
(514) 457-0701, (800) 361-6820
Spectron, Inc.

NEBULIZERS

Savillex
Email: info@savillex.com
www.savillex.com
(952) 935-4100
See ad on page 45

MICROCONCENTRIC

Savillex
Email: info@savillex.com
www.savillex.com
(952) 935-4100
See ad on page 45

TEMPERATURE CONTROL DEVICES

Bruker Optics
+1 (978) 430-2394
BV Thermal Systems
Harrick Scientific Products Inc

Wavelength Electronics
Email: sales@teamwavelength.com
www.teamwavelength.com
(406) 587-4910

WINDOW/CUVETTE MATERIAL TYPES

BK7 GLASS
REFLEX Analytical Corporation
(201) 444-8958

CRYSTALLINE QUARTZ
REFLEX Analytical Corporation
(201) 444-8958

DIAMOND
S.T.Japan-Europe GmbH

INFRASIL
REFLEX Analytical Corporation
(201) 444-8958

METHACRYLATE
REFLEX Analytical Corporation
(201) 444-8958

PYREX
REFLEX Analytical Corporation
(201) 444-8958

SAPPHIRE
REFLEX Analytical Corporation
(201) 444-8958

SODIUM CHLORIDE
REFLEX Analytical Corporation
(201) 444-8958

UV-GRADE FUSED SILICA
REFLEX Analytical Corporation
(201) 444-8958

PRODUCTS AND SERVICES FOR SPECTROSCOPY

SPECTROSCOPY SOFTWARE/ COMPUTER HARDWARE/ AUTOMATION PRODUCTS

AUTOMATION EQUIPMENT

AUTOSAMPLERS
Shimadzu Scientific Instruments

SOFTWARE

CHEMOMETRICS SOFTWARE

DATA ACQUISITION SOFTWARE
Coherent, Inc.
Diffraction Limited
Lambert Instruments BV
Metrohm
866-METROHM

DISCRIMINANT ANALYSIS
Sartorius Data Analytics AB

PARTIAL LEAST SQUARES
Sartorius Data Analytics AB
Metrohm
866-METROHM

PRINCIPAL COMPONENT REGRESSION
Coherent, Inc.
Metrohm
866-METROHM

DATA PROCESSING SOFTWARE

3-D VISUALIZATION SOFTWARE
International Centre for Diffraction Data
Sartorius Data Analytics AB

CHEMICAL STRUCTURE SOFTWARE
Wiley Science Solutions

DATA MANAGEMENT
International Centre for Diffraction Data
LabVantage Solutions
NeoSpectra by Si-Ware
Shimadzu Scientific Instruments
Wiley Science Solutions

ELECTROSPRAY MAXIMUM ENTROPY SOFTWARE
Diffraction Limited

INSTRUMENT CONTROL SOFTWARE
Diffraction Limited
Edinburgh Instruments
+44 15 06425300
ELODIZ Ltd
Ocean Insight
+1 (407) 673-0041
Optiwave Systems Inc

MOLECULAR MODELING/ SIMULATION
International Centre for Diffraction Data

PEAK FITTING
International Centre for Diffraction Data

PEAK PICKING
Metrohm
866-METROHM
S.T.Japan-Europe GmbH

QUANTITATION
International Centre for Diffraction Data
Metrohm
866-METROHM

SMOOTHING
International Centre for Diffraction Data
Metrohm
866-METROHM

SPECTRAL SEARCH SOFTWARE
International Centre for Diffraction Data
S.T.Japan-Europe GmbH
Wiley Science Solutions

STATISTICAL PROCESS CONTROL/QUALITY CONTROL SOFTWARE
Sartorius Data Analytics AB

SPECTRAL LIBRARIES

FORENSICS/ILLICIT DRUG COMPOUNDS
International Centre for Diffraction Data
PerkinElmer, Inc.
S.T.Japan-Europe GmbH
Wiley Science Solutions

IR
PerkinElmer, Inc.
S.T.Japan-Europe GmbH
Wiley Science Solutions

MS
Wiley Science Solutions

NMR
Wiley Science Solutions

OTHER SPECTRAL LIBRARIES
International Centre for Diffraction Data
S.T.Japan-Europe GmbH
Shimadzu Scientific Instruments
Wiley Science Solutions

PHARMACEUTICAL COMPOUNDS
International Centre for Diffraction Data
S.T.Japan-Europe GmbH

POLYMER COMPOUNDS
International Centre for Diffraction Data
Metrohm
866-METROHM
S.T.Japan-Europe GmbH

RAMAN
Edinburgh Instruments
+44 15 06425300
IS Instruments
Metrohm
866-METROHM
Nanobase, Inc.
+82 70 8666 0233
S.T.Japan-Europe GmbH
Wiley Science Solutions
WITec Raman Imaging Solutions
+49(0)731 140 700

SPECTROSCOPY SERVICES

CONSULTING

Excellims
Metrohm
866-METROHM
Ocean Insight
+1 (407) 673-0041

CONTRACT RESEARCH & ANALYSIS

Excellims
IS Instruments
Malvern Panalytical
McPHERSON
Physical Electronics

EDUCATION/TRAINING

Inorganic Ventures
International Centre for Diffraction Data
Metrohm
866-METROHM
PerkinElmer, Inc.

INSTRUMENT DESIGN

ELODIZ Ltd
Harrick Scientific Products Inc
McPHERSON
Optiwave Systems Inc
RaySpec Ltd
Wasatch Photonics

LABORATORY EQUIPMENT REPAIR

Edinburgh Instruments
+44 15 06425300

McPHERSON
SCP SCIENCE
(514) 457-0701, (800) 361-6820

PROFESSIONAL ORGANIZATIONS

International Centre for Diffraction Data

PUBLISHING

International Centre for Diffraction Data

SPECTRAL INTERPRETATION

International Centre for Diffraction Data

PRODUCTS AND SERVICES FOR SPECTROSCOPY

GENERAL SCIENTIFIC EQUIPMENT AND ACCESSORIES

ANALYZERS, SENSORS, AND TESTING INSTRUMENTS

CALORIMETERS

Hitachi High-Tech Analytical Science
PerkinElmer, Inc.

COLORIMETERS

Newsight Imaging
Shimadzu Scientific Instruments

DYNAMIC MECHANICAL ANALYZERS

Hitachi High-Tech Analytical Science

EDDY CURRENT EQUIPMENT

Hitachi High-Tech Analytical Science

ELEMENTAL ANALYZERS

Applied Rigaku Technologies, Inc.
+1 (512) 225-1796
EDAX
(201) 529-4880
Elementar Analysensysteme GmbH
Exum Instruments
Hitachi High-Tech Analytical Science
HORIBA Scientific
Malvern Panalytical
Verder Scientific Inc

FLOW METERS

Bruker Optics
+1 (978) 430-2394

HARDNESS TESTING EQUIPMENT

Shimadzu Scientific Instruments
Verder Scientific Inc

MICROPLATE READERS

Coherent, Inc.
HORIBA Scientific
LTB Lasertechnik Berlin GmbH

MOLECULAR WEIGHT ANALYZERS

Malvern Panalytical

NONDESTRUCTIVE TESTING/INSPECTION EQUIPMENT, GENERAL

Applied Rigaku Technologies, Inc.
+1 (512) 225-1796
Bruker Optics
+1 (978) 430-2394
EDAX
(201) 529-4880
Hitachi High-Tech Analytical Science
PerkinElmer, Inc.
Shimadzu Scientific Instruments

OTHER ANALYZERS

Applied Rigaku Technologies, Inc.
+1 (512) 225-1796
Bruker Optics
+1 (978) 430-2394
EDAX
(201) 529-4880
HORIBA Scientific
Metrohm
866-METROHM
Verder Scientific Inc

PARTICLE SIZE ANALYZERS

Shimadzu Scientific Instruments
HORIBA Scientific
Malvern Panalytical
Shimadzu Scientific Instruments
Verder Scientific Inc
WITec Raman Imaging Solutions
+49(0)731 140 700

PHOTOMETERS

HORIBA Scientific

PYROLYSIS EQUIPMENT

Verder Scientific Inc

SENSORS

Bruker Optics
+1 (978) 430-2394
Diffraction Limited
Newsight Imaging

SURFACE ANALYZERS

HORIBA Scientific
Verder Scientific Inc

TENSILE TESTING EQUIPMENT

Shimadzu Scientific Instruments

THERMOGRAVIMETRIC ANALYZERS

Hitachi High-Tech Analytical Science
PerkinElmer, Inc.
Shimadzu Scientific Instruments
Verder Scientific Inc

THERMOMECHANICAL ANALYZERS

Hitachi High-Tech Analytical Science
PerkinElmer, Inc.
Shimadzu Scientific Instruments

VISCOMETERS

PerkinElmer, Inc.

WATER PURIFICATION EQUIPMENT

Newsight Imaging

LABORATORY CHEMICALS, GASES, AND MATERIALS

CHEMICALS

Inorganic Ventures

OTHER LABORATORY CHEMICALS, GASES AND MATERIALS

Inorganic Ventures

REAGENTS

Inorganic Ventures
SCP SCIENCE
(514) 457-0701, (800) 361-6820

STANDARDS

Inorganic Ventures
SCP SCIENCE
(514) 457-0701, (800) 361-6820

LABORATORY EQUIPMENT

BALANCES

Shimadzu Scientific Instruments

DISTILLATION SYSTEMS

American Cannabis Technologies
Milestone, Inc.
(866) 995-5100
SCP SCIENCE
(514) 457-0701, (800) 361-6820

FILTRATION/ PURIFICATION EQUIPMENT

Bruker Optics
+1 (978) 430-2394
SCP SCIENCE
(514) 457-0701, (800) 361-6820

FITTINGS/FLANGES

American Cannabis Technologies

FLUID HANDLING EQUIPMENT

Bruker Optics
+1 (978) 430-2394
SCP SCIENCE
(514) 457-0701, (800) 361-6820

GLASSWARE

American Cannabis Technologies
Spectron, Inc.

HEATERS/COOLERS

Wavelength Electronics
Email: sales@teamwavelength.com
www.teamwavelength.com
(406) 587-4910

HOMOGENIZERS

Bruker Optics
+1 (978) 430-2394
Verder Scientific Inc

PLASTIC WARE

Savillex
Email: info@savillex.com
www.savillex.com
(952) 935-4100
See ad on page 45

SHAKERS/STIRRERS
Verder Scientific Inc

TEMPERATURE/ PRESSURE CONTROLLERS
BV Thermal Systems
Verder Scientific Inc

Wavelength Electronics
Email: sales@teamwavelength.com
www.teamwavelength.com
(406) 587-4910

TUBING
Spectron, Inc.

LABORATORY FURNISHINGS

FURNITURE
Verder Scientific Inc

WORKBENCHES
Verder Scientific Inc

MICROSCOPES, MICROSPECTROMETERS, AND IMAGING EQUIPMENT

IMAGING EQUIPMENT/ ACCESSORIES

CCD CAMERAS
Diffraction Limited
e-con Systems
HORIBA Scientific
Lambert Instruments BV
PerkinElmer, Inc.
Thermo Scientific - CIDTEC

FIBER OPTICS
Edinburgh Instruments
+44 15 06425300
FiberTech Optica

HYPERSPECTRAL IMAGING EQUIPMENT/SOFTWARE
ABB Measurement and Analytics
418 877 2944
HORIBA Scientific
HySpex by NEO
WITec Raman Imaging Solutions
+49(0)731 140 700

IMAGE ANALYZERS/ INTENSIFIERS
Lambert Instruments BV

OTHER IMAGING EQUIPMENT/ ACCESSORIES
Edinburgh Instruments
+44 15 06425300
HORIBA Scientific
Mad City Labs Inc.
WITec Raman Imaging Solutions
+49(0)731 140 700

MICROSCOPES

ATOMIC FORCE MICROSCOPES
HORIBA Scientific
Mad City Labs Inc.
WITec Raman Imaging Solutions
+49(0)731 140 700

CONFOCAL MICROSCOPES
Bruker Optics
+1 (978) 430-2394
Edinburgh Instruments
+44 15 06425300
HORIBA Scientific
WITec Raman Imaging Solutions
+49(0)731 140 700

FLUORESCENCE MICROSCOPES
Edinburgh Instruments
+44 15 06425300
HORIBA Scientific
Mad City Labs Inc.
PerkinElmer, Inc.
WITec Raman Imaging Solutions
+49(0)731 140 700

INFRARED MICROSCOPES/ FT-IR MICROSPECTROMETERS
Bruker Optics
+1 (978) 430-2394
DRS Daylight Solutions
PerkinElmer, Inc.
Shimadzu Scientific Instruments

NEAR-FIELD SCANNING MICROSCOPES
Mad City Labs Inc.
WITec Raman Imaging Solutions
+49(0)731 140 700

OTHER MICROSCOPES
HORIBA Scientific
Mad City Labs Inc.

RAMAN MICROSCOPES/ MICROSPECTROMETERS
Bruker Optics
+1 (978) 430-2394
Edinburgh Instruments
+44 15 06425300
HORIBA Scientific
Malvern Panalytical
Nanobase, Inc.
+82 70 8666 0233
WITec Raman Imaging Solutions
+49(0)731 140 700

SCANNING PROBE MICROSCOPES
Mad City Labs Inc.
Physical Electronics
WITec Raman Imaging Solutions
+49(0)731 140 700

MICROSCOPE ACCESSORIES

OTHER MICROSCOPE ACCESSORIES
Diffraction Limited
Edinburgh Instruments
+44 15 06425300
Mad City Labs Inc.
PIKE Technologies
(608) 274-2721
S.T.Japan-Europe GmbH
WITec Raman Imaging Solutions
+49(0)731 140 700

SLIDES AND MOUNTS
PIKE Technologies
(608) 274-2721
S.T.Japan-Europe GmbH

SOFTWARE
Bruker Optics
+1 (978) 430-2394
Edinburgh Instruments
+44 15 06425300
Lambert Instruments BV

SPECIMEN PREPARATION
S.T.Japan-Europe GmbH

PROCESS ANALYTICAL INSTRUMENTATION

APPLIED SPECTROSCOPIC OR PHOTOMETRIC ANALYZERS

ARC/SPARK SPECTROMETERS
Hitachi High-Tech Analytical Science

ATOMIC/ELEMENTAL SPECTROMETERS
Applied Rigaku Technologies, Inc.
+1 (512) 225-1796
Malvern Panalytical

FIBER-OPTIC SPECTROPHOTOMETERS
FiberTech Optica
Ocean Insight
+1 (407) 673-0041

FLUORESCENCE SPECTROMETERS
Edinburgh Instruments
+44 15 06425300
Ocean Insight
+1 (407) 673-0041
PerkinElmer, Inc.

FOURIER TRANSFORM-IR SPECTROMETERS
ABB Measurement and Analytics
Email: contact.center@us.abb.com
https://global.abb
418 877 2944
See ad on page 5

Bruker Optics
+1 (978) 430-2394
PerkinElmer, Inc.
Thermo Scientific
+1 (800) 532-4752

GC-IR ANALYZERS
Thermo Scientific
+1 (800) 532-4752

GC-MS ANALYZERS
Thermo Scientific
+1 (800) 532-4752

INFRARED (NON-FT) SPECTROMETERS
DRS Daylight Solutions
PerkinElmer, Inc.

LASER-INDUCED BREAKDOWN SPECTROMETERS
Ocean Insight
+1 (407) 673-0041

MASS SPECTROMETERS
Exum Instruments
Physical Electronics

MICROSPECTROMETERS
Ocean Insight
+1 (407) 673-0041

NEAR-IR SPECTROMETERS
ABB Measurement and Analytics
Email: contact.center@us.abb.com
https://global.abb
418 877 2944
See ad on page 5

Bruker Optics
+1 (978) 430-2394
Malvern Panalytical
Metrohm
866-METROHM
Ocean Insight
+1 (407) 673-0041
PerkinElmer, Inc.
Spectra Vista Corporation

PHOTOMETERS
ABB Measurement and Analytics
418 877 2944
Bruker Optics
+1 (978) 430-2394

RAMAN SPECTROMETERS
Bruker Optics
+1 (978) 430-2394
Coherent, Inc.
Edinburgh Instruments
+44 15 06425300
IS Instruments
Metrohm
866-METROHM
Nanobase, Inc.
+82 70 8666 0233
Ocean Insight
+1 (407) 673-0041

THERMOGRAVIMETRIC ANALYZERS-INFRARED SPECTROMETERS
DRS Daylight Solutions
PerkinElmer, Inc.

UV SPECTROMETERS
Ocean Insight
+1 (407) 673-0041

UV/VIS SPECTROMETERS
Bruker Optics
+1 (978) 430-2394
Edinburgh Instruments
+44 15 06425300
Ocean Insight
+1 (407) 673-0041
PerkinElmer, Inc.

VISIBLE SPECTROMETERS
Ocean Insight
+1 (407) 673-0041

X-RAY SPECTROMETERS (ENERGY-DISPERSIVE)
Applied Rigaku Technologies, Inc.
+1 (512) 225-1796
Hitachi High-Tech Analytical Science
Malvern Panalytical

X-RAY SPECTROMETERS (WAVELENGTH-DISPERSIVE)
AXT - Scientific Solutions for Industry and Academia
Malvern Panalytical

CHROMATOGRAPHIC PROCESS ANALYZERS

GAS CHROMATOGRAPHS (GC), PROCESS
ABB Measurement and Analytics
418 877 2944
Thermo Scientific
+1 (800) 532-4752

GC-INFRARED SPECTROMETERS, PROCESS
Thermo Scientific
+1 (800) 532-4752

LC-INFRARED SPECTROMETERS
DRS Daylight Solutions

LC-MASS SPECTROMETERS, PROCESS
IonSense

LIQUID CHROMATOGRAPHS (LC), PROCESS
IonSense

CONDITION/PROPERTY ANALYZERS

AIR QUALITY MONITORS
Thermo Scientific
+1 (800) 532-4752

GAS ANALYZERS, AMBIENT
ABB Measurement and Analytics
418 877 2944
Thermo Scientific
+1 (800) 532-4752
Verder Scientific Inc

GAS ANALYZERS, COMBUSTIBLE
Verder Scientific Inc

GAS ANALYZERS, LAB-BASED
ABB Measurement and Analytics
Email: contact.center@us.abb.com
https://global.abb
418 877 2944
See ad on page 5

IS Instruments
Thermo Scientific
+1 (800) 532-4752
Verder Scientific Inc

GAS ANALYZERS, ON-LINE
ABB Measurement and Analytics
Email: contact.center@us.abb.com
https://global.abb
418 877 2944
See ad on page 5

IS Instruments
Thermo Scientific
+1 (800) 532-4752

GAS ANALYZERS, STACK/FLUE EMISSIONS
Thermo Scientific
+1 (800) 532-4752

GAS ANALYZERS, TOXIC
Thermo Scientific
+1 (800) 532-4752

MOISTURE ANALYZERS
ABB Measurement and Analytics
418 877 2944
Metrohm
866-METROHM
Verder Scientific Inc

OXYGEN ANALYZERS
Verder Scientific Inc

SOLIDS/SLURRIES ANALYZERS, LAP-BASED
Metrohm
866-METROHM

SOLIDS/SLURRIES ANALYZERS, ON-LINE
Malvern Panalytical

INDUSTRIAL ENVIRONMENTAL MONITORING INSTRUMENTS

CONTINUOUS EMISSIONS MONITORS
AXT - Scientific Solutions for Industry and Academia
Bruker Optics
+1 (978) 430-2394

FENCELINE/PERIMETER MONITORING INSTRUMENTS
Bruker Optics
+1 (978) 430-2394

FIELD-BASED SPECTROSCOPY EQUIPMENT
Bruker Optics
+1 (978) 430-2394

HYPERSPECTRAL IMAGING EQUIPMENT
ABB Measurement and Analytics
418 877 2944
Bruker Optics
+1 (978) 430-2394
HySpex by NEO

LIDAR
IS Instruments

MOBILE/PORTABLE LABORATORIES
Spectra Vista Corporation

OPTICAL REMOTE SENSING INSTRUMENTS
ABB Measurement and Analytics
Email: contact.center@us.abb.com
https://global.abb
418 877 2944
See ad on page 5

STACK/FLUE GAS EMISSIONS MONITORS
ABB Measurement and Analytics
418 877 2944

OTHER INDUSTRIAL ANALYZERS AND TESTING EQUIPMENT

CALORIMETERS
PerkinElmer, Inc.

FLOWMETERS
Bruker Optics
+1 (978) 430-2394

INFRARED ANALYZERS

ABB Measurement and Analytics
Email: contact.center@us.abb.com
https://global.abb
418 877 2944
See ad on page 5

Bruker Optics
+1 (978) 430-2394
DRS Daylight Solutions
Keit Spectrometers
PerkinElmer, Inc.

LASER-BASED ANALYZERS

ABB Measurement and Analytics
418 877 2944
Bruker Optics
+1 (978) 430-2394
Hitachi High-Tech Analytical Science
LTB Lasertechnik Berlin GmbH
Metrohm
866-METROHM

NONDESTRUCTIVE TESTING EQUIPMENT

ABB Measurement and Analytics
418 877 2944
Applied Rigaku Technologies, Inc.
+1 (512) 225-1796
Hitachi High-Tech Analytical Science
Metrohm
866-METROHM

PH INSTRUMENTS

ABB Measurement and Analytics
418 877 2944

PARTICLE ANALYZERS, LAB-BASED

Bruker Optics
+1 (978) 430-2394
Verder Scientific Inc

PARTICLE ANALYZERS, ON-LINE

Bruker Optics
+1 (978) 430-2394
Verder Scientific Inc

PETROLEUM TESTING EQUIPMENT

Applied Rigaku Technologies, Inc.
+1 (512) 225-1796
Bruker Optics
+1 (978) 430-2394

SENSORS, OPTICAL

ABB Measurement and Analytics
418 877 2944
Bruker Optics
+1 (978) 430-2394
Metrohm
866-METROHM
Princeton Infrared Technologies, Inc.

SENSORS, OTHER

Princeton Infrared Technologies, Inc.

Wavelength Electronics
Email: sales@teamwavelength.com
www.teamwavelength.com
(406) 587-4910

STRESS/STRAIN ANALYZERS

PerkinElmer, Inc.

TENSILE STRENGTH ANALYZERS

PerkinElmer, Inc.

TEST AND MEASUREMENT EQUIPMENT, GENERAL

ABB Measurement and Analytics
418 877 2944
Applied Rigaku Technologies, Inc.
+1 (512) 225-1796
Bruker Optics
+1 (978) 430-2394
Hitachi High-Tech Analytical Science
Metrohm
866-METROHM
Verder Scientific Inc

Wavelength Electronics
Email: sales@teamwavelength.com
www.teamwavelength.com
(406) 587-4910

THERMAL ANALYZERS

Bruker Optics
+1 (978) 430-2394
Hitachi High-Tech Analytical Science
PerkinElmer, Inc.

VISCOMETERS

PerkinElmer, Inc.

X-RAY ANALYSIS EQUIPMENT

Applied Rigaku Technologies, Inc.
+1 (512) 225-1796
Hitachi High-Tech Analytical Science
Physical Electronics

PROCESS ANALYTICAL ACCESSORIES/ ANCILLARY PRODUCTS

CALIBRATION EQUIPMENT/SERVICES

Bruker Optics
+1 (978) 430-2394
Ocean Insight
+1 (407) 673-0041

FIBER OPTICS AND RELATED PRODUCTS

Armadillo SIA
FiberTech Optica
Ocean Insight
+1 (407) 673-0041

Wavelength Electronics
Email: sales@teamwavelength.com
www.teamwavelength.com
(406) 587-4910

SAFETY EQUIPMENT

Bruker Optics
+1 (978) 430-2394

SOFTWARE, INSTRUMENT CONTROL

Bruker Optics
+1 (978) 430-2394
Optiwave Systems Inc

SOFTWARE, VALIDATION

Bruker Optics
+1 (978) 430-2394

PRODUCTS AND SERVICES FOR SPECTROSCOPY

BIOANALYSIS INSTRUMENTS

BIOANALYZERS AND RELATED EQUIPMENT

AUTOSAMPLERS

Excellims
Verder Scientific Inc

BIOSENSORS

Ionica Sciences

CHROMATOGRAPHY, LIQUID

Malvern Panalytical
Newsight Imaging

FLUORIMETERS

Avantes

LUMINESCENCE SPECTROMETERS

Avantes

PHOTOMETERS

Newsight Imaging

PLATE READERS, SPECTROMETERS, FLUORESCENCE

LTB Lasertechnik Berlin GmbH

SPECTROMETERS, IR

Metrohm
866-METROHM
PerkinElmer, Inc.
PhaseTech Spectroscopy

SPECTROMETERS, MASS

Excellims

SPECTROMETERS, RAMAN

Avantes
IS Instruments
LTB Lasertechnik Berlin GmbH
Metrohm
866-METROHM
Nanobase, Inc.
WITec Raman Imaging Solutions
+49(0)731 140 700

SPECTROMETERS, UV/VIS

Avantes
Edinburgh Instruments
+44 15 06425300
Excellims
Newsight Imaging
PerkinElmer, Inc.
PhaseTech Spectroscopy

SPECTROMETERS, OTHER

Edinburgh Instruments
+44 15 06425300
Newsight Imaging
PhaseTech Spectroscopy

IMAGING/MICROSCOPY/ MICROANALYSIS PRODUCTS

CCD CAMERAS/ DETECTORS

Axiom Optics
Diffraction Limited
HORIBA Scientific
Lambert Instruments BV
PerkinElmer, Inc.
PhaseTech Spectroscopy
Princeton Infrared Technologies, Inc.
Thermo Scientific - CIDTEC

IMAGE INTENSIFIERS

Lambert Instruments BV

IMAGING ANALYSIS SOFTWARE

Diffraction Limited
HORIBA Scientific
PerkinElmer, Inc.
Physical Electronics
WITec Raman Imaging Solutions
+49(0)731 140 700

IMAGING EQUIPMENT, GENERAL

Edinburgh Instruments
+44 15 06425300
HORIBA Scientific
Lambert Instruments BV
PerkinElmer, Inc.
PIKE Technologies
(608) 274-2721
Shimadzu Scientific Instruments
WITec Raman Imaging Solutions
+49(0)731 140 700

MICROSCOPES, ATOMIC FORCE

Mad City Labs Inc.
WITec Raman Imaging Solutions
+49(0)731 140 700

MICROSCOPES, CONFOCAL

Edinburgh Instruments
+44 15 06425300
HORIBA Scientific
WITec Raman Imaging Solutions
+49(0)731 140 700

MICROSCOPES, NEAR-FIELD SCANNING OPTICAL

Mad City Labs Inc.
WITec Raman Imaging Solutions
+49(0)731 140 700

MICROSCOPES, SCANNING ELECTRON

MOXTEK, Inc.

MICROSPECTROMETERS, RAMAN

Coherent, Inc.
Edinburgh Instruments
+44 15 06425300
Malvern Panalytical
WITec Raman Imaging Solutions
+49(0)731 140 700

MOLECULAR BIOLOGY INSTRUMENTS

NUCLEIC ACID ANALYZERS

AXT - Scientific Solutions for Industry and Academia

MANUFACTURER DIRECTORY

ABB MEASUREMENT AND ANALYTICS
3400 rue Pierre-Ardouin,
Quebec G1P 0B2,
Canada
Phone: 418 877 2944
Email: contact.center@us.abb.com
https://global.abb
See our ad on page 5

ACUTECH SCIENTIFIC INC
2311 S. 2nd Avenue,
Arcadia, California 91006,
United States
Phone: (626) 606-8810;
(626) 461-2894
Email: sales@acutechscientific.com
www.acutechscientific.com

ALPHA RESOURCES LLC
3090 Johnson Road,
Saint Joseph, Michigan 49085-2144,
United States
Phone: (269) 465-559
Email: info@alpharesources.com
www.alpharesources.com

ALLUXA
3660 North Laughlin Road
Santa Rosa, CA 95403
Phone: (855) 4-ALLUXA
Email: info@alluxa.com
www.alluxa.com
See our ad on pages 21, 81

AMERICAN CANNABIS TECHNOLOGIES
14775 E Hinsdale Avenue,
Centennial, Colorado 80112,
United States
Phone: (303) 517-1425
https://americancannabis-technologies.com

ANALYTIK JENA US
2066 W 11th Street
Upland, CA 91786-3509
Phone: (909) 946-3197, (800) 452-6788
Email: info@analytik-jena.com
www.analytik-jena.com
See our ad on page 3

APPLIED RIGAKU TECHNOLOGIES, INC.
9825 Spectrum Drive,
Building 4, Suite 475,
Austin, Texas 78717,
United States
Phone: +1 (512) 225-1796
Email: info@rigakuedxrf.com
www.rigakuedxrf.com
See our ad on page 27

ARMADILLO SIA
Krisjana Valdemara 33-11A
LV-1010, Latvia
Phone: +1 (408) 834-7422
Email: info@armadillosia.com
https://armadillosia.com

ART PHOTONICS
Rudower Chaussee 46,
Bezirk Treptow-Köpenick, Berlin,
Berlin 12489, Germany
Phone: +49 30 67798870
Email: sales@artphotonics.com
https://artphotonics.com
See our ad on page 39

ASI STANDARDS
27635 Commerce Oaks Drive #100
Oak Ridge North, Texas 77385,
United States
Phone: (281) 419-9229
Email: sales@asistandards.com
www.asistandards.com

AVANTES
2586 Trailridge Drive East, Suite 100,
Lafayette, Colorado 80026,
United States
Phone: (303) 410-8668
Email: info@avantes.com
www.avantes.com

AXIOM OPTICS
444 Somerville Avenue,
Massachusetts 02143-3260,
United States
Phone: (617) 221-6636
Email: info@axiomoptics.com
www.axiomoptics.com

AXT - SCIENTIFIC SOLUTIONS FOR INDUSTRY AND ACADEMIA
1/3 Vuko Place,
Warriewood, NSW 2102,
Australia
Phone: +61 2 9450 1359
www.axt.com.au

BAYSPEC
1101 Mckay Dr
San Jose, CA 95131
Phone: (408) 512-5928
Email: info@bayspec.com
www.bayspec.com
See our ad on page 81

BRUKER OPTICS
40 Manning Road,
Billerica, Massachusetts 01821,
United States
Phone: +1 (978) 430-2394
Email: productinfo@bruker.com
www.bruker.com
See our ad on page 19

BV THERMAL SYSTEMS
38241 Willoughby Parkway
Willoughby, Ohio 44094,
United States
Phone: (209) 522-3701
Email: Sales@BVThermal.com
www.bvthermal.com

CEM CORP.
3100 Smith Farm Road,
Matthews, North Carolina 28104,
United States
Phone: (704) 821-7015
Email: info@cem.com
https://cem.com

COHERENT, INC.
850 E Duarte Road,
Monrovia, California 91016,
United States
Phone: (626) 803-5734
Email: customer.support@coherent.com
www.coherent.com

DESIGNS & PROTOTYPES, LTD. D/B/A D&P INSTRUMENTS
17 Herman Dr. , Ste A
Simsbury, CT 06070
United States
Phone: (860) 658-0458
Email: info@dpinstruments.com
www.dpinstruments.com

DIFFRACTION LIMITED
59 Grenfell Crescent, Unit B,
Ottawa, Ontario K2G 0G2,
Canada
Phone: (613) 225-2732
www.lightmachinery.com

DRS DAYLIGHT SOLUTIONS
16465 Via Esprillo,
San Diego, California 92127,
United States
Phone: (858) 362-8971
Email: dls-info@drs.com
https://daylightsolutions.com

E-CON SYSTEMS
Suite 565, 2003 Gateway Pl,
California 95110,
United States
Phone: +1 (408) 766-7503
www.e-consystems.com

EDAX
5794 W. Las Positas Blvd.,
Pleasanton, California 94588,
United States
Phone: (201) 529-4880
Email: info.edax@ametek.com
www.edax.com
See our ad on page 23

EDINBURGH INSTRUMENTS
2 Bain Square, Kirkton Campus EH54 7DQ, United Kingdom
Phone: +44 15 06425300
Email: sales@edinst.com
www.edinst.com
See our ad on page 17

ELEMENTAR ANALYSENSYSTEME GMBH
Elementar-Straße 1,
Langenselbold, Hesse 63505,
Germany
Phone: +49 6184 9393 - 0
Email: info-us@elementar.com
www.elementar.com

ELODIZ LTD
Unit 29, Riverside Business Centre,
Victoria Street, High Wycombe,
Buckinghamshire HP11 2LT,
United Kingdom
Phone: 01494 708 811
Email: info@elodiz.com
www.elodiz.com

ENDRESS+HAUSER
2350 Endress Place,
Greenwood, Indiana 46143,
United States
Phone: (888) 363-7377
Email: info@endress.com
www.endress.com

EXCELLIMS
20 Main Street Suite A,
Acton, Massachusetts 01720-3575,
United States
Phone: +1 (978) 264-1980
https://excellims.com

EXUM INSTRUMENTS
747 Sheridan Blvd Unit 9A,
Denver, Colorado 80214,
United States
Email: info@exuminstruments.com
www.exuminstruments.com

FIBERTECH OPTICA
330 Gage Avenue , Suite I,
Kitchener, Ontario N2M 5C6,
Canada
Phone: (860) 747-4487;
(514) 352-6666
Email: info@fto.ca
https://fibertech-optica.com

GLASS EXPANSION
31 Jonathan Bourne Dr, Unit 7,
Pocasset, Massachusetts 02559,
United States
Phone: (508) 563-1800
Email: geusa@geicp.com
www.geicp.com

HARRICK SCIENTIFIC PRODUCTS INC
141 Tompkins Ave, PO Box277,
Pleasantville, New York 10570,
United States
Phone: +1 (914) 747-7202,
(800) 248-3847
Email: info@harrickscl.com
www.harrickscl.com

HITACHI HIGH-TECH ANALYTICAL SCIENCE
2 Technology Park Drive, 2nd Floor,
Westford, Massachusetts 01886,
United States
Phone: (888) 850-5588
https://hha.hitachi-hightech.com

HORIBA SCIENTIFIC
20 Knightsbridge Road,
Piscataway, New Jersey 08854,
United States
Phone: (732) 494-8660
Email: info.sci@horiba.com
www.horiba.com/scientific

HÜBNER PHOTONICS - HIGH PERFORMANCE LASERS
Vretenvagen 13 17154,
Sweden
Phone: +46 854 591 230
Email: sales@hubner-photonics.com
https://hubner-photonics.com
See our ad on page 7

HYSPEX BY NEO
65 Plain Street,
Clinton, Massachusetts 01510,
United States
Phone: +1 (954) 270-0132;
+47 40 00 18 58 (HQ Oslo, Norway)
https://neo.no

INORGANIC VENTURES
300 Technology Drive,
Christiansburg, Virginia 24073,
United States
Phone: (540) 585-3030
Email: info@inorganicventures.com
www.inorganicventures.com

INTERNATIONAL CENTRE FOR DIFFRACTION DATA
12 Campus Blvd.,
Newtown Square, Pennsylvania 19073,
United States
Phone: (610) 325-9814
Email: sales@icdd.com
www.icdd.com

IONICA SCIENCES
413 Weill Hall,
Ithaca, New York 14853,
United States
Phone: (626) 676-3076
www.ionicasci.com

IONSENSE
999 Broadway, 4th Floor,
Saugus, Massachusetts 01906,
United States
Phone: (781) 484-1043
Email: support@ionsense.com
www.ionsense.com

IS INSTRUMENTS
220 Vale Road,
Rochester, Kent TN91SP,
United Kingdom
Phone: 01732 373 020
Email: info@is-instruments.com
https://is-instruments.com

■ JASCO, INCORPORATED
28600 Mary's Court,
Easton, Maryland 21601,
United States
Phone: (410) 822-1220
Email: sales@jascoinc.com
https://jascoinc.com
See our ad on page 49

KEIT SPECTROMETERS
Unit 4, Zephyr Building, Eighth St.,
Harwell Campus, Oxford,
Oxfordshire OX11 0RL,
United Kingdom
Phone: +44 12 35431260
https://keit.co.uk

KIMMON KOHA USA, INC.
7002 S. Revere Parkway, Suite 85,
Centennial, Colorado 80112,
United States
Phone: (303) 754-0401
Email: japan@kimmon.com
https://optics.org

LABVANTAGE SOLUTIONS
265 Davidson Ave Ste 220,
Somerset, New Jersey 08873,
United States
Phone: (908) 707-4100
www.labvantage.com

LAMBERT INSTRUMENTS BV
Leonard Springerlaan 19,
5e Etage 9727KB,
Netherlands
Phone: +31 5 0501 8461
www.lambertinstruments.com

■ LECO CORP
3000 Lakeview Avenue
St Joseph, MI 49085
Phone: 269-985-5496, 800-292-6141
Email: info@leco.com
www.leco.com
See our ad on page 29

LIGHT IN MOTION
1525 McCarthy Blvd Suite 1000,
Milpitas, California 95035,
United States
Phone: (800) 886-6808,
(408) 930-3789
Email: Customer.Service@
Lightinmotion.com
www.lightinmotion.com

■ LIGHTMACHINERY
80 Colonnade Road North, Unit #1
Ottawa, ON K2E 7L2
Canada
Phone: +1 (613) 749-4895
www.lightmachinery.com
See our ad on page 55

LTB LASERTECHNIK BERLIN GMBH
Am Studio 2c,
Berlin 12489, Germany
Phone: +4930912075-100-208
Email: info@ltb-berlin.de
www.ltb-berlin.de

MAD CITY LABS INC.
2524 Todd Drive,
Madison, Wisconsin 53713,
United States
Phone: (608) 298-0855
Email: mclgen@madcitylabs.com
www.madcitylabs.com

MALVERN PANALYTICAL
2400 Computer Drive , Suite 2100,
Westborough, Massachusetts 01581,
United States
Phone: (800) 279-7297
www.malvernpanalytical.com

MCPHERSON
7 Stuart Road, #A,
Chelmsford, Massachusetts 01824-
4107, United States
Phone: (978) 256-4512
Email: Sales@McPhersonInc.com
https://mcphersoninc.com

■ METROHM
9250 Camden Field Pkwy,
Florida 33578,
United States
Phone: 866-METROHM
https://web.metrohmusa.com
See our ad on page 9

■ MILESTONE, INC.
25 Controls Drive,
Shelton, Connecticut 06484,
United States
Phone: (866) 995-5100
Email: mwave@milestonesci.com
www.milestonesci.com
See our ad on page 53

MOXTEK, INC.
452 West 1260 North,
Orem, Utah 84057,
United States
Phone: 1 (800) 758-3110
https://moxtek.com

■ NANOBASE, INC.
1406-1, 196 Gasan-digital-1-ro,
Geumcheon-gu, Seoul 08502,
South Korea
Phone: +82 70 8666 0233
Email: nbsales@nanobase.co.kr
https://www.nanobase.co.kr
See our ad on page CV4

NEOSPECTRA BY SI-WARE
101 Jefferson Dr, 1st Floor,
Menlo Park, California 94025,
United States
Phone: +1(650) 257-9680,
+1(859) 620-9828
www.si-ware.com

NEWPORT CORPORATION
1791 Deere Avenue,
Irvine, California 92606,
United States
Phone: 1 (978) 645-5500;
1 (800) 227-8766 (International)
www.newport.com

NEWSIGHT IMAGING
Golda Meir 3, Ness Ziona 7414002,
Israel
Phone: +972 8 373 0635,
+972 5 0541 7178
Email: info@nstimg.com
www.nstimg.com

NIKALYTE LTD
Heyford Park Innovation Centre,
77 Heyford Park,
Oxford, Oxfordshire OX25 5HD,
United Kingdom
Phone: 01869 238 042
Email: sales@nikalyte.com
www.nikalyte.com

NLIR
Hirsemarken 1, Farum,
Farum, Copenhagen 3520 ,
Denmark
Phone: +45 7174 7870
Email: info@nlir.com
https://nlir.com

■ OCEAN INSIGHT
3500 Quadrangle Blvd. ,
Orlando, Florida 32817,
United States
Phone: +1 (407) 673-0041
www.oceaninsight.com
See our ad on pages CV2, 81

OPTIWAVE SYSTEMS INC
7 Capella Court, Suite 300 K2E 8A7,
Canada
Phone: +1(613) 224-4700
Email: info@optiwave.com
https://optiwave.com

PERKINELMER, INC.
940 Winter Street,
Waltham, Massachusetts 02451,
United States
Phone: (203) 925-4602
Email: customercareus@
perkinelmer.com
www.perkinelmer.com

PHASETECH SPECTROSCOPY
4916 East Broadway, Suite 125,
Madison, Wisconsin 53716,
United States
Phone: +1 (608) 712-1857
Email: contact@
phasetechspectroscopy.com
http://phasetechspectroscopy.com

PHYSICAL ELECTRONICS
18725 Lake Drive East,
Chanhassen, Minnesota 55317,
United States
Phone: (952) 828-6100
www.phi.com

■ PIKE TECHNOLOGIES
6125 Cottonwood Dr.,
Madison, Wisconsin 53719,
United States
Phone: (608) 274-2721
Email: info@piketech.com
www.piketech.com
See our ad on pages 25, 34

PRINCETON INFRARED TECHNOLOGIES, INC.
7 Deerpark Dr., Suite E,
Monmouth Junction, New Jersey
08852, United States
Phone: +1(609) 917-3380
Email: contact@princetoneirtech.com
www.princetonirtech.com

QUANTUM ANALYTICS
The Woodlands, Texas,
United States
Phone: (800) 992-4199
Email: info@lqa.com
www.quananalytics.com

RAYSPEC LTD
1 The Valley Centre, Gordon Road,
High Wycombe, Buckinghamshire
HP13 6EQ,
United Kingdom
Phone: +44 (0) 1628 511770
www.rayspec.co.uk

■ REFLEX ANALYTICAL CORPORATION
PO Box 119
Ridgewood, New Jersey 07451
United States
Phone: (201) 444-8958
Email: reflexusa@att.net
www.reflexusa.com
See our ad on page 82

■ RENISHAW
1001 Wesemann Dr
West Dundee, IL 60118
Phone: (847) 286-9953
Email: usa@renishaw.com
www.renishaw.com
See our ad on page 43

RPMC LASERS INC
8495 Veterans Memorial Pkwy,
OFallon, Missouri 63366,
United States
Phone: (636) 272-7227
Email: info@rpmclasers.com
www.rpmclasers.com

SARTORIUS DATA ANALYTICS AB
Östra Strandgatan 24,
Umeå 90333,
Sweden
Phone: +46 90 184800
Email: info@sartorius.com
www.sartorius.com

■ SAVILLEX
10321 W 70 Street
Eden Prairie, MN 55344
Phone: (952) 935-4100
Email: info@savillex.com
www.savillex.com
See our ad on page 45

SCHOTT NORTH AMERICA, INC. - LIGHTING AND IMAGING
122 Charlton Street,
Southbridge , Massachusetts
01550, United States
Phone: +1 (508) 765-3201
www.schott.com

SCP SCIENCE
21800 Clark Graham,
Baie D'Urfe, Quebec, H9X 4B6,
Canada
Phone: (514) 457-0701,
(800) 361-6820 (Toll-Free US/Canada)
Email: sales@scpscience.com
www.scpscience.com

SHIMADZU SCIENTIFIC INSTRUMENTS
7102 Riverwood Drive,
Columbia, Maryland 21046,
United States
Phone: (410) 381-1227
www.ssi.shimadzu.com

SPECTRA VISTA CORPORATION - VISNIR SPECTROMETERS AND SPECTRORADIOMETERS
29 Firemen's Way,
Poughkeepsie, New York 12603,
United States
Phone: (845) 471-7007
Email: svcinfo@spectravista.com
https://spectravista.com

SPECTROLIGHT, INC.
19800 Macarthur Blvd. Suite #300,
Irvine, California 92612,
United States
Phone: +1 (909) 630-6237
Email: info@spectrolightinc.com
www.spectrolightinc.com

SPECTRON, INC.
2387 Portola Road, Suite A,
Ventura, California 93003,
United States
Phone: (805) 642-0400
Email: Spectron@SpectronUS.com
https://spectronus.com

■ **SPECTROSCOPY MEDIA**
485 US Highway 1
Iselin, New Jersey 08830,
United States
Phone: (732) 710-2175
www.spectroscopyonline.com
See our ad on pages 47, 59, 65, 71

S.T.JAPAN-EUROPE GMBH
Suelzburgstrasse 203,
Cologne, North-Rhine
Westphalia 50937,
Germany
Phone: +49 (0)2234 956372
Email: contact@stjapan.de
www.stjapan.de

TELEDYNE PRINCETON INSTRUMENTS
3660 Quakerbridge Road,
Trenton, New Jersey 08619,
United States
Phone: (609) 587-9797
Email: pi.info@Teledyne.com
www.princetoninstruments.com

THERMO SCIENTIFIC - CIDTEC
101 Commerce Blvd,
Liverpool, New York 13088-4507,
United States
Phone: (315) 451-9410
Email: sales.cidtec@
thermofisher.com
www.thermofisher.com/cidtec

■ **THERMO SCIENTIFIC**
5225-1 Verona Road,
Madison, Wisconsin 53711,
United States
Phone: +1 (800) 532-4752
Email: info.spectroscopy@
thermofisher.com
www.thermoscientific.com/
spectroscopy
See our ad on page 67

TOPTICA PHOTONICS AG
Lochhamer Schlag 19
82166 Graefelfing
Munich, Germany
Phone: +49 89 85837-0
Email: sales@toptica.com
www.toptica.com

■ **TOPTICA PHOTONICS, INC.**
5847 County Road 41
Farmington, NY 14425
United States
Phone: +1 (585) 657-6663
Email: sales@toptica-usa.com
www.toptica.com
See our ad on page 41

VERDER SCIENTIFIC INC
11 Penns Trail, Suite 300,
Newtown, Pennsylvania 18940,
United States
Phone: (267) 757-0351
www.verder-scientific.com

WASATCH PHOTONICS
808 Aviation Parkway, Suite 1400,
Morrisville, North Carolina 27560,
United States
Phone: +1 (919) 544-7785
https://wasatchphotonics.com

WAVELENGTH ELECTRONICS
51 Evergreen Drive
PO Box 865
Bozeman, MT 59771
Phone: (406) 587-4910
Email: sales@teamwavelength.com
www.teamwavelength.com

WILEY SCIENCE SOLUTIONS
111 River Street,
Hoboken, New Jersey 07030,
United States
https://sciencesolutions.wiley.com

■ **WITEC RAMAN IMAGING SOLUTIONS**
Lise-Meitner-Str. 6,
Ulm, Germany 89081
Phone: +49(0)731 140 700
Email: info@WITec.de
https://raman.oxinst.com
See our ad on page 35

■ **SEE DISPLAY AD IN THIS ISSUE**

PRODUCT PROFILES

Emission Line Filters

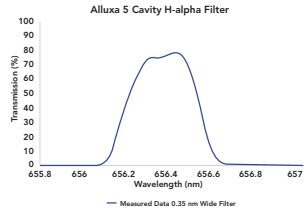

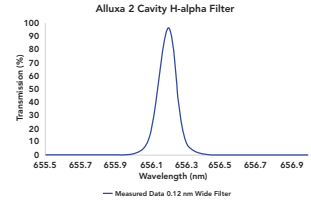

Alluxa's two Hydrogen Alpha (H-Alpha) Emission Line Filters are designed to monitor H-alpha spectra in astronomy. According to the company, the filters can be used in any application where spectral line discrimination is critical, including spectroscopy, plasma monitoring, fusion research, and more.

The novel 5 Cavity H-alpha Filter sets a new standard for narrow filters with regard to squareness. It has a 50% BW of only 0.35 nm, a 1% BW of <0.6 nm, peak transmission of approximately 80%, and is fully blocked to OD6 out of band. Alluxa's 2 Cavity H-alpha Filter features an even narrower design, with a FWHM of 0.12 nm and peak transmission of greater than 90%.

Alluxa, Inc.,
Santa Rosa, CA.
www.alluxa.com

Microspectrometer

The Ocean ST is a powerful microspectrometer that provides excellent UV response, high-speed spectral acquisition, and high signal-to-noise ratio performance for applications ranging from DNA absorbance to color characterization. Despite its small size and light weight, Ocean ST delivers full spectral analysis at a performance level comparable to larger and more expensive spectrometers. Models are available for UV (185–650 nm), visible (350–810 nm), and shortwave NIR (645–1085 nm) wavelength coverage. The Ocean ST has optical resolution to 2.2 nm (FWHM), and is suitable for both everyday laboratory use and integration into other devices and setups where space is limited.

Ocean Insight,
Orlando, FL.
www.oceaninsight.com/OceanSTspectrometer

Palm Spectrometer

BaySpec's Breeze™ palm spectrometer for 400–2500 nm is designed with one-button operation. Proprietary miniaturized optics give Breeze maximum sensitivity with ultrafast acquisition. According to the company, the Breeze Dual-IS provides even higher accuracy with an integrating sphere.

BaySpec, Inc.,
San Jose, CA.
www.bayspec.com/category/spectroscopy/uv-vis-nir-spectrometers/

Miniature Spectrometer

The new Ocean SR2 spectrometer provides high-speed spectral acquisition and excellent signal-to-noise ratio (SNR) performance. The spectrometer is well suited for applications including challenging absorbance and fluorescence measurements, LED/laser characterization, plasma monitoring, and water analysis. Ocean SR2's combination of speed (integration times to 10 µs), SNR (380:1), and a novel high-speed averaging mode provide application versatility without the trade-offs typical of comparable spectrometers. Also, Ocean SR2's precision slit aperture and rugged electronic accessory connector ensure reliable performance, and models are available that cover multiple wavelengths across UV, visible and NIR ranges from 185–1100 nm.

Ocean Insight,
Orlando, FL.
www.oceaninsight.com/OceanSR2spectrometer

PRODUCT PROFILES

Pellet Die

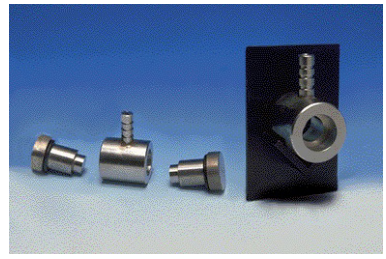

The University Pellet Die from REFLEX Analytical, also known as the Uni-Die, is designed as a unique 13-mm evacuable pellet die that forms a pellet within the assembly's barrel chamber after compressing the sample matrix between two polished mandrels using a laboratory press. According to the company, the mandrels are easily removed while the pellet remains intact within the center of the barrel. The barrel is then placed in the path of the spectrophotometer's beam for analysis. The three-piece design is fabricated from hardened stainless steel with an evacuable connection permitting interface with a vacuum pump. It can manage applied pressure up to 5 tons.

REFLEX Analytical Corporation,
Ridgewood, NJ.
www.reflexusa.com

• Continued from Page 24

(5) R.A. Talewar, V.M. Gaikwad, P.K. Tawalare, and S.V. Moharil, *Opt. Laser Technol.* **115,** 215–221 (2019).

(6) Z.J. Wang, X.Z. Li, G.J. Wang, M.J. Song, Q. Wei, G.F. Wang, and X.F. Long, *J. Lumines.* **128,** 451–456 (2008).

(7) Z.J. Wang, X.Z. Li, Q. Wei, and X.F. Long, *Mater. Res. Innovations* **12,** 174–178 (2013).

(8) Y. Ohishi, A. Mori, M. Yamada, H. Ono, Y. Nishida, and K. Oikawa, *Opt. Lett.* **23,** 274–276 (1998).

(9) P. Peterka, B. Faure, W. Blanc, M. Karásek, and B. Dussardier, *Opt. Quantum Electron.* **36,** 201–212 (2004).

(10) Z. Chen, J. Zhang, S. Pan, X. Wang, and J. Pan, *J. Lumines.* **225,** 117347 (2020).

(11) M.P. Hehlen, A. Kuditcher, A.L. Lenef, H. Ni, Q. Shu, S.C. Rand, J. Rai, and S. Rai, *Phys. Rev. B* **61,** 1116–1128 (2000).

(12) S.D. Jackson and S. Mossman, *Appl. Opt.* **42,** 2702–2707 (2003).

(13) A. Braud, S. Girard, J.L. Doualan, M. Thuau, R. Moncorgé, and A.M. Tkachuk, *Phys. Rev. B* **61,** 5280–5292 (2000).

(14) L. Feng, Q. Tang, L. Liang, J. Wang, H. Liang, and Q. Su, *J. Alloys Compd.* **436,** 272–277 (2007).

(15) M. Liao, L. Wen, H. Zhao, Y. Fang, H. Sun, and L. Hu, *Mater. Lett.* **61,** 470–472 (2007).

(16) X. Mateos, R. Solé, J. Gavaldà, M. Aguiló, J. Massons, and F. Díaz, *Opt. Mater.* **28,** 423–431 (2006).

(17) W. Xu, X. Xu, W. Feng, G. Zhao, Z. Zhao, G. Zhou, and J. Xu, *Opt. Commun.* **272,** 182–185 (2007).

(18) H. Cañibano, G. Boulon, L. Palatella, Y. Guyot, A. Brenier, M. Voda, R. Balda, and J. Fernandez, *J. Lumines.* **102-103,** 318–326 (2003).

(19) Y.K. Voron'Ko, K.A. Subbotin, V.E. Shukshin, D.A. Lis, S.N. Ushakov, A.V. Popov, and E.V. Zharikov, *Opt. Mater.* **29,** 246–252 (2006).

(20) C. Borel, *Opt. Commun.* **142,** 239–243 (1997).

(21) W.A. Bollig, R.A. Clarkson, and D.C. Hayward, *Opt. Commun.* **154,** 35–38 (1998).

(22) P. Song, Z. Zhao, X. Xu, B. Jang, P. Deng, and J. Xu, *J. Cryst. Growth* **270,** 433–437 (2004).

(23) N.Y. Garces, M.M. Chirila, H.J. Murphy, J.W. Foise, E.A. Thomas, C. Wicks, K. Grencewicz, L.E. Halliburton, and N.C. Giles, *J. Phys. Chem. Solids* **64,** 1195–1200 (2003).

(24) D.J. Daniel, H.J. Kim, S. Kim, and S. Khan, *Opt. Mater.* **70,** 120–126 (2017).

(25) Y. Dong, H. Xia, L. Fu, S. Li, X. Gu, J. Zhang, D. Wang, Y. Zhang, H. Jiang, and B. Chen, *Optoelectron. Lett.* **10,** 262–265 (2014).

(26) P. Yu, L. Su, H. Zhao, X. Guo, H. Li, X. Feng, Q. Yang, and J. Xu, *Opt. Mater.* **33,** 831–834 (2011).

(27) J. Zhang, I.R. Pandey, S. Pan, H. Kim, J. Pan, and H. Chen, *J. Lumines.* **212,** 184–190 (2019).

(28) S. Pan, J. Zhang, J. Pan, G. Ren, J. Lee, and H. Kim, *J. Cryst. Growth* **498,** 56–61 (2018).

(29) X. Wang, Z. Li, K. Li, L. Zhang, J. Cheng, and L. Hu, *Opt. Mater.* **35,** 2290–2295 (2013).

(30) A. Méndez-Blas, M. Rico, V. Volkov, C. Cascales, C. Zaldo, C. Coya, A. Kling, and L.C. Alves, *J. Phys. Condens. Matter* **16,** 2139–2160 (2004).

(31) C. Cascales, M. Serrano, F. Estebanbetegón, C. Zaldo, R. Peters, K. Petermann, G. Huber, L. Ackermann, D. Rytz, and C. Dupré, *Phys. Rev. B* **74,** 3840–3845 (2006).

(32) M. Rico, U. Griebner, V. Petrov, P. Ortega, X.M. Han, C. Cascales, and C. Zaldo, *J. Opt. Soc. Am. B* **23,** 1083–1090 (2006).

(33) P. Shi, Z. Xia, M.S. Molokeev, and V.V. Atuchin, *Dalton Trans.* **43,** 9669–9676 (2014).

(34) J. Huang, J. Huang, Y. Lin, X. Gong, Y. Chen, Z. Luo, and Y. Huang, *J. Lumines.* **187,** 235–239 (2017).

(35) X. Li, Z. Lin, L. Zhang, and G. Wang, *Opt. Mater.* **29,** 728–731 (2007).

Xi Wang, Zongyue Chen, Jianyu Zhang, and **Shangke Pan** are with the State Key Laboratory Base of Novel Function Materials and Preparation Science at the School of Material Sciences and Chemical Engineering of Ningbo University, in Ningbo, Zhejiang, China. **Shangke Pan** and **Jianguo Pan** are with the Key Laboratory of Photoelectric Materials and Devices of Zhejiang Province, in Zhejiang, China. Direct correspondence to: panshangke@nbu.edu.cn ●

Medical World News®

powered by MJH life sciences

A 24-hour streaming program

For Health Care Professionals, By Health Care Professionals

Season 7 is streaming now!

www.medicalworldnews.com

Discover the latest innovation in Raman customization.

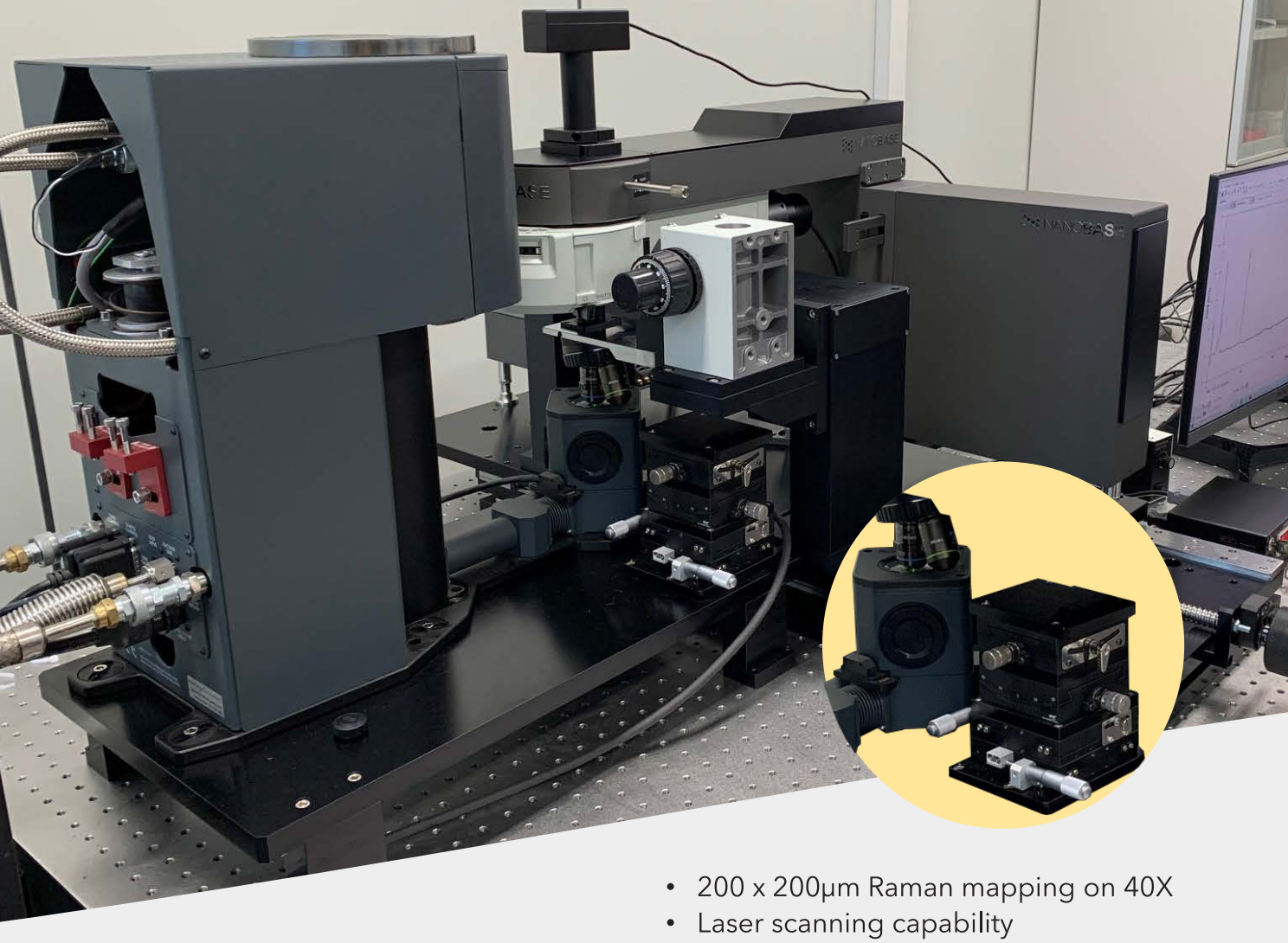

Introducing our Raman module integrated with *Cryostation*®* for cold Raman measurement

- 200 x 200μm Raman mapping on 40X
- Laser scanning capability
- High efficiency spectrometer
- VPH transmission grating selections
- Multiple laser selections
- Raman measurement in low temperature or in ambient environment
- Easy measurement mode switch by stage movement
- Also customizable to *CryoAdvance*™*

NANOBASE

www.nanobase.co.kr
nbsales@nanobase.co.kr

* *Cryostation*® and *CryoAdvance*™ are the products made by Montana Instruments.